

AD-A267 867 ENTATION PAGE

Form Approved
OMB No. 0704-0188

time to review and respond to requests for information, including the time for reviewing instructions, searching existing data sources, gathering and reviewing the collection of information, and reviewing the collection of information. Send comments regarding this burden estimate or any other aspect of this collection of information, including suggestions for reducing this burden, to Washington Headquarters Services, Directorate for Information Operations and Reports, 1215 Jefferson Davis Highway, Suite 1204, Arlington, VA 22202-4302, and to the Office of Management and Budget, Paperwork Reduction Project (0704-0188), Washington, DC 20503.

1. AGENCY USE ONLY (Leave blank)		2. REPORT DATE Aug 1993		3. REPORT TYPE AND DATES COVERED THESIS/ DISSERTATION	
4. TITLE AND SUBTITLE LEUKOCYTE DEFORMATION AND ENDOTHELIAL CELL CONTACT MECHANICS DURING INCIPIENT MEMBRANE PEELING AND CELL ROLLING				5. FUNDING NUMBERS	
6. AUTHOR(S) Erika J. Struble					
7. PERFORMING ORGANIZATION NAME(S) AND ADDRESS(ES) AFIT Student Attending: Penn State University				8. PERFORMING ORGANIZATION REPORT NUMBER AFIT/CI/CIA- 93-063	
9. SPONSORING / MONITORING AGENCY NAME(S) AND ADDRESS(ES) DEPARTMENT OF THE AIR FORCE AFIT/CI 2950 P STREET WRIGHT-PATTERSON AFB OH 45433-7765				10. SPONSORING / MONITORING AGENCY REPORT NUMBER	
11. SUPPLEMENTARY NOTES					
12a. DISTRIBUTION / AVAILABILITY STATEMENT Approved for Public Release IAW 190-1 Distribution Unlimited MICHAEL M. BRICKER, SMSgt, USAF Chief Administration				12b. DISTRIBUTION CODE	
13. ABSTRACT (Maximum 200 words)					
 93-18708 					
14. SUBJECT TERMS				15. NUMBER OF PAGES 130	
				16. PRICE CODE	
17. SECURITY CLASSIFICATION OF REPORT	18. SECURITY CLASSIFICATION OF THIS PAGE	19. SECURITY CLASSIFICATION OF ABSTRACT	20. LIMITATION OF ABSTRACT		

92-063

The Pennsylvania State University

The Graduate School

College of Engineering

**LEUKOCYTE DEFORMATION AND ENDOTHELIAL CELL
CONTACT MECHANICS DURING INCIPIENT MEMBRANE
PEELING AND CELL ROLLING**

A Thesis in

Bioengineering

by

Erika J. Struble

**Submitted in Partial Fulfillment
of the Requirements
for the Degree of**

Master of Science

August 1993

I grant The Pennsylvania State University the nonexclusive right to use this work for the University's own purposes and to make single copies of the work available to the public on a not-for-profit basis if copies are not otherwise available.

Erika J Struble

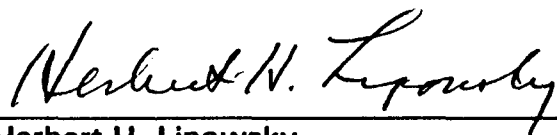
Erika J. Struble

DTIC QUALITY INSPECTED 3

Accession For	
NTIS GRA&I	<input checked="checked" type="checkbox"/>
DTIC TAB	<input type="checkbox"/>
Unannounced	<input type="checkbox"/>
Justification	
By	
Distribution/	
Availability Codes	
Dist	Avail and/or Special
A-1	

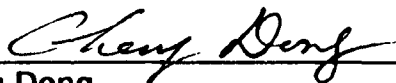
We approve the thesis of Erika J. Struble.

Date of Signature



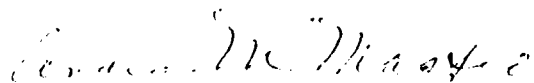
Herbert H. Lipowsky
Professor and Chair of Bioengineering
Thesis Advisor

4/27/93



Cheng Dong
Assistant Professor of Bioengineering

4/28/93



Andrea M. Mastro
Professor of Microbiology and Cell Biology

4/29/93

Abstract

Leukocyte (WBC) adhesion to venular endothelium (EC) is an important step in the immune response which precedes their emigration through the microvessel wall. To assess the relationship between membrane WBC mechanics and the formation and disruption of WBC-EC bonds, measurements of transients in contact area and WBC shape were made during adhesion in postcapillary venules of the rat mesentery during control conditions (spontaneous adhesion), in response to exposure to the chemoattractant N-formyl-methionyl-leucyl-phenylalanine (FMLP) and following tissue exposure to interleukin-1 β (IL-1). To assess the roles of WBC deformability, adhesion was also studied during suffusion with colchicine and cytochalasin B (CB). Frame-by-frame analysis of video recordings facilitated measurement of the length of the contact zone between WBC and EC (L_c) and the acute angle (θ) between the trailing edge of the WBC membrane and EC surface. During the initial adhesion, L_c was found to steadily increase with time as new bonds were formed, and to subsequently decrease with time as the trailing edge of the WBC membrane began to peel away from the EC. The contact angle at the trailing edge of the cell decreased exponentially for control, IL-1, CB, and colchicine. For

FMLP the angle initially decreased then subsequently increased as the WBC became more activated. Both θ and L_c plotted against τ_w furnished a measure of deformability for control, FMLP, IL-1, and colchicine which was consistent with current data. θ decreased with τ_w for control, IL-1, and colchicine treatment indicating the cells were deformable. θ increased with τ_w for FMLP indicating that the more activated and stiffest cells adhered at the highest shear rates. L_c versus τ_w provided consistent results with the exception of IL-1 stimulated adhesion in which L_c was invariant with τ_w . The time of transition between bonding and peeling, t_p , was assumed to correspond to the life span of bonds formed during the initial WBC-EC contact. A logarithmic decline of t_p with wall shear stress, τ_w , suggested a mode of peeling consistent with the kinetic theory of fracture. The logarithmic relationship was significant for peeling under control, FMLP, and IL-1 conditions. Employing the kinetic theory of fracture, the bond energy (U_o) and bond force (f_o) were calculated for each condition and were 3% greater for FMLP as compared to control and IL-1 ($p < 0.05$). U_o for both control and IL-1 was not significantly different ($p > 0.05$), indicating that both stimulants for adhesion induce WBC sticking through similar mechanisms. To model the adhesion process and elucidate the relative roles of cell deformability and strength of the adhesion bond as determinants of the peeling process, a theoretical analysis was performed in which the bond, normal stress, and membrane tension distributions were analyzed. Since the

avidity of the receptor-ligand bonds for FMLP and IL-1 adhesion were similar in magnitude, the FMLP adhesion appeared to be much stronger due to increased bond density rather than bond force.

Table of Contents

List of Tables	viii
List of Figures	ix
Chapter 1 Introduction	1
1.1 Rationale	1
1.2 Background	3
Chapter 2 Experimental Methods and Data Acquisition	8
2.1 Methods	8
2.2 Data Analysis	12
2.3 Statistical Analysis	17
Chapter 3 Experimental and Analytical Results	18
3.1 Formation and Disruption of WBC-EC Bonds	18
3.1.1 Kinetic Theory of Fracture	25
3.2 WBC Membrane Mechanics	35
Chapter 4 Force Equilibrium Analysis of an Adherent White Blood Cell in Shear Flow	53
4.1 Analysis	54
4.1.1 Peeling Region	59

4.1.2 Bonded Region - Outside of the Peeling Region	65
4.2 Model Validation	68
Chapter 5 Discussion of Bond Density Distributions for Control Conditions and FMLP and IL-1 Stimulated Adhesion	91
Chapter 6 Summary and Conclusion	102
References	105
Appendix A Hemodynamic Data	110
A.1 Control	111
A.2 FMLP	113
A.3 IL-1	114
A.4 CB	115
A.5 Colchicine	116
Appendix B Experimental Analysis	117
B.1 Control	118
B.2 FMLP	120
B.3 IL-1	121
B.4 CB	122
B.5 Colchicine	123
Appendix C Bond Distribution Program	125

List of Tables

Table 3.1	Hemodynamic parameters	19
Table 3.2	L_c vs. time regression parameters	23
Table 3.3	Experimental time to peeling and contact length measurements	26
Table 3.4	Regression parameters and statistics for $\ln(t_p)$ versus r_w . .	29
Table 3.5	Adhesion energy and force per bond	33
Table 3.6	Regression parameters and statistics for $L_{c\ tp}$ versus r_w . . .	39
Table 3.7	Contact angle measurements for control, FMLP, IL-1, CB, and colchicine	43
Table 3.8	Regression parameters and statistics for θ_{tp} versus r_w . . .	47
Table 3.9	Regression parameters and statistics for θ_{tp} versus t_p	52
Table 4.1	Parameter estimates	69
Table 5.1	Model parameters and average bond density for control, FMLP, and IL-1 conditions	92

List of Figures

Figure 2.1	Experimental set-up	10
Figure 2.2	Schematic of adherent WBC	15
Figure 3.1	Representative trends of contact length versus time for WBCs under control conditions and FMLP and IL-1 stimulated adhesion	21
Figure 3.2	Representative trends of contact length versus time for WBCs with CB and colchicine treatment	22
Figure 3.3	Comparison plot of L_c versus time for control, FMLP, and IL-1 and the determination of time to peeling (t_p)	24
Figure 3.4	Time to peeling versus wall shear stress for control conditions and FMLP and IL-1 stimulated adhesion	27
Figure 3.5	Time to peeling versus wall shear stress for CB and colchicine treatment	28
Figure 3.6	Comparison of linear regressions of t_p versus τ_w for control conditions and FMLP and IL-1 stimulated adhesion	30
Figure 3.7	Adhesion energy and bond force for control, FMLP, IL-1, CB, and colchicine treatment	34

Figure 3.8	Contact length at t_p versus wall shear stress for control conditions and FMLP and IL-1 stimulated adhesion	37
Figure 3.9	Contact length at t_p versus wall shear stress for CB and colchicine treatments	38
Figure 3.10	Representative trends of contact angle versus time for WBCs under control conditions and FMLP and IL-1 stimulated adhesion	40
Figure 3.11	Representative trends of contact angle versus time for WBCs under CB and colchicine treatment	41
Figure 3.12	Contact angle at t_p versus wall shear stress for control, FMLP, and IL-1	45
Figure 3.13	Contact angle at t_p versus wall shear stress for CB and colchicine	46
Figure 3.14	Angle at t_p versus t_p for control conditions and FMLP and IL-1 stimulated adhesion	49
Figure 3.15	Angle at t_p versus t_p for CB and colchicine	50
Figure 4.1	Schematic view of an adhering WBC	55
Figure 4.2	Schematic illustration of stresses acting on the bridged region of the membrane	57
Figure 4.3	Membrane displacement from equilibrium	62
Figure 4.4	Membrane displacement from equilibrium for various values of parameter c	71

Figure 4.5 Bond density model sensitivity curve for independent parameter c	72
Figure 4.6 Bond normal stress versus non-dimensional distance from trailing edge for various gap thickness decay rates	73
Figure 4.7 Membrane tension versus non-dimensional distance from trailing edge, where δ is the fraction of the contact zone with non-zero shear stresses (τ_s)	75
Figure 4.8 Membrane distributions for $\tau_w = 1.0$ dyne/cm ² and zero internal shear stress	76
Figure 4.9 Membrane distributions for $\tau_w = 2.0$ dyne/cm ² and zero internal shear stress	77
Figure 4.10 Membrane distributions for $\tau_w = 4.0$ dyne/cm ² and zero internal shear stress	78
Figure 4.11 Membrane distributions for $\tau_w = 6.0$ dyne/cm ² and zero internal shear stress	79
Figure 4.12 Membrane distributions for $\tau_w = 6.0$ dyne/cm ² and $\tau_p = 3.0$ dyne/cm ²	81
Figure 4.13 Effect of contact length on bond density distribution . . .	83
Figure 4.14 Bond density model sensitivity curves for f_o , the force per bond	85
Figure 4.15 Schematic diagram of a leukocyte rolling on vascular endothelium	86

Figure 4.16	Surface density of adhesion bonds as a function of distance along the vascular endothelium	86
Figure 4.17	Bond density distribution for small membrane gap	88
Figure 4.18	Bond density distribution for larger membrane gap	89
Figure 5.1	Membrane distributions for WBC adhesion under control conditions	93
Figure 5.2	Membrane distributions for WBC FMLP stimulated adhesion	94
Figure 5.3	Membrane distributions for WBC IL-1 stimulated adhesion	95
Figure 5.4	Average bond density versus force per bond	97
Figure 5.5	Bond density comparison for control conditions and FMLP and IL-1 stimulated adhesion	98
Figure 5.6	Average bond density for control conditions and FMLP and IL-1 stimulated adhesion	99

Chapter 1

Introduction

1.1 Rationale

Adhesion of leukocytes to post-capillary venular endothelium is a central component of the immune response which precedes the extravasation of white blood cells (WBCs) through the vessel wall. Elucidation of the mechanics of the adhesion process is necessary to understand the etiology of pathological conditions which result from either weak or excessive WBC adhesion to the endothelium.

For example, leukocyte adhesion deficiency syndrome results from the absence of a specific adhesion molecule and manifests itself in virulent bacterial infections, and early death (Lasky, 1992). Excessive leukocyte adhesion may also have deleterious consequences. Progressive leukocyte adhesion has been implicated in the "no re-flow phenomenon" following periods of myocardial, brain, and bowel ischemia and acute hemorrhagic shock (Bagge, 1984; Barroso-Arnanda *et al.*, 1988; Dahlgren *et al.*, 1984; Engler *et al.*, 1983 and 1986; Engler, 1989, Granger *et al.*, 1989). Concomitant to the period of ischemia, there is a progressive increase in

vascular resistance due to the continual entrapment of WBCs in the microcirculation and edema formation (Engler *et al.*, 1986). The entrapment or leukocyte capillary plugging occurs at points within the capillary bed that require the WBC to deform in order to pass, such as, capillary entrances and tapered segments caused by protruding endothelial cell nuclei (Dahlgren *et al.*, 1984). Upon reperfusion, hemodynamic forces are insufficient to disrupt the adhesion between the leukocyte and endothelium; therefore, a "no-reflow phenomenon" occurs and tissue ischemia is exacerbated. While trapped in the microcirculation and parenchymal tissue, the activated WBCs may release a number of toxic substances, such as, lytic enzymes and oxygen free radicals, resulting in endothelial injury and edema which further increases vascular resistance (Barroso-Arnanda *et al.*, 1988). Anti-adhesive treatments are currently being investigated to aid in the prevention of the "no-reflow phenomenon" and reduction of tissue injury following ischemic episodes (Engler *et al.*, 1986; Suzuki *et al.*, 1991; Granger *et al.*, 1989; Schmid-Schönbein and Engler, 1990). Leukocyte mediated injury has also been implicated in allograft rejection, rheumatoid arthritis, inflammatory skin disease, and adult respiratory distress syndrome (Harlan *et al.*, 1992). For these reasons, the study of WBC adhesion is a pertinent and compelling topic of microvascular research.

In vivo, leukocytes can be observed rolling along the vascular endothelium, particularly the venules. During inflammation, the WBCs

adhere to the endothelium and emigrate across the microvessel wall to the site of injury (Grant, 1973). Their adhesion, and ultimately the progression of the inflammatory response, rests upon the balance of the adhesive and hemodynamic forces acting upon the leukocyte. Various agents may be employed to alter adhesive and hemodynamic forces acting on the WBC. There are several modes of adhesion, two of which can be stimulated with separate agents, N-formyl-methionyl-leucyl-phenylalanine (FMLP) and interleukin-1 β (IL-1); therefore, possibly manifesting distinct adhesive forces. Hemodynamic forces can be altered by affecting WBC deformability. Two agents are specifically proposed for this purpose; cytochalasin-B and colchicine, both which cause an increase in cell deformability by acting on the WBC's cytoskeleton. In addition FMLP has been shown to significantly decrease WBC deformability. In studying the relationship between adhesive and hemodynamic forces under these different conditions, a greater understanding of the mechanical properties of the adhesion molecules may provide new insight into the therapeutic management of leukocyte-endothelium adhesion.

1.2 Background

Historically, the strength of the adhesive force between leukocytes and vascular endothelium has been estimated indirectly by measurements of

white blood cell rolling velocity (V_{wbc}) and/or the number of cells per unit area of endothelium. Atherton and Born (1973) concluded that leukocyte rolling was governed by two forces: the hemodynamic shear force and the adhesive force between WBC and endothelium. Further, if the adhesive force was assumed to be similar for all WBCs, the proportionality between the velocity of blood (red blood cell velocity, V_{rbc}) and V_{wbc} was due to the balance of these shear forces. Mayrovitz and Wiedeman (1976) showed that wall shear stress was indeed an important parameter in determining whether leukocyte adherence would occur. Using leukocyte flux in arterioles (bat wing) as a measure of the strength of adhesion, they concluded that the initial adherence of WBCs was dependent upon the magnitude of shear stress, up to a critical or threshold value of 8 dyne/cm², above which no WBC adhesion could be observed. Contrastingly, they found that once the cells were rolling along the endothelium, there was no clear relationship between V_{wbc} and shear stress except for at low blood velocities. Similar findings were published by Firrell and Lipowsky (1989) based upon observations in postcapillary venules (mesentery). The invariance of V_{wbc} with shear stress indicated that further mechanisms needed to be considered, such as, cell to cell adhesive forces and cell deformability.

Cell to cell adhesive forces are derived from the interaction of receptors on the WBC and endothelial cells. Preliminary evidence indicates that "rolling receptors" or selectins enable neutrophils to roll along the

endothelium. The slowing of the white cell and the close proximity to the vascular wall, in turn, promotes the engagement of the integrins (adhesion molecules), thereby, facilitating adhesion and ultimately cell emigration, Lawrence and Springer (1991) and Figdor and Van Kooyk (1992). Leukocyte deformability may aid in the adhesion process by helping to balance the adhesive and hemodynamic forces. The more deformable the WBC, the longer the cell will stretch and the larger the area of contact between the cell membrane and endothelium. Contact area may be the principal determinant of the maximal force that can be withstood before hemodynamic stresses disrupt the bond between WBC and EC. Schmid-Schönbein *et al.* (1987) presented an analysis affirming this relationship. They showed that the force per unit length it takes to break the adhesive bonds (fracture stress) between a steady rolling white cell and endothelium is inversely proportional to the ratio of V_{wbc}/V_{rbc} . Therefore, the lower the velocity ratio; the higher will be the fracture stress. Since, the fracture stress (adhesion energy density) is equal to adhesion energy divided by contact area, a larger contact area, will yield a greater adhesive energy between the WBC and EC for a given fracture stress. Therefore, a highly deformable cell may have a larger contact area which will increase the strength of the cell to cell adhesion. Firrell and Lipowsky (1989) hypothesized that the stretching and elongation of the WBC in shear flow may also help temper hemodynamic shear forces by reducing the extent of the vessel lumen obstructed by the cell; thereby,

reducing the wall shear stress acting on the cell. Thus, cell deformability influences WBC-endothelium interaction by increasing contact length and decreasing hemodynamic shear forces, hence, influencing the balance of bond and hemodynamic forces in an adherent cell.

It can be seen by the research discussed above that contact area is an important determinant in assessing adhesive strength, yet little attention has been given to this parameter. Schmid-Schönbein *et al.* (1975) estimated contact lengths of adhered cells in venules of the rabbit omentum in order to estimate the shear force on the WBCs due to differing blood hematocrits. Firrell and Lipowsky made measurements of contact length (L_c) as a function of wall shear rate finding that L_c increased in an exponential fashion as wall shear rate increased. Yet, there are no published reports to date examining contact length change over time in an adhered cell.

The aim of this present experimental study was to look specifically at the transients in contact length (L_c) between the WBC and endothelium and acute angle of contact (θ) the WBC forms with the endothelium during spontaneous intermittent adhesion and relate these parameters to bond life time and cell deformability. It was hypothesized that the breaking of the bonds responsible for adhesion in shear flow would follow the kinetic theory of fracture. This relationship served to elucidate the mechanical strength parameters of the adhesion bonds which in turn were used as part of a

theoretical analysis of WBC membrane mechanics assuming force equilibrium between hemodynamic and adhesive forces.

Chapter 2

Experimental Methods and Data Acquisition

2.1 Methods

Female Wistar rats, 100-200 g in weight were anesthetized intraperitoneally with a Nembutal pentobarbital sodium (Abbott Laboratories) injection (35 mg/kg). After a tracheostomy, the left jugular vein and right carotid artery were cannulated with polyethylene tubing (PE-50) for administration of supplemental anesthetic (1/10th of original dose) and monitoring of blood pressure, respectively.

A Century Technology CP-02 Physiologic Pressure Transducer was connected to the rats carotic artery catheter and to a Beckman Instruments Dynograph Recorder R611. Recorder components included TYPE 9853A Voltage/Pulse/Pressure Coupler, preamplifier type 461D, and power amplifier type R-411. Blood pressure was monitored throughout the experiment to assess physiologic state and level of anesthesia.

A midline abdominal incision was made and a section of the distal intestinal mesentery exteriorized. The rat was placed on a plexiglass stage, and the intestine and associated mesentery were draped on a glass slide for

direct observation with transmitted light. Figure 2.1 is a schematic of the experimental set-up. The intestine was handled gingerly to prevent not only tissue damage but peristalsis due to over stimulation. The tissue was continuously suffused with warmed Ringer's gelatin solution (37° C) buffered with sodium bicarbonate and adjusted to a pH of 7.4 with hydrochloric acid. The mesentery was allowed to stabilize for a 20 minute period prior to the start of data acquisition. If an abundance of leukocyte sticking or significant stasis in the microvessels was observed, the mesenteric section was not used.

Venules were observed at high magnification, Zeiss 40/0.75 water-immersion objective (magnification/numerical apperture) and projected by a 79 mm eyepiece onto a silicon diode video camera (DAGE-MTI SIT-66X). The images were then recorded on 1/2 inch VHS videotape (Panasonic Omnivision II VHS Video Cassette Recorder NV-8950) for off-line analysis. A video time code generator (FOR.A Video Timer VTG-33) was used to provide a time reference for off-line analysis. White cell saltation and intermittent adhesion were recorded while focusing upon the lateral edges of post-capillary venules. During each adhesion event, the transient deformations of the WBCs were recorded for subsequent frame by frame analysis.

These observations were repeated for five different protocols: (1) Spontaneous adhesion during a "control" state, (2) adhesion in response to

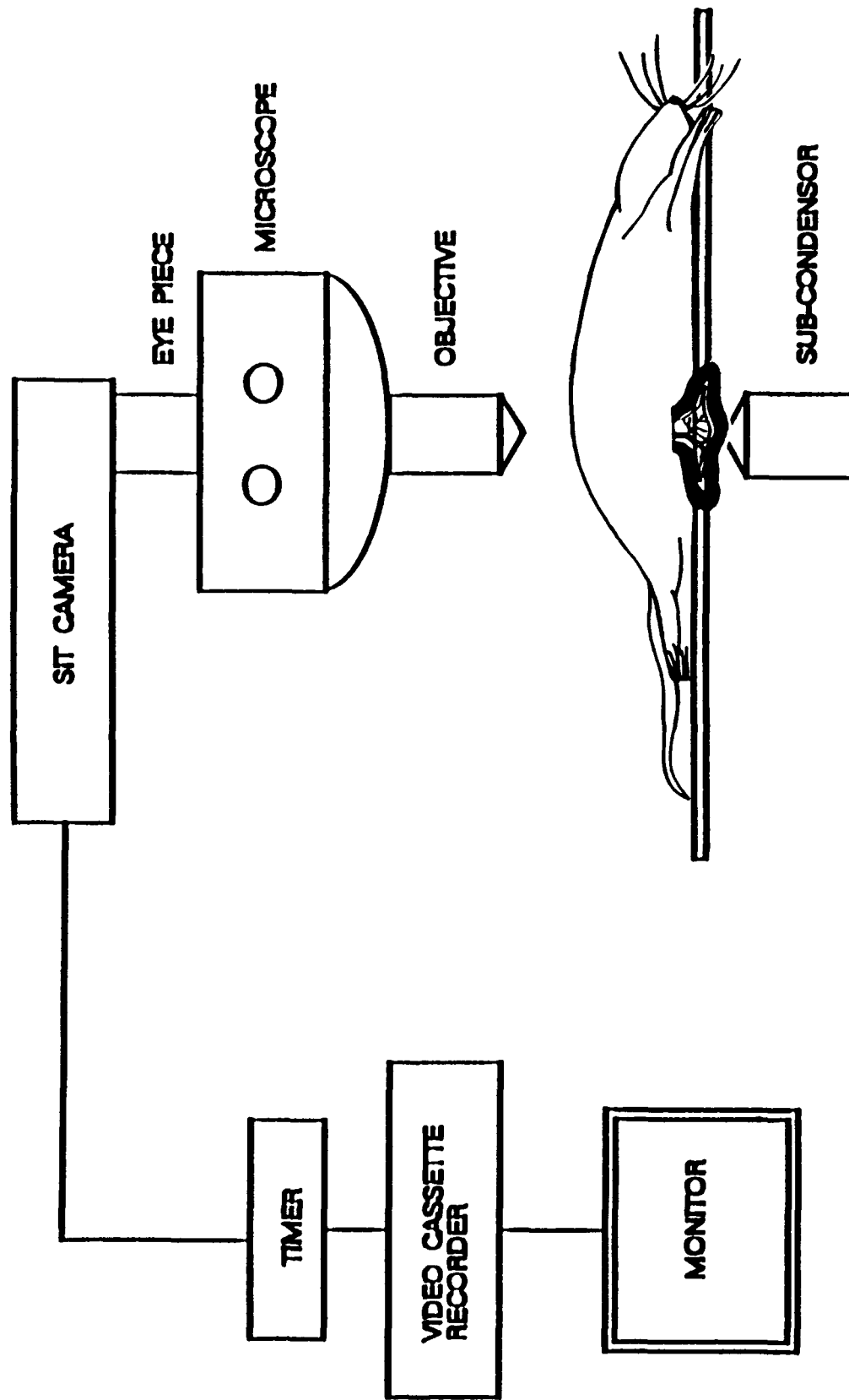


Figure 2.1 Experimental set-up.

topical application of the chemoattractant N-formyl-methionyl-leucyl-phenylalanine (FMLP) at a concentration of 10^{-7} M dissolved in the Ringer's irrigation solution, (3) adhesion in response to stimulation by the cytokine, interleukin- 1β (IL-1), administered to the animal intraperitoneally at 50 U in 1 ml normal saline per hour for two hours prior to mesentery exteriorization, (4) adhesion during suffusion of the tissue with Ringer's solution containing cytochalasin B (CB) at a concentration of $10\text{ }\mu\text{M}$, (5) with the addition of colchicine ($100\mu\text{g/ml}$) to the irrigation solution.

Studies of adhesion in response to FMLP and IL-1 were performed in light of the two different modes of adhesion stimulated by those agents. FMLP is a chemotactic peptide that directly activates the WBC, and has been shown to significantly decrease WBC deformability at concentrations of 10^{-7} M (Kawaoka *et al.*, 1981; House and Lipowsky, 1991; and Lipowsky *et al.*, 1991). IL-1 is a major cytokine that induces expression of adhesion molecules on the endothelium with little effect on WBC adhesion molecules. Resting endothelium typically lacks the molecules to support adhesion; however, upon addition of a cytokine there is an increase in the expression of three known adhesion molecules; intercellular adhesion molecule-1 (ICAM-1), vascular cell adhesion molecule-1 (VCAM-1), and endothelial leukocyte adhesion molecule (ELAM-1) (Vedas *et al.*, 1992). The deformation properties of the WBC in response to adhesion due to IL-1 endothelial

stimulation have been shown to decrease; however, not statistically different from that of control (Lipowsky *et al.*, 1991).

Cytochalasin (CB) and colchicine have both been shown to increase WBC deformability (Lipowsky *et al.*, 1991). Cytochalasin B is one of a broad family of cytochalasins and is a naturally occurring organic molecule that binds to actin and inhibits its polymerization. It permeates the cell membrane and causes the inhibition of polymerization and depolymerization; therefore, the cell becomes more flaccid (Cooper, 1987). Colchicine is an anti-mitotic agent commonly used in the treatment of inflammatory disorders; such as, rheumatoid arthritis. It has been proposed that colchicine attenuates the inflammation process by disrupting the microtubules, which are a major structural component of the WBC, thereby, decreasing cell stiffness. Increased WBC deformability in response to colchicine has been confirmed *in vivo* (Lipowsky *et al.*, 1991 and Asako *et al.*, 1992).

2.2 Data Analysis

After completion of the experiments, the video tape recordings were analyzed off-line. It should be noted at this point that several video recordings were used from previous experiments which utilized the same protocol. The recordings were not previously analyzed for the information desired in this present study. Use of these recordings was by permission of

the principal investigator of the 1988 study, Dr. H. H. Lipowsky. The combination of current and past experimental data served to provide a larger pool of data and reduce the number of animals required to complete this study.

Intermittently adherent cells in the venules, with durations of adhesion which lasted for at least 2.5 seconds, but not permanently, were identified. Venule diameters was assessed by the video image shearing technique, using an IPM (Instrumentation for Physiology and Medicine, Inc) Image Shearing Monitor model 908. Measurements of centerline red cell velocity (V_{rbc}) were made using video two-slit photometric technique. Using a photoanalyzer (IPM Video Photoanalyzer model 204), two photodetectors were aligned along the venule of interest at a spacing ranging from 30 to 60 μ ms. The output of the photoanalyzer was coupled to an on-line self-tracking correlator (IPM Velocity Tracker Model 102b). The signals from the photodetectors were cross-correlated to determine the time shift. The spacing between the detectors was then divided by the time shift to yield the V_{rbc} .

Estimates of mean blood velocity (V_{mean}) were then determined using the empirical relationship peculiar to the two-slit method (Lipowsky and Zweifach, 1978).

$$V_{mean} = V_{rbc} / 1.6 \quad . \quad (2.1)$$

The wall shear rate ($\dot{\gamma}$) was then estimated as the Newtonian value,

$$\dot{\gamma} = 8 V_{mean} / D \quad (2.2)$$

where D denotes vessel diameter. Wall shear stress (τ_w) was calculated as the product of the wall shear rate and blood viscosity (an average value of blood viscosity of 0.025 Poise was assumed).

Images of WBC deformation and membrane peeling were analyzed to measure transient changes in white blood cell-endothelium (WBC-EC) contact length (L_c) and the acute angle of contact (θ) over the entire time the cell remained adherent. Figure 2.2 depicts both the length and angle of interest. The images were digitized in successive frames by an image sampling program, IMP.EXE, originally written by Michael Kent in Turbo-C. The program allowed the user to sample up to sixteen consecutive frames at a rate specified by the user, identify a 128 by 128 pixel region of interest (ROI) from each frame, and create a montage of the 16 ROIs in time sequence order. For each cell, a minimum of sixteen frames were digitized over the duration of the cell adhesion with more frames being "grabbed" as required to adequately analyze the transient changes in L_c and θ .

The next step in the data analysis was to measure the WBC-EC contact length with the measurement capability of the sampling program.

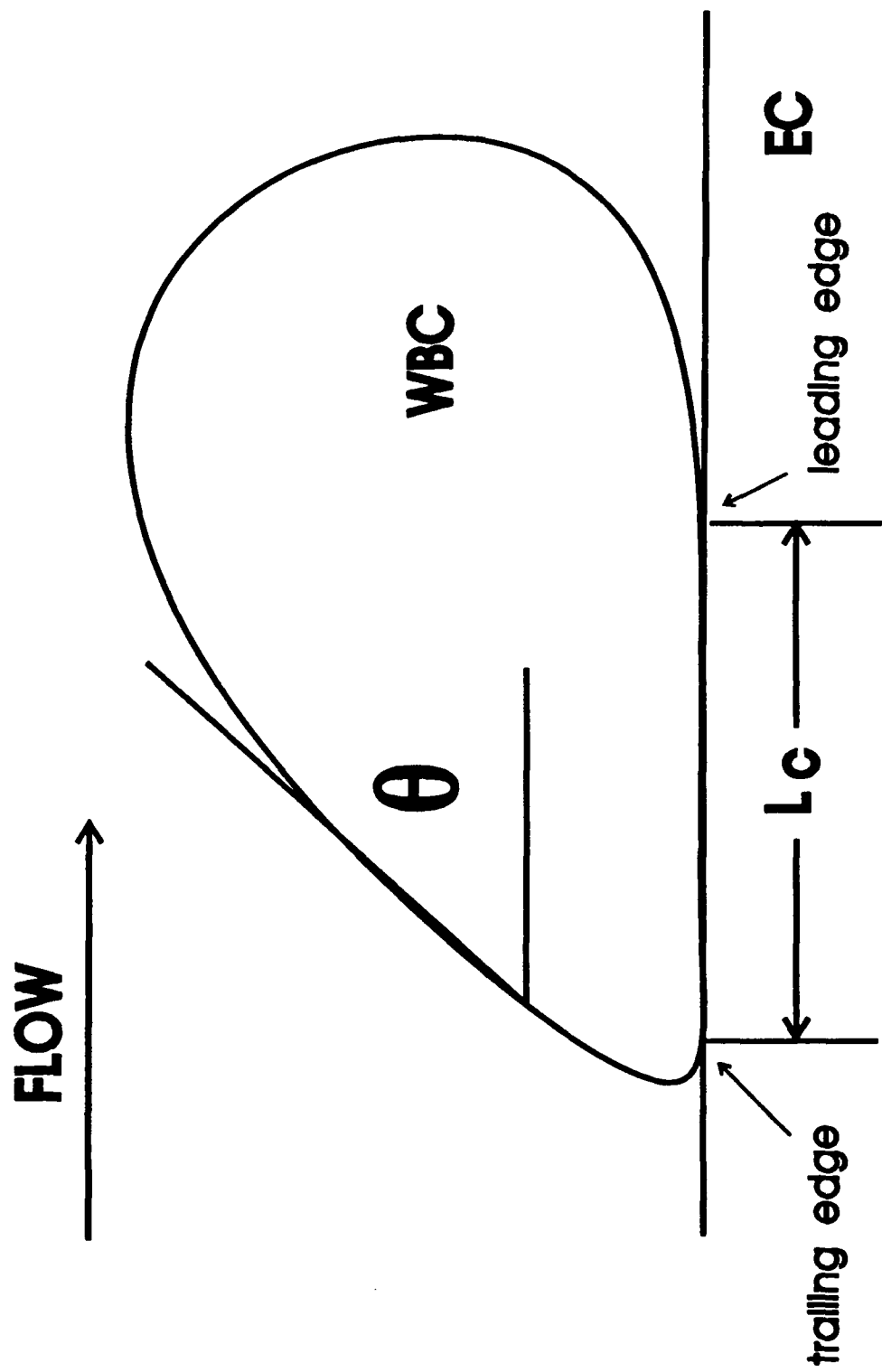


Figure 2.2 Schematic of adherent WBC. θ is the contact angle between the WBC and EC. L_c represents the contact length.

However, the digitization process created a distortion in the projected image where the number of pixels per micron differed in the horizontal and vertical directions. Therefore, the program was first modified to allow for separate horizontal and vertical calibrations, thereby, increasing the accuracy of the contact length measurements. The separate calibration factors were incorporated into the length calculation with the following equation:

$$\text{segment length} = \sqrt{(HCAL \cdot HLEN)^2 + (VCAL \cdot VLEN)^2} \quad (2.3)$$

where HCAL is the horizontal calibration factor ($\mu\text{m}/\text{pixel}$), HLEN (pixels) is the horizontal length measurement, VCAL is the vertical calibration factor ($\mu\text{m}/\text{pixel}$), and VLEN (pixels) is the vertical length measurement. At the magnification used in the present experiments, the width of the entire video field was approximately $114 \mu\text{m}$. Scale calibration factors averaged $0.2278 \mu\text{m}/\text{pixel}$ for HCAL and $0.1553 \mu\text{m}/\text{pixel}$ for VCAL. The program was also enhanced to allow the automatic storage of length, width, and time measurements for each cell in an ASCII file that could be read directly into a statistical program.

The contact angle, θ , was measured by making a thermal print of the image file and judging the angle of the WBC membrane by eye. The angle was measured the old fashion way, with a protractor. The information was then typed into an analysis program.

2.3 Statistical Analysis

Measurements of L_c and θ were input to Sigma Plot scientific graphing system for preliminary analysis and graph generation. The data was further analyzed using the statistical software Minitab Release 7.1.

Chapter 3

Experimental and Analytical Results

To assess the relationship between membrane WBC mechanics and the formation and disruption of WBC-EC bonds, transients in contact area and WBC shape were made during spontaneous adhesion. Tables of the hemodynamic data for each WBC are provided in Appendix A while, the experimental analysis for each cell is listed in Appendix B.

3.1 Formation and Disruption of WBC-EC Bonds

The hemodynamic environment experienced by each cell of interest was very important in assessing the adhesive force required to keep the WBC adherent to the EC. Therefore, the wall shear rate and wall shear stress were calculated as described in Chapter 2 for each cell of interest. Table 3.1 lists the mean values and standard deviations of the experimental hemodynamic conditions for control, FMLP, IL-1, CB, and colchicine treatments. Venule diameters ranged from 16.2 to 43.3 μm . The mean τ_w was greatest for FMLP and least for colchicine; indicating the WBC adhesive strength was greatest for the FMLP treatment and least for colchicine.

Table 3.1

Hemodynamic parameters

Treatment	Vessel Diameter Range (μm)	Mean Vessel Diameter (μm)	V_{rec} (mm/sec)	Shear Rate (1/sec)	τ_w (dyne/cm ²)
Control n = 18	16.20 - 43.30	26.40 \pm 9.57 SD	1.50 \pm 0.76 SD	285.35 \pm 88.67 SD	7.13 \pm 2.22 SD
FMLP n = 13	22.00 - 39.00	27.69 \pm 5.23 SD	2.43 \pm 0.48 SD	465.95 \pm 165.52 SD	11.65 \pm 4.14 SD
IL-1 n = 12	18.0 - 31.9	26.45 \pm 4.81 SD	1.57 \pm 0.63 SD	297.26 \pm 100.43 SD	7.43 \pm 2.51 SD
CB n = 13	20.60 - 26.00	23.93 \pm 1.72 SD	1.66 \pm 0.36 SD	347.47 \pm 70.02 SD	8.69 \pm 1.75 SD
Colchicine n = 11	25.20 - 41.20	34.30 \pm 6.73 SD	1.17 \pm 0.21 SD	179.12 \pm 53.50 SD	4.48 \pm 1.34 SD

• Values shown are mean \pm standard deviation (SD)

Typical examples of WBC-EC contact length (L_c) versus time for each treatment are shown in Figure 3.1 (a), (b), and (c) for control, FMLP, and IL-1 conditions, respectively. Figure 3.2 (a) and (b) depict representative examples of L_c versus time for treatments with CB and colchicine, respectively. Since the fluid shear stress was not controlled during the experiments, the representative curves are at differing wall shear stresses. During the initial adhesion, L_c steadily increased with time as new bonds were formed at the leading edge, and L_c subsequently decreased with time as the trailing edge of the WBC membrane peeled away from the EC during initiation of a rolling movement of the WBC. Linear regressions through both the periods of increasing and decreasing L_c enabled identification of the maximum L_c . This point was considered to represent the equilibrium between bond formation and disruption, as the WBC began to roll and the corresponding time was denoted as the time to peeling, t_p .

Table 3.2 lists the regression parameters and correlation or r-value for each regression depicted in Figures 3.1 and 3.2. In general all treatments, excluding FMLP, exhibited a greater rate of decrease in L_c than increase which can be interpreted as the bonds were broken faster than they were formed. Figure 3.3 is a comparison of L_c versus time for control, FMLP, and IL-1 and corresponding t_p . As demonstrated in the figure, the FMLP treated cells remained adhered to the endothelium significantly longer than all others. The time to peeling is also much greater for FMLP than control or IL-1.

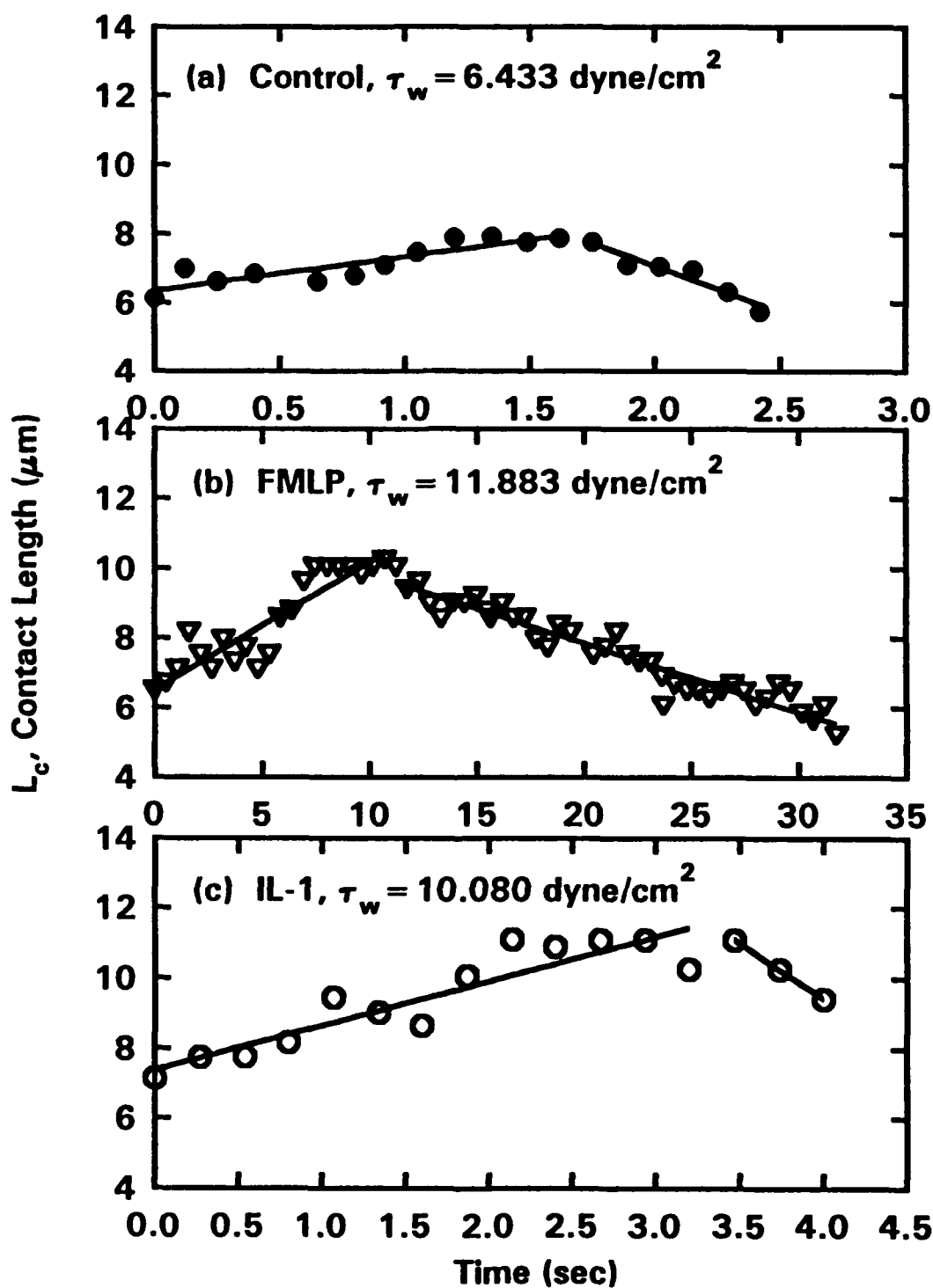


Figure 3.1 Representative trends of contact length versus time for WBCs under (a) control conditions and (b) FMLP and (c) IL-1 stimulated adhesion.

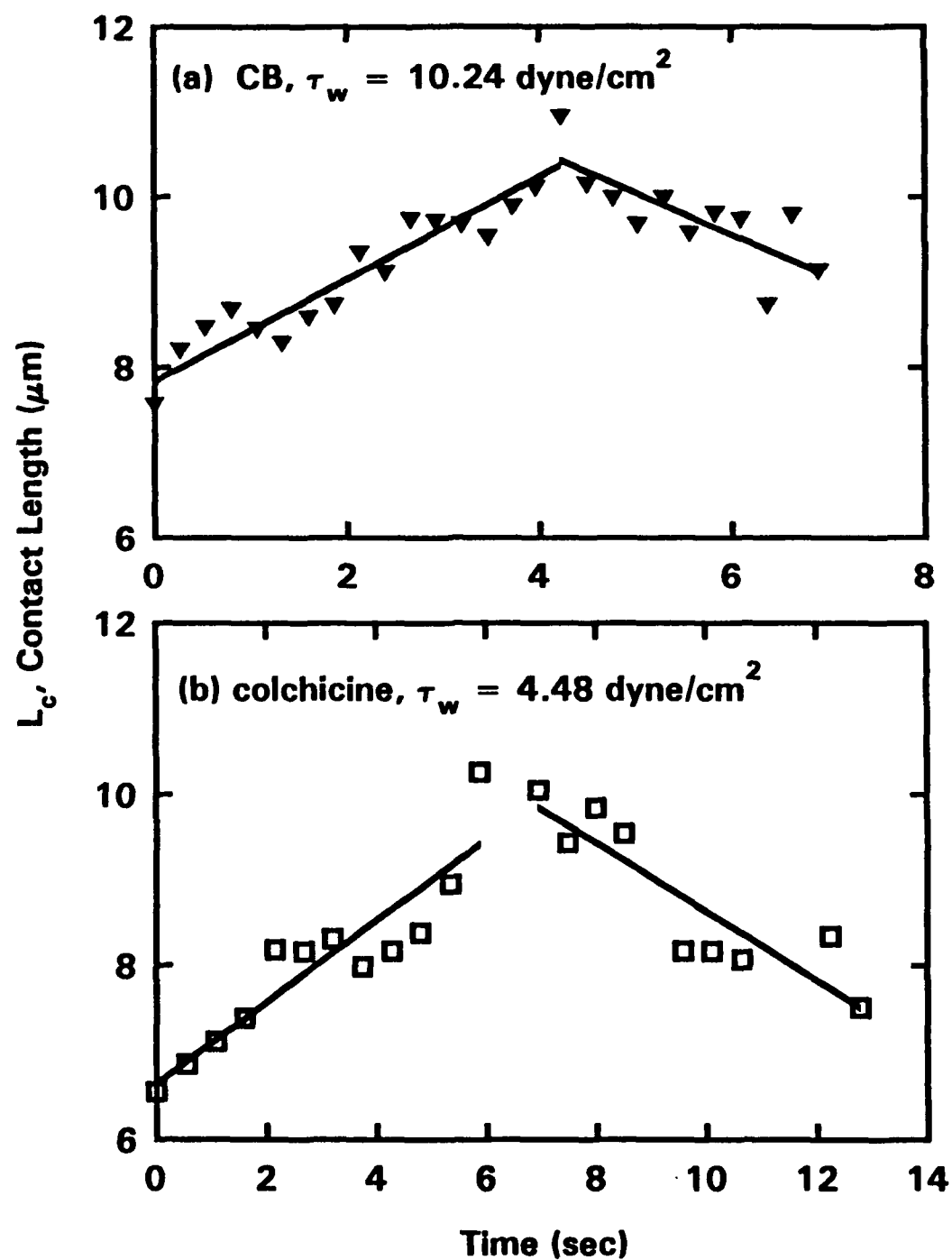


Figure 3.2 Representative trends of contact length versus time for WBCs with (a) CB and (b) colchicine treatment.

Table 3.2

 L_c vs. time regression parameters

$$L_c = \beta_0 + \beta_1 t$$

Treatment	Increasing $L_c(t)$			Decreasing $L_c(t)$		
	β_0	β_1	r	β_0	β_1	r
Control	6.355	0.986	0.89	12.445	-2.694	0.96
FMLP	6.534	0.366	0.92	11.799	-0.198	0.96
IL-1	7.391	1.263	0.91	22.026	-3.151	0.99
CB	7.836	0.599	0.94	12.480	-0.488	0.77
colchicine	6.646	0.470	0.91	12.621	-0.399	0.89

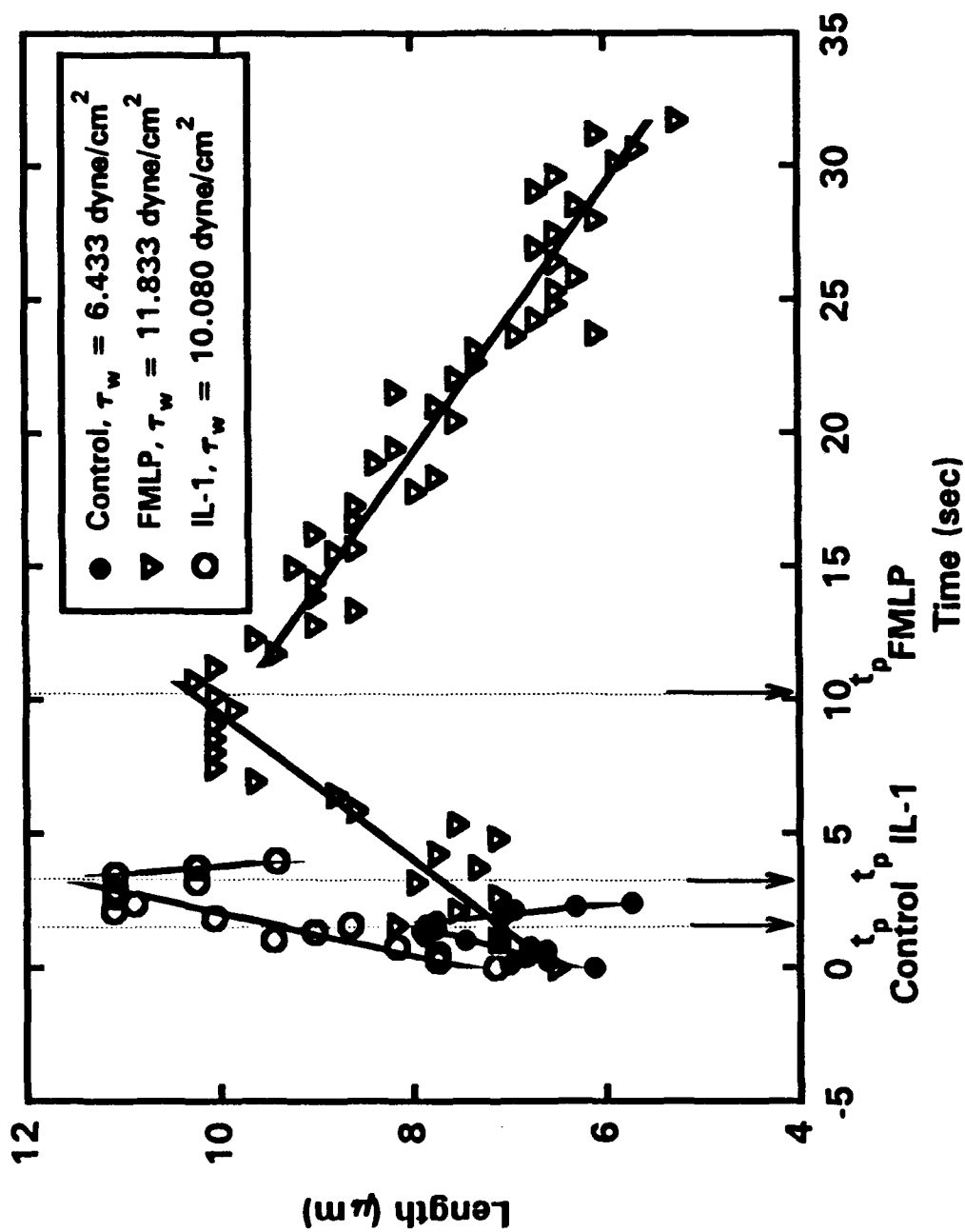


Figure 3.3 Comparison plot of L_o versus time for control, FMLP, and IL-1, and the determination of time to peeling (t_p). FMLP stimulated adhesion was sustained for a greater period of time and correspondingly had a greater t_p .

Table 3.3 lists the mean and standard deviation of τ_w , t_p , L_c at t_p , and total time the cell remained adherent to the endothelium (t_{tot}) for all five conditions. As previously noted, τ_w , t_p and t_{tot} are greatest for the FMLP treated cells, thereby, indicating a strong bond adhesive force.

Figures 3.4 and 3.5 show t_p versus τ_w for all treatments on a semi-log scale. The regression of $\ln(t_p)$ and τ_w was statistically significant for control, FMLP, and IL-1 for $p < 0.01$. The regressions for CB and colchicine were not statistically significant ($p > 0.05$) due to limited range of data. Parameters, t-ratios, p-values, and r-value are listed in Table 3.4 for each regression.

Figure 3.6 is a composite of all three significant regressions; control, FMLP, and IL-1. The slopes for each of the treatments were not significantly different from one another; while, the intercept for the FMLP treatment was significantly greater than either the control or IL-1 ($p < 0.05$). The logarithmic relationship between t_p and τ_w , suggested a mode of peeling consistent with the kinetic theory of fracture (Zhurkov, 1965).

3.1.1 Kinetic Theory of Fracture

Zhurkov's theory considered the fracture of solids as a time process whose rate is determined by mechanical stress and temperature. A universal rate relation was suggested as follows:

Table 3.3
Experimental time to peeling and contact length measurements

Treatment	τ_w (dyne/cm ²)	t_p (sec)	L_c at t_p (μ m)	t_{tot} (sec)
Control n = 18	7.13 \pm 2.22 SD	3.44 \pm 1.50 SD	8.41 \pm 1.58 SD	5.04 \pm 2.21 SD
FMLP n = 13	11.65 \pm 4.14 SD	9.44 \pm 5.45 SD	8.82 \pm 2.26 SD	26.07 \pm 9.04 SD
IL-1 n = 12	7.43 \pm 2.51 SD	4.87 \pm 1.93 SD	10.22 \pm 1.82 SD	5.71 \pm 1.93 SD
CB n = 13	8.69 \pm 1.75 SD	4.73 \pm 1.73 SD	11.39 \pm 2.24 SD	8.04 \pm 3.18 SD
Colchicine n = 11	4.48 \pm 1.34 SD	7.08 \pm 3.03 SD	10.94 \pm 1.84 SD	10.53 \pm 7.46 SD

* Values shown are means \pm standard deviations (SD).

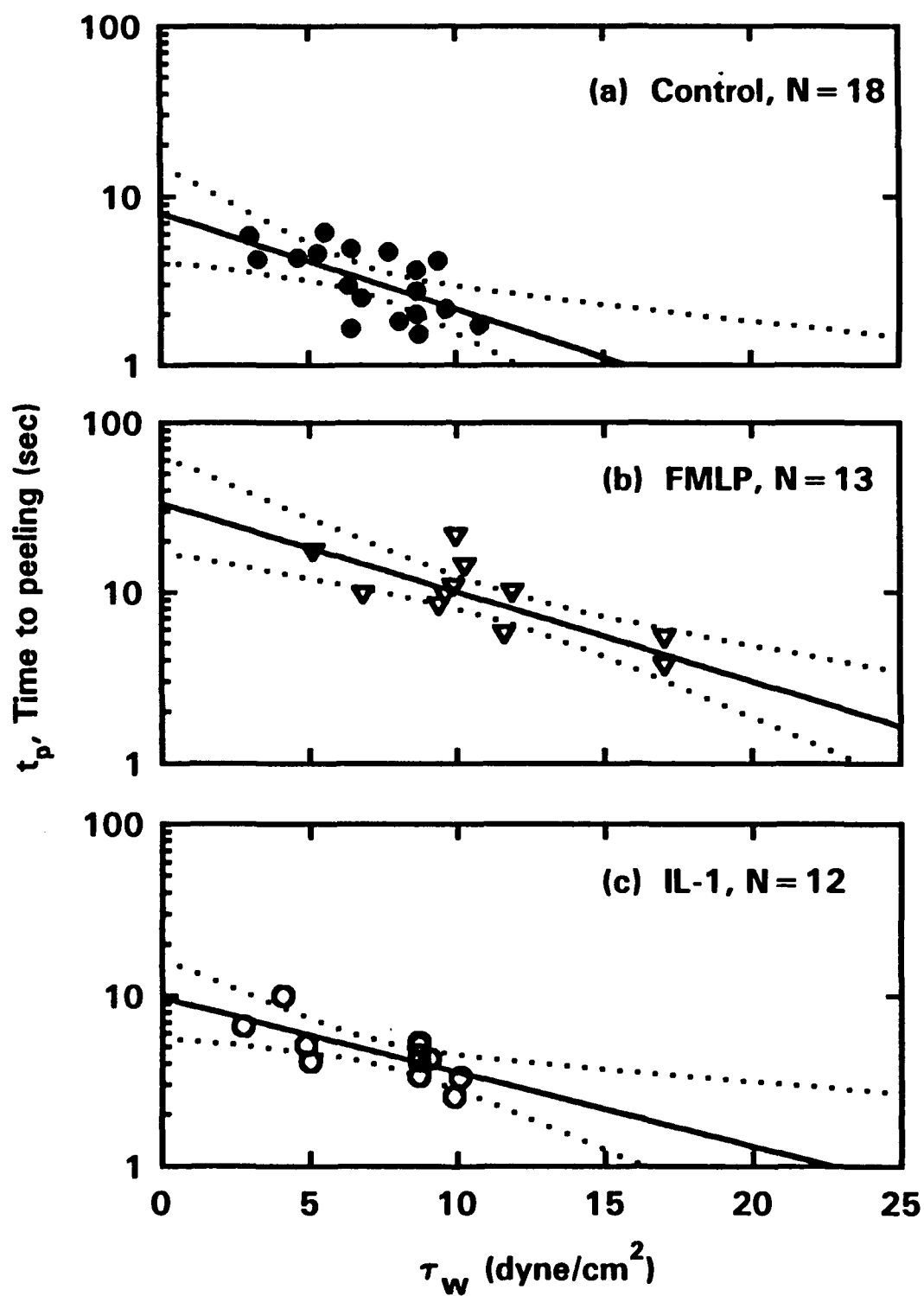


Figure 3.4 Time to peeling versus wall shear stress for (a) control conditions and (b) FMLP and (c) IL-1 stimulated adhesion. All regressions were statistically significant for $p < 0.01$.

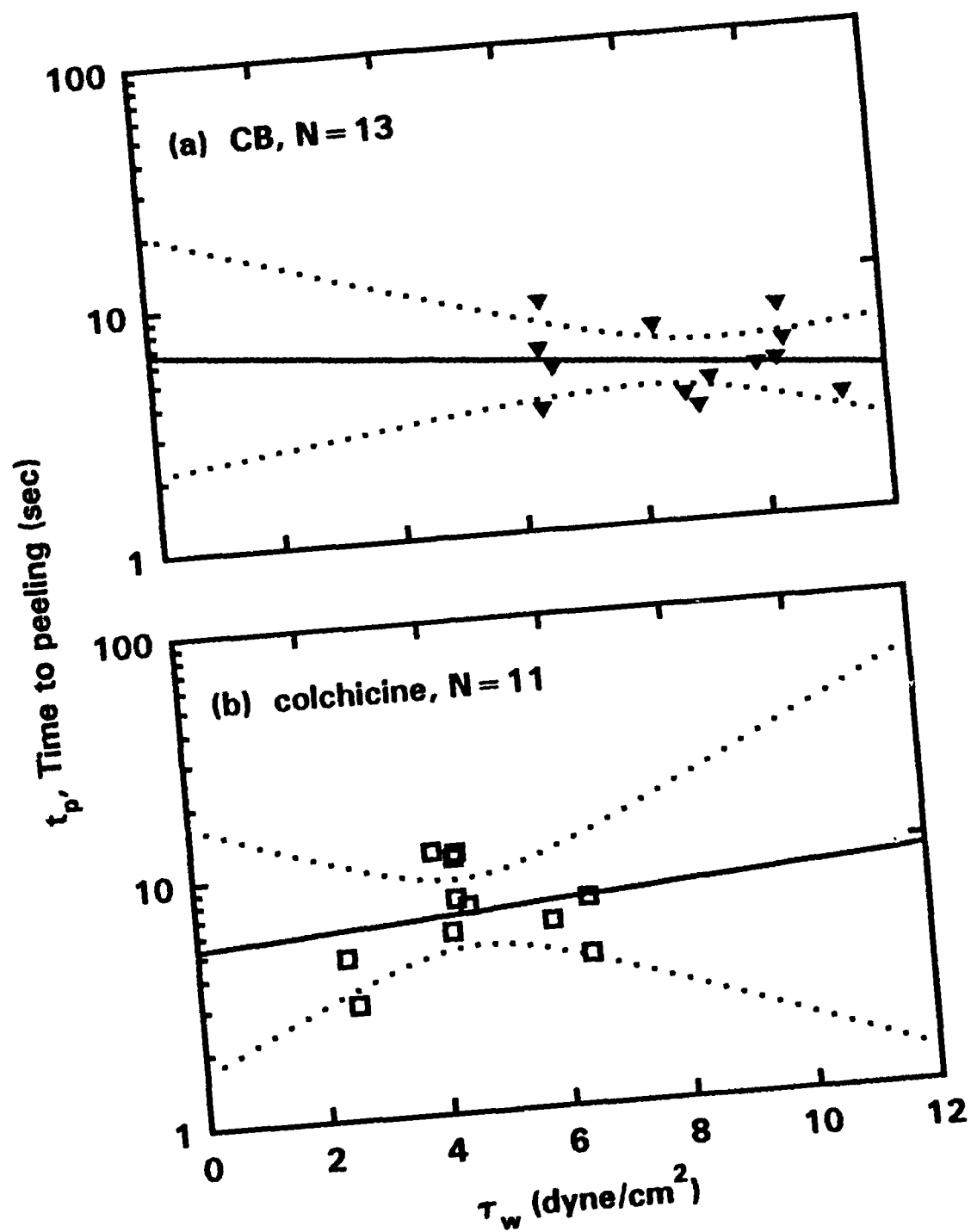


Figure 3.5 Time to peeling versus wall shear stress for (a) CB and (b) colchicine treatment. The regression of $\ln(t_p)$ versus τ_w was not statistically significant for either treatment ($p > 0.05$).

Table 3.4

Regression parameters and statistics for $\ln(t_p)$ versus τ_w

$$\ln(t_p) = \beta_0 + \beta_1 \tau_w$$

Treatment	β_0 parameter	β_0 t-ratio	β_0 p-value	β_1 parameter	β_1 t-ratio	β_1 p-value	r
Control	2.07	6.69	0.0001	-0.131	-3.15	0.006	0.62
FMLP	3.50	11.75	0.0001	-0.120	-4.99	0.0001	0.83
IL-1	2.27	9.43	0.0001	-0.100	-3.26	0.009	0.72
CB	1.89	3.69	0.004	-0.046	-0.79	0.447	0.23
Colchicine	1.67	3.26	0.010	0.044	0.400	0.697	0.13

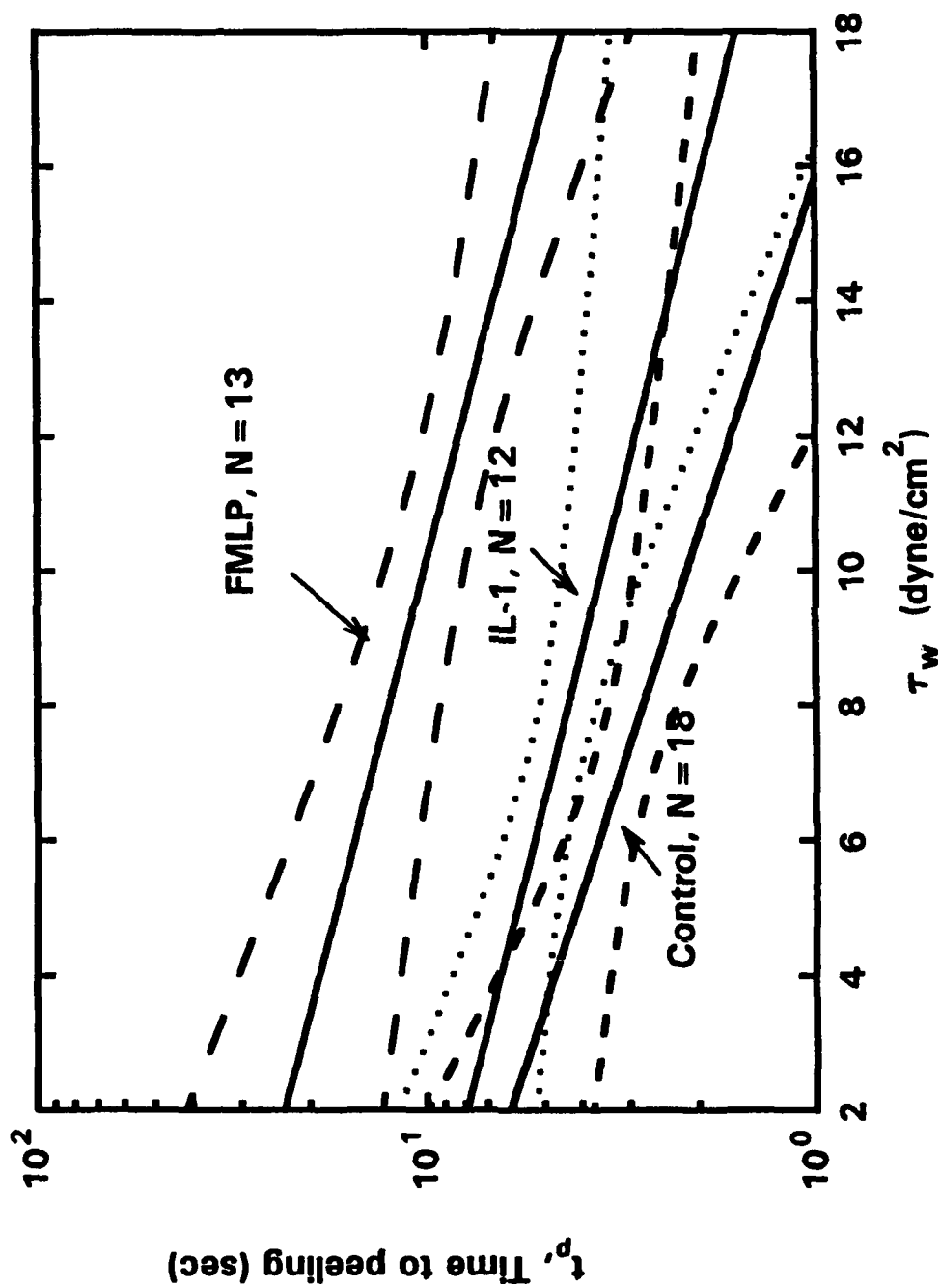


Figure 3.6 Comparison of linear regressions of t_p versus τ_w for control conditions and FMLP and IL-1 stimulated adhesion. While the slopes of the regressions were not statistically different, the intercept of FMLP were statistically different from both control and IL-1.

$$\tau = \tau_o \exp\left[\frac{(U_o - \gamma\sigma)}{kT}\right] \quad (3.1)$$

where τ is the lifetime of a bond under load, σ is the load tensile stress, T is the absolute temperature, k is Boltzman's constant and τ_o , U_o , and γ are constant coefficients which represent material constants of the solid. For the case of constant temperature, as in the case of the present study, equation (3.1) can be rewritten as:

$$\ln(\tau) = [\ln(\tau_o) + \frac{U_o}{kT}] - \frac{\gamma\sigma}{kT} \quad (3.2)$$

τ_o is the reciprocal of the natural frequency of oscillation of atoms in a solid. Zhurkov reported τ_o to be in the order of magnitude of 10^{-13} seconds for all solids, independent of structure and chemical nature. Using the kinetic theory of strength of solids, Bell (1978) calculated this parameter to be 10^{-8} seconds for receptor-ligand bonds. U_o can be interpreted as the magnitude of the energy barrier which determines the probability of bond breakage. γ , represents an empirical parameter that accounts for the structure of the solid and its imperfections.

The logarithmic regression of t_p versus τ_w ,

$$\ln(t_p) = \beta_0 + \beta_1 \tau_w \quad (3.3)$$

can be related to equation (3.2). Therefore, t_p is equivalent to Zhurkov's τ , β_0 is equivalent to:

$$\beta_0 = \ln(\tau_0) + \frac{U_0}{kT} \quad (3.4)$$

and β_1 is equivalent to:

$$\beta_1 = \frac{C\gamma}{kT} \quad (3.5)$$

C is a constant relating the fluid shear stress to the normal tensile stress acting on the receptor-ligand bonds. C can be solved through the balance of moment if the normal stress distribution on the adherent membrane is known or assumed. Using the parameters listed in Table 3.4, Boltzman's constant = 1.38×10^{-23} J/K, and $T = 310$ K, the parameter U_0 representing the strength of the bond responsible for adhesion was obtained for each of the three treatments with significant $\ln(t_p)$ versus τ_w regressions; control, FMLP, and IL-1. Bell (1978) interpreted the kinetic theory of fracture, such that, at τ equal to τ_0 , U_0 equalled the product of the maximum

force per bond (f_o) and the maximum stretch per bond (r_o). Therefore,

$$U_o = f_o \cdot r_o \quad (3.6)$$

Using the values of U_o calculated above and $r_o = 0.5 \times 10^{-7}$ cm, f_o for control, FMLP, IL-1, CB, and colchicine was calculated. Table 3.5 lists the calculated mean values for each of the three treatments, as well as, the standard deviations. Figure 3.7 compares the values graphically. The values of both U_o and f_o were statistically significantly greater for FMLP than for either IL-1 or control. However, the increase in U_o and f_o was only

Table 3.5
Adhesion energy and force per bond

Treatment	U_o (dyne-cm)	f_o (dyne/bond)
Control n = 18	$8.192 \times 10^{-13} \pm$ 0.060×10^{-13} SD	$1.638 \times 10^{-5} \pm$ 0.012×10^{-5} SD
FMLP n = 13	$8.417 \times 10^{-13} \pm$ 0.035×10^{-13} SD	$1.683 \times 10^{-5} \pm$ 0.007×10^{-5} SD
IL-1 n = 12	$8.231 \times 10^{-13} \pm$ 0.043×10^{-13} SD	$1.646 \times 10^{-5} \pm$ 0.009×10^{-5} SD
CB n = 13	$8.154 \times 10^{-13} \pm$ 0.102×10^{-13} SD	$1.631 \times 10^{-5} \pm$ 0.020×10^{-5} SD
Colchicine n = 11	$8.100 \times 10^{-13} \pm$ 0.115×10^{-13} SD	$1.620 \times 10^{-5} \pm$ 0.023×10^{-5} SD

* Values shown are mean \pm standard deviation (SD).

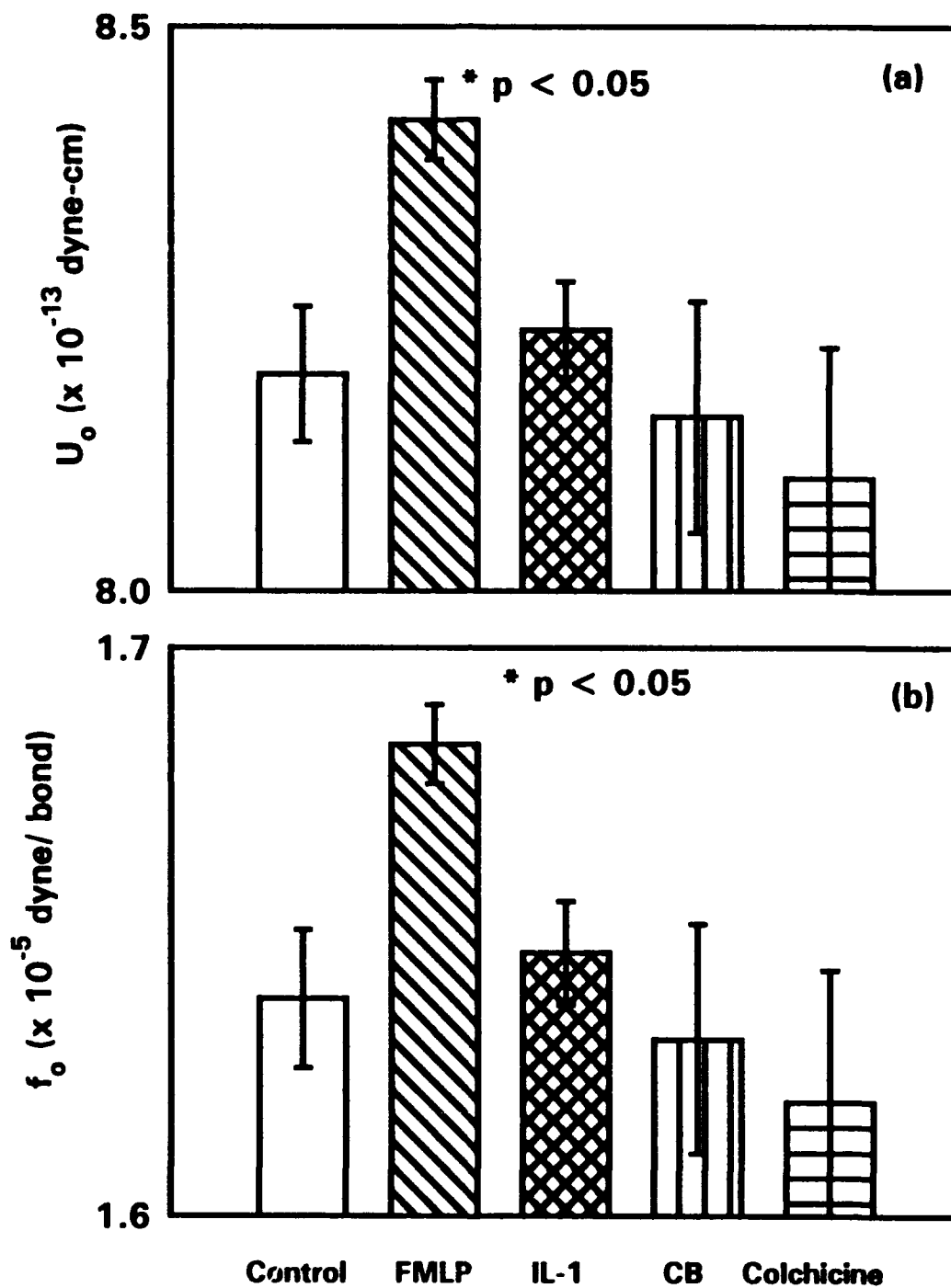


Figure 3.7 (a) Adhesion energy and (b) bond force for control, FMLP, IL-1, CB, and colchicine treatment. U_o and f_o were significantly greater for FMLP than all others. Values shown are means \pm standard deviations.

3% greater for FMLP versus control or IL-1. The difference in magnitude was not significant enough to conclude whether adhesion through FMLP stimulation occurred due to a different bond or bonding mechanism. However, the similarity of U_0 and f_0 for control and IL-1 stimulated adhesion did indicate that these two conditions induced WBC adhesion through similar mechanisms. U_0 and f_0 were significantly less for CB and colchicine as compared to the other three conditions. The decrease in bond energy and bond strength may be due to the WBC and EC cytoskeletal deterioration caused by the two treatments. In all cases, U_0 and f_0 are comparable to values calculated by Bell (1977) using kinetic theory.

The force per bond, f_0 , as well as, the mean hemodynamic values for each of the treatments were incorporated into a mechanical analysis of the force equilibrium required to keep a WBC adherent to the EC. Thereby, the minimum bond density was elucidated for control conditions and FMLP and IL-1 stimulated adhesion. Such an analysis is addressed in Chapter 4.

3.2 WBC Membrane Mechanics

As a measure of the mechanical properties of the WBC membrane, the contact length and angle of contact between the WBC and EC were studied versus τ_w .

L_c was calculated at t_p for each cell using the linear regressions employed earlier to determine t_p . The contact length at t_p ($L_{c, tp}$) was then plotted against the corresponding wall shear stress. Figure 3.8 and 3.9 depict $L_{c, tp}$ versus τ_w , the associated first order linear regressions, and 95% confidence intervals. The parameters, t-ratios, p-values, and correlation are listed in Table 3.6 for each treatment. Although none of the regressions were statistically significant, the general trends could be loosely interpreted. Under control conditions, $L_{c, tp}$ increased with τ_w indicating that the cells were easily deformable. With FMLP stimulated adhesion, there was the opposite trend which was interpreted as the cells that adhered at higher shear stresses were less deformable due to activation and subsequent polymerization of the f-actin. The WBCs under IL-1 stimulated adhesion showed a trend similar to that of control. $L_{c, tp}$ increased with τ_w for both CB and colchicine. This was expected since both of these treatments have been shown to increase cell deformability. The rate of increase was almost four times greater for colchicine than CB. Statistical insignificance of all of these regressions was probably due to the limited range of data.

The contact angle between WBC and EC was measured for all five conditions. Figure 3.10 shows representative trends of contact angle, θ , versus time for control, FMLP, and IL-1. Figure 3.11 shows representative trends for CB and colchicine. All conditions except FMLP stimulated

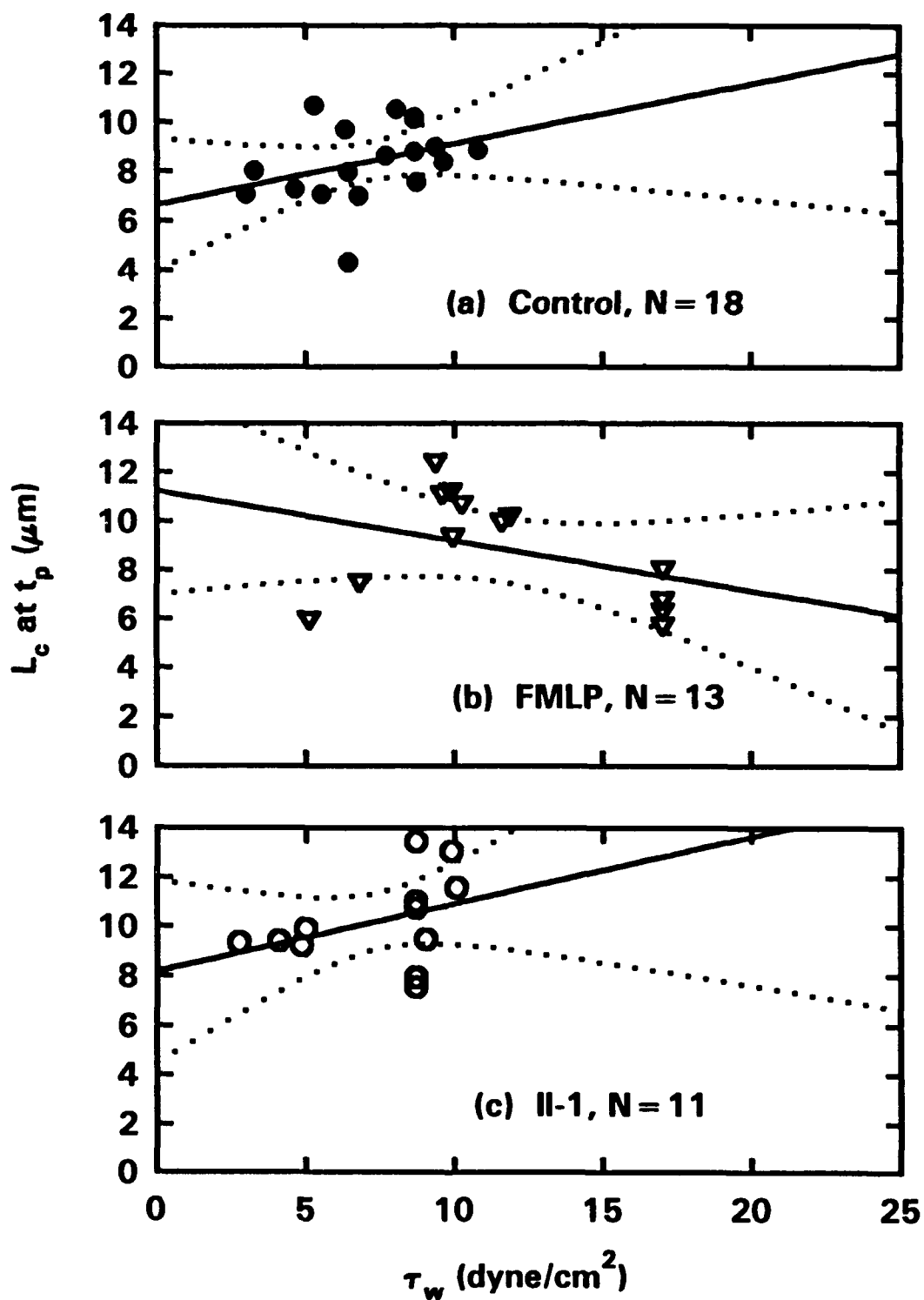


Figure 3.8 Contact length at t_p versus wall shear stress for (a) control conditions and (b) FMLP and (c) IL-1 stimulated adhesion. Regressions were not statistically significant ($p > 0.05$).

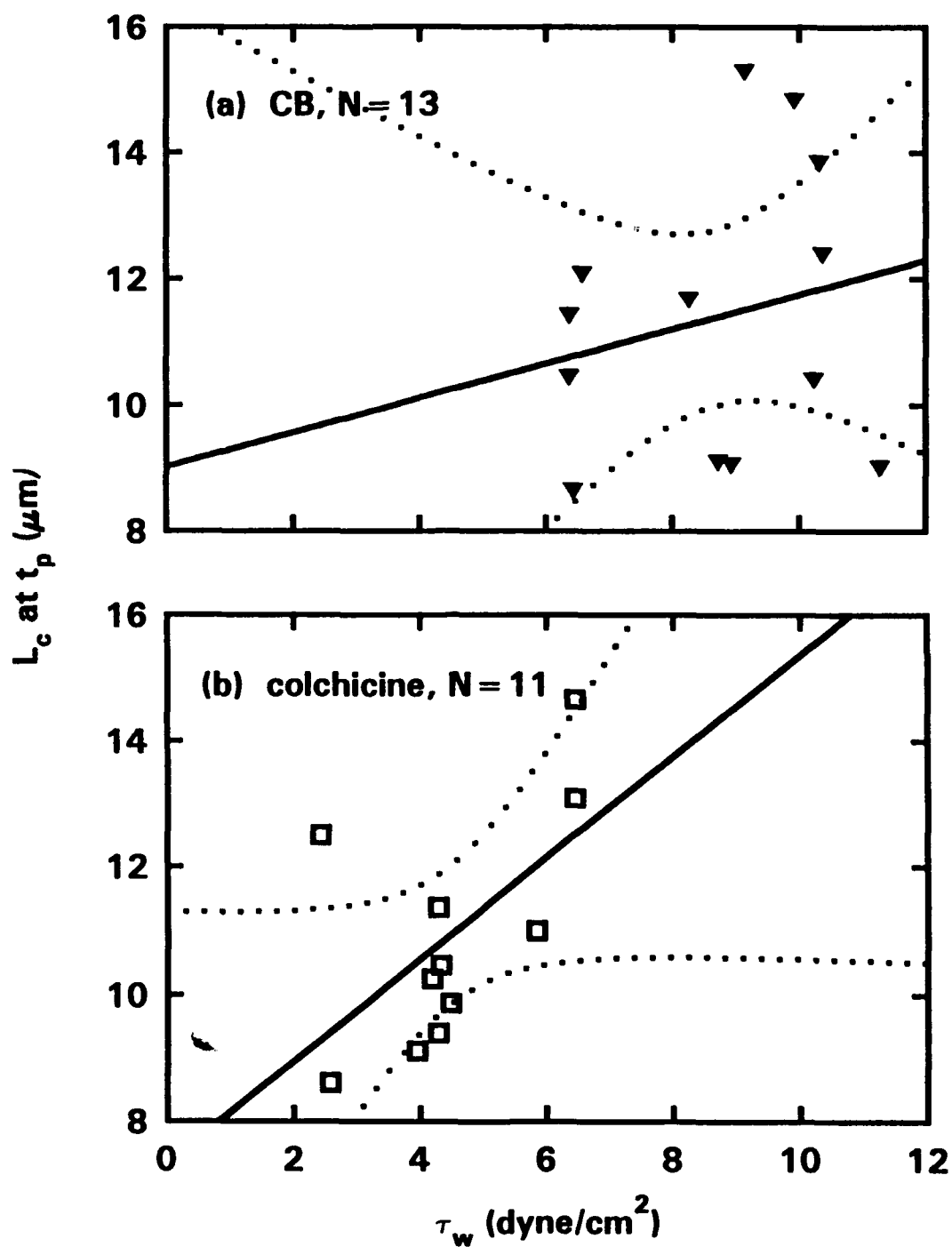


Figure 3.9 Contact length at t_p versus wall shear stress for (a) CB and (b) colchicine treatments. Regressions were not statistically significant ($p > 0.05$).

Table 3.6

Regression parameters and statistics for L_c at t_p versus τ_w

$$L_c \text{ at } t_p = \beta_0 + \beta_1 \tau_w$$

Treatment	τ_w (dyne/cm ²)	L_c at t_p (μ m)	β_0 parameter	β_0 t-ratio	β_0 p-value	β_1 parameter	β_1 t-ratio	β_1 p-value	r
Control n = 18	7.13 \pm 2.22 SD	8.41 \pm 1.58 SD	6.66	5.26	0.0001	0.246	1.45	0.167	0.34
FMLP n = 13	11.65 \pm 4.14 SD	8.82 \pm 2.26 SD	11.22	5.84	0.0001	-0.204	-1.31	0.215	0.37
IL-1 n = 12	7.43 \pm 2.51 SD	10.22 \pm 1.82 SD	8.19	4.93	0.0001	0.274	1.29	0.227	0.38
CB n = 13	8.69 \pm 1.75 SD	11.39 \pm 2.24 SD	9.02	2.70	0.021	0.273	0.72	0.484	0.21
Colchicine n = 11	4.48 \pm 1.34 SD	10.94 \pm 1.84 SD	7.35	4.22	0.002	0.801	2.14	0.061	0.13

• Values shown for τ_w and L_c at t_p are means \pm standard deviations (SD).

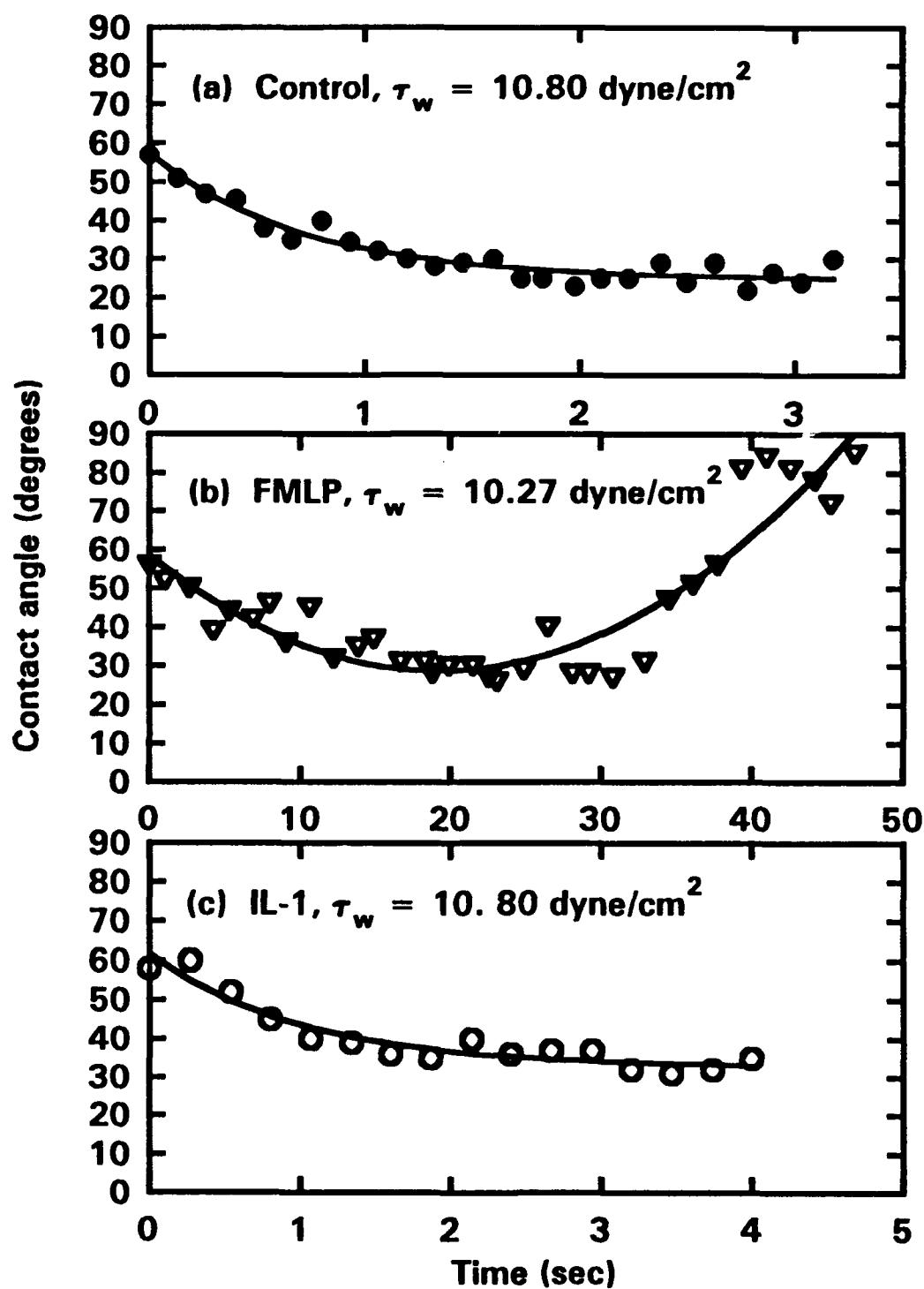


Figure 3.10 Representative trends of contact angle versus time for WBCs under (a) control conditions and (b) FMLP and (c) IL-1 stimulated adhesion.

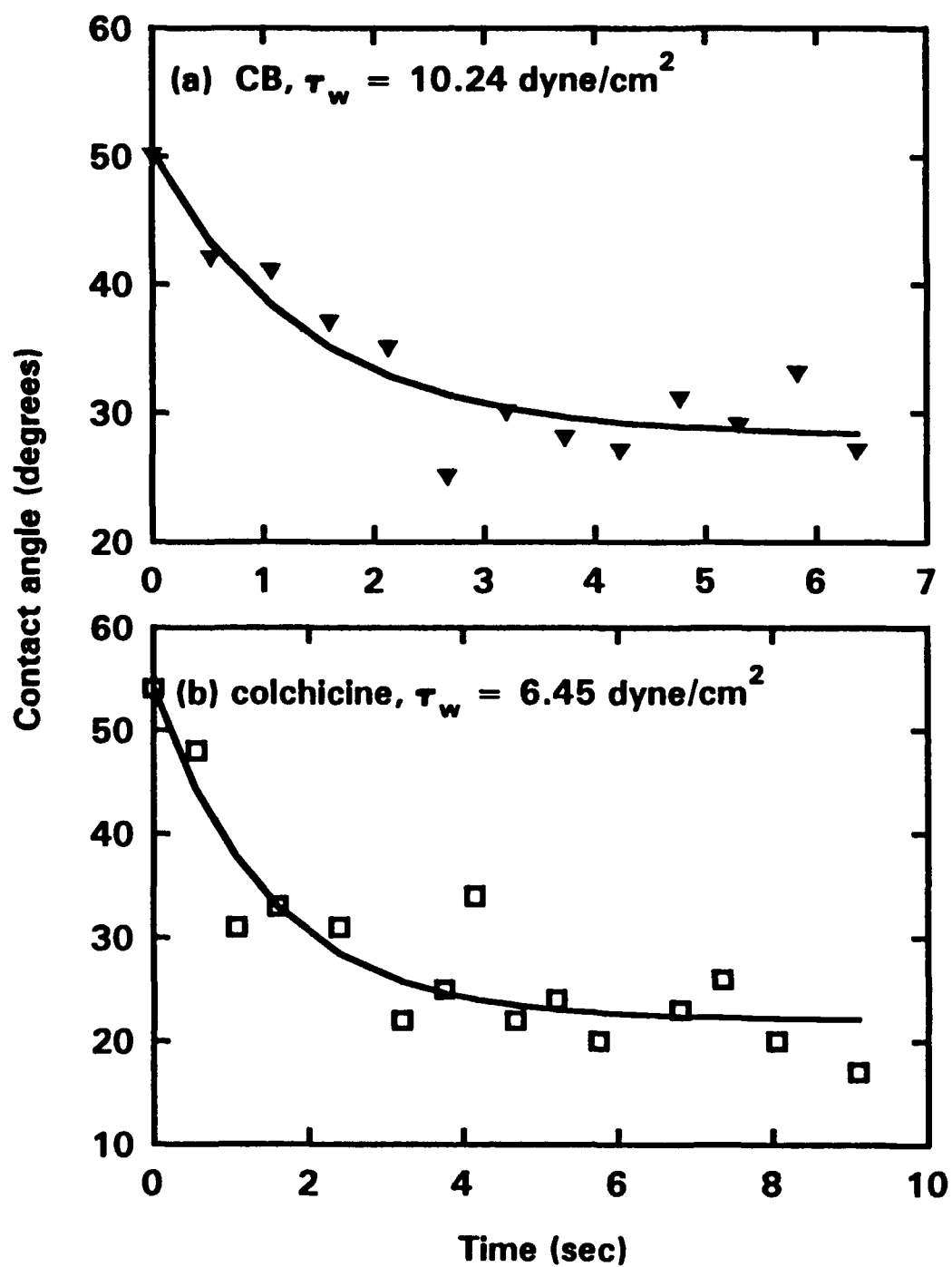


Figure 3.11 Representative trends of contact angle versus time for WBCs under (a) CB and (b) colchicine treatment.

adhesion exhibited an exponential decrease in θ versus time that was fitted with the equation:

$$\theta(t) = a(1 + b e^{-t/\alpha}) \quad (3.7)$$

where a and b are parameters such that θ_0 , the initial contact angle, equals $a(1 + b)$ and α is the time constant for $0 \leq t \leq t_{\text{act}}$. The contact angle versus time for FMLP stimulated adhesion demonstrated an initial decrease followed by a steady increase in θ to 90° or a perfectly spherical cell. A second order linear regression was used to curve fit the FMLP stimulated WBC change in θ with time. The steady increase in θ with time for FMLP cells corresponded with the increased polymerization of f-actin as the cells became more activated. Half of the FMLP stimulated WBCs exhibited an initial exponential decrease in θ with time and were also fitted with equation (3.7).

Using the equations for $\theta(t)$ for the adherent WBCs, the mean value of θ at t_p was calculated for each of the conditions. It was also of interest to determine if the cells had reached a steady state value of θ by t_p . This was determined by calculating the percent of total change in θ that had occurred by t_p . The percent of total change by t_p was not a meaningful parameter for the FMLP cells since they exhibited an initial decrease and subsequent increase in contact angle with time. Table 3.7 lists the mean and standard deviation for the wall shear stress, contact angle at t_p , as well

Table 3.7

Contact angle measurements for control, FMLP, IL-1, CB, and colchicine

Treatment	τ_w (dyne/cm ²)	Time Constant, α	θ_o (degrees)	θ at t_p (degrees)	% Angle change by t_p
Control n = 16	7.09 \pm 2.28 SD	2.11 \pm 2.37 SD	74.22 \pm 15.17 SD	46.78 \pm 9.53 SD	96.39 \pm 5.57 SD
FMLP n = 12	11.31 \pm 3.92 SD	*	*	60.47 \pm 19.39 SD	*
FMLP** n = 6	10.88 \pm 3.40 SD	7.15 \pm 5.57 SD	79.96 \pm 16.18 SD	**	**
IL-1 n = 11	7.32 \pm 2.60 SD	2.99 \pm 2.56 SD	87.10 \pm 19.19 SD	48.98 \pm 12.32 SD	95.89 \pm 4.52 SD
CB n = 12	8.55 \pm 1.76 SD	4.87 \pm 6.21 SD	60.20 \pm 19.79 SD	32.99 \pm 12.82 SD	89.05 \pm 10.73 SD
Colchicine n = 9	4.77 \pm 1.26 SD	4.47 \pm 4.06 SD	64.25 \pm 7.50 SD	35.25 \pm 10.93 SD	92.31 \pm 19.17 SD

* Not determined; see text for explanation.

** Includes only those cells that exhibited an initial exponential decrease in θ with time.

as, % angle change by t_p , time constant, α , and θ_0 for each condition. The number of cells in each condition group is smaller than that used for the contact length data; this was due to the contact angle not being discernable for several cells due to poor image quality. As seen in Table 3.7, greater than 95% of total angle change had occurred by t_p for WBCs under control conditions and IL-1 stimulated adhesion. Therefore, a steady state in cell deformation had essentially been reached.

Figures 3.12 and 3.13 depict the contact angle calculated at t_p (θ_p) for each cell versus the corresponding wall shear stress for control, FMLP, IL-1, CB, and colchicine. The parameters and statistical analysis for each regression are listed in Table 3.8. The regression for control conditions was significant at $p < 0.02$; the regression for FMLP stimulated adhesion was significant at a level of $p < 0.053$; the regression for colchicine treatment was significant only at a level of $p < 0.10$, while the regressions for IL-1 stimulated adhesion and CB treatment were not significant.

The results of contact angle versus wall shear stress were consistent with the earlier conclusions made from the contact length data for control conditions, FMLP stimulated adhesion, and colchicine treatment. WBCs under control conditions were readily deformable, WBCs with FMLP stimulated adhesion tended to adhere at higher shear rates and were more activated, therefore, less deformable, and WBCs under colchicine treatment were highly deformable. The contact angle and contact length results for

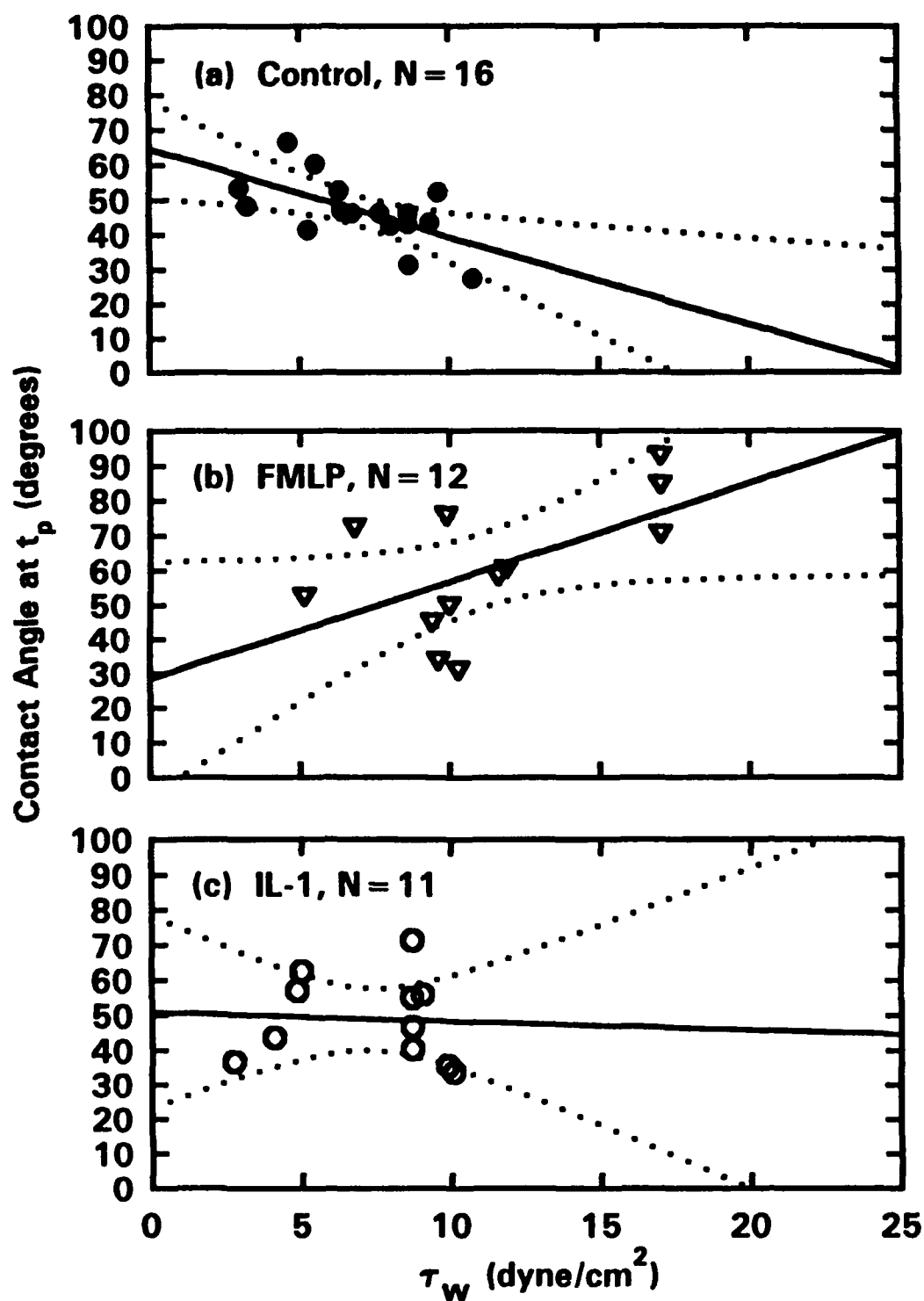


Figure 3.12 Contact angle at t_p versus wall shear stress for (a) control, (b) FMLP, and (c) IL-1. The regression for control was statistically significant for $p < 0.02$, while the regression for FMLP was only significant at $p < 0.06$. The regression for IL-1 was not statistically significant.

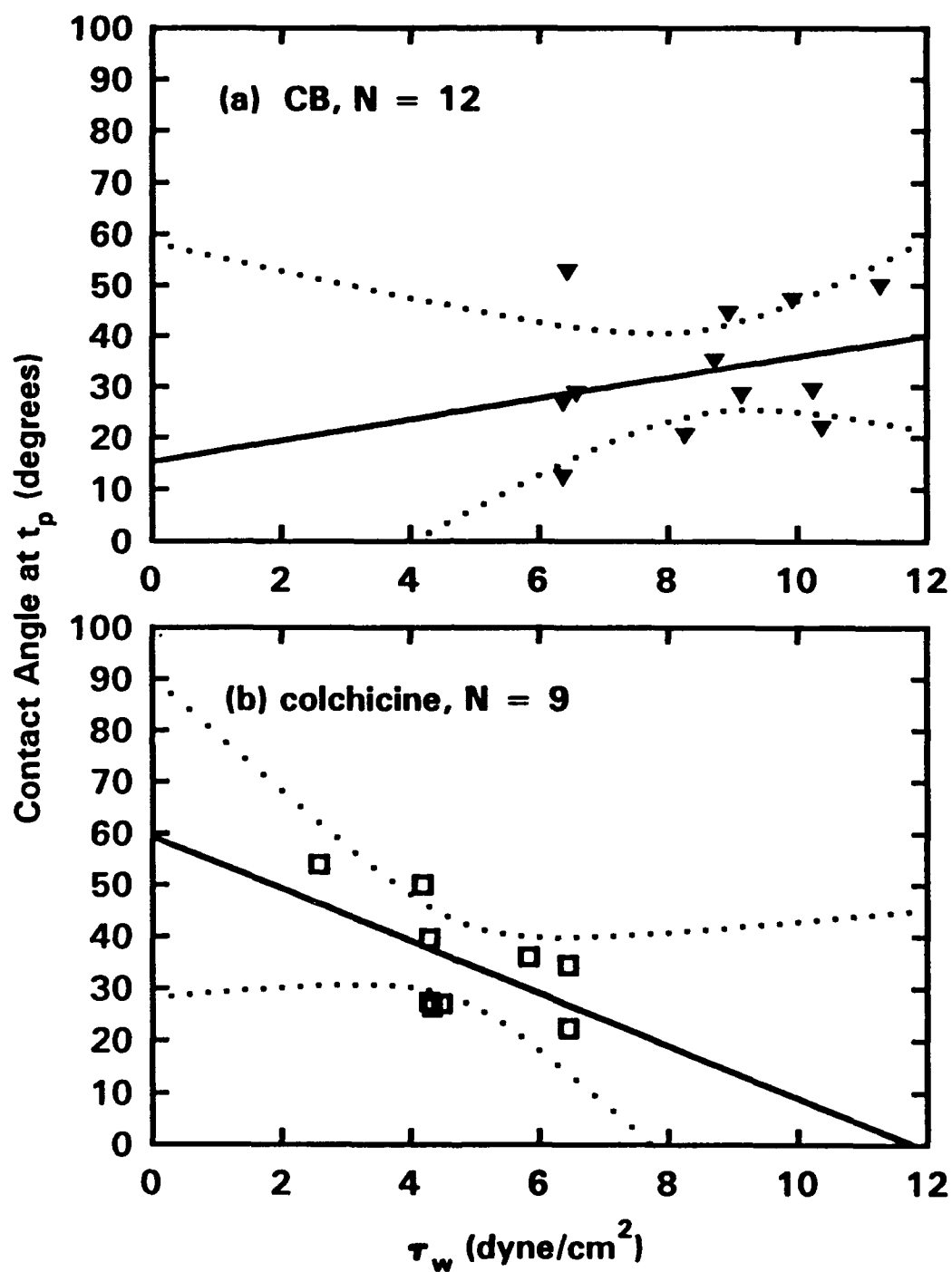


Figure 3.13 Contact angle at t_p versus wall shear stress for (a) CB and (b) colchicine. The regression for CB was not statistically significant, while the regression for colchicine was significant at $p < 0.11$.

Table 3.8

Regression parameters and statistics for θ_w versus τ_w

$$\theta_w = \beta_0 + \beta_1 \tau_w$$

Treatment	τ_w (dyne/cm ²)	θ_w (degrees)	β_0 parameter	β_0 t-ratio	β_0 p-value	β_1 parameter	β_1 t-ratio	β_1 p-value	r
Control n = 16	7.13 ± 2.22 SD	46.78 ± 9.53 SD	64.60	9.84	0.0001	-2.52	-2.84	0.013	0.60
FMLP n = 12	11.65 ± 4.14 SD	60.47 ± 19.39 SD	28.51	1.86	0.092	2.83	2.20	0.052	0.57
IL-1 n = 11	7.43 ± 2.51 SD	48.98 ± 12.32 SD	50.79	4.17	0.002	-0.25	-0.16	0.879	0.05
CB n = 12	8.55 ± 1.76 SD	32.99 ± 12.82 SD	15.31	0.79	0.446	2.07	0.93	0.373	0.28
Colchicine n = 9	4.77 ± 1.26 SD	35.25 ± 10.93 SD	59.25	4.51	0.0001	-5.04	-1.88	0.10	0.58

* Values shown for τ_w and θ_w are means ± standard deviations (SD).

IL-1 and CB appeared to contradict one another. The lack of decrease in contact angle at t_p for IL-1 stimulated WBCs with wall shear stress seemed to indicate that the cells were less deformable, while the contact length data suggested the WBCs were readily deformable. The contact angle data was consistent with earlier studies by Lipowsky *et al.* (1991). For CB, the contact length data increased with wall shear stress which was congruous with increased deformability and previous studies published by Lipowsky *et al.* (1991) while the contact angle data suggested the opposite trend. Since neither the regression of $L_{c\ t_p}$ versus τ_w or the regression of θ_{t_p} versus τ_w were statistically significant for either IL-1 or CB it was not reasonable to make any firm conclusions.

It was also of interest to investigate how contact angle calculated at t_p varied with t_p . It had been shown in the present study that t_p varied inversely with τ_w for control, FMLP and IL-1 and was virtually invariant for colchicine and CB. Contact angle decreased with increasing τ_w for control conditions and colchicine treatment, increased with τ_w for FMLP stimulated adhesion, and did not vary significantly with τ_w for IL-1 stimulated adhesion and CB treatment. Therefore, it was expected that θ would vary with t_p in a direction opposite to that of θ and τ_w . As seen by Figures 3.14 and 3.15, the expected outcome held true for all except for the colchicine treatment. For control conditions, as t_p increased, indicating a strong adhesive force between the WBC and EC and increased cell activation, the contact angle

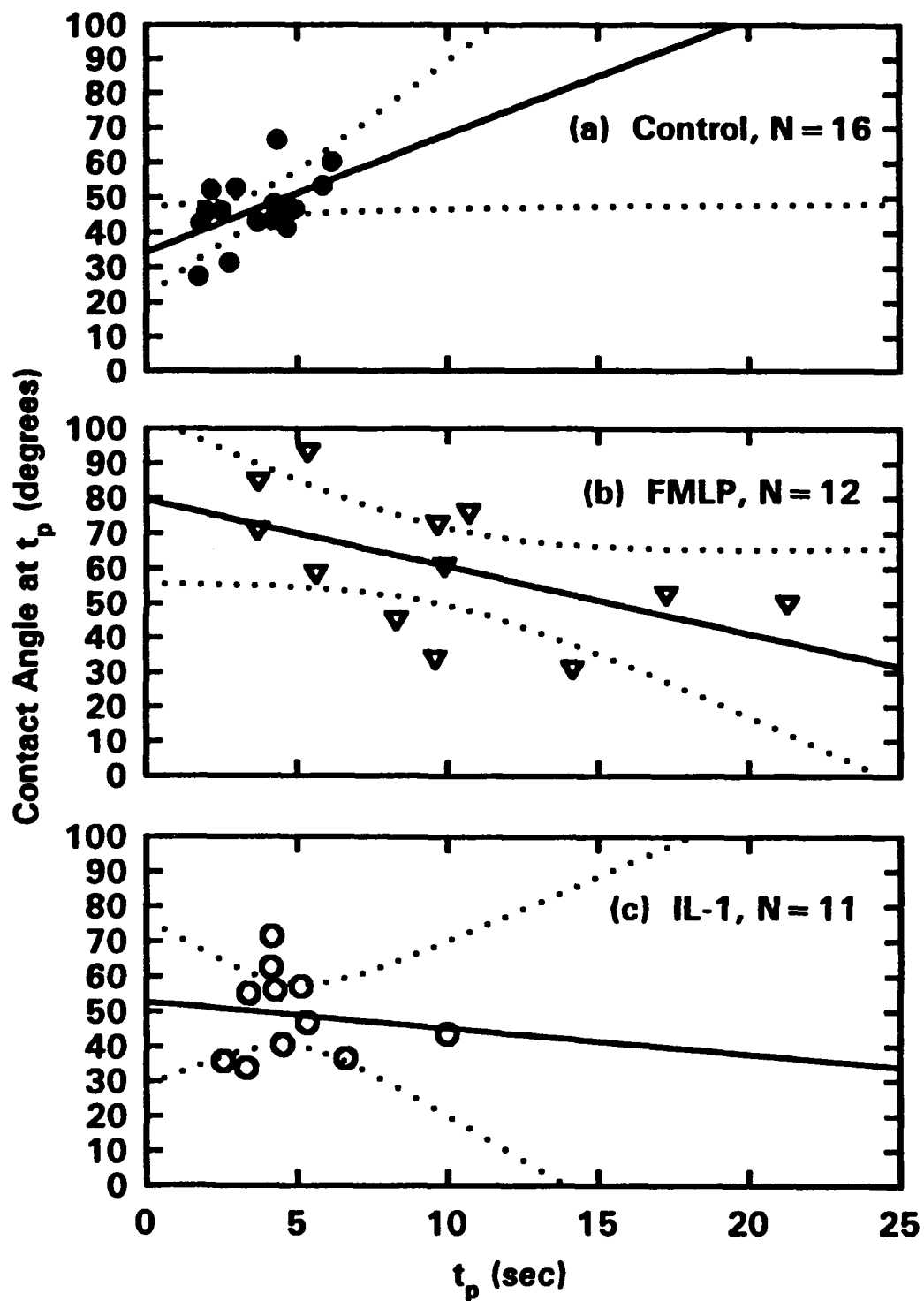


Figure 3.14 Angle at t_p versus t_p for (a) control conditions and (b) FMLP and (c) IL-1 stimulated adhesion. The regression of angle(t_p) is significant only for control conditions at $p < 0.05$.

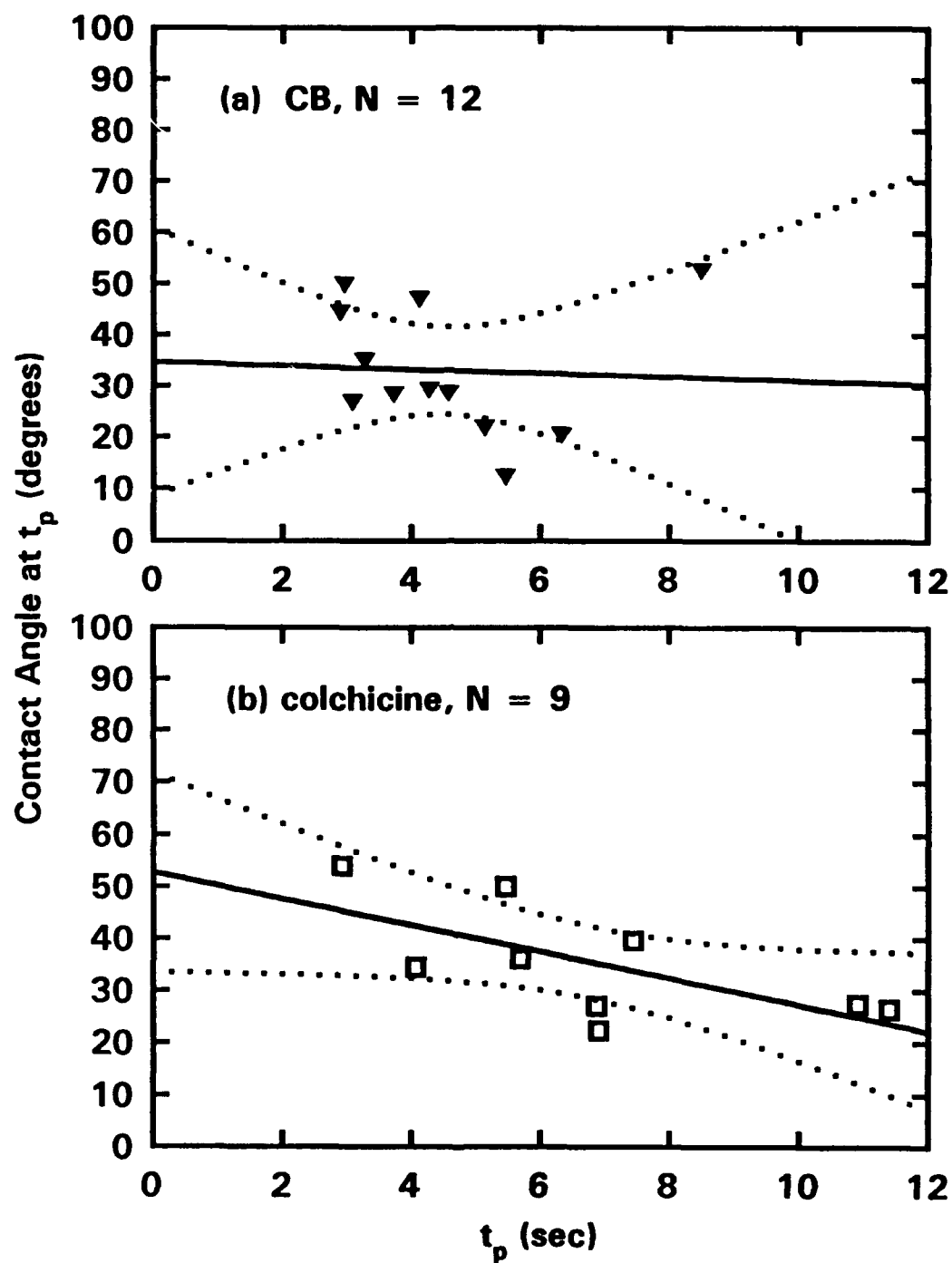


Figure 3.15 Angle at t_p versus t_p for (a) CB and (b) colchicine. The regression was statistically significant for colchicine at $p < 0.06$.

also increased. The regression of θ calculated at t_p versus t_p for control was statistically significant for $p < 0.05$. The FMLP activated WBCs demonstrated the opposite behavior although the regression was not statistically significant ($p > 0.05$). The higher values of t_p were coincident with lower shear stresses and adhesion of less activated WBCs. Since the WBCs were not as activated, they were more deformable and θ decreased as t_p increased. The regression of θ for IL-1 activated adhesion and CB treatment versus t_p was fairly invariant and not statistically significant ($p > 0.05$). For colchicine treatment, contact angle calculated at t_p decreased with t_p ($p < 0.06$). This may indicate that the cells remained deformable due to microtubule disruption regardless of the degree of WBC activation and strength of adhesion between WBC and EC. The regression parameters and statistics for all conditions are listed in Table 3.9.

The results obtained for both L_e and θ were consistent with current knowledge of WBC deformability; thus, both parameters appear to be a good measure of WBC membrane mechanics and deformability.

Table 3.9

Regression parameters and statistics for θ_{tp} versus t_p

$$\theta_{t_p} = \beta_0 + \beta_1 t_p$$

Treatment	t_p (sec)	θ_{tp} (degrees)	β_0 parameter	β_0 t-ratio	β_0 p-value	β_1 parameter	β_1 t-ratio	β_1 p-value	r
Control n = 16	3.44 ± 1.50 SD	46.78 ± 9.53 SD	34.42	5.71	0.0001	3.37	2.19	0.046	0.51
FMLP n = 12	9.44 ± 5.45 SD	60.47 ± 19.39 SD	79.47	7.39	0.0001	-1.91	-1.99	0.074	0.53
IL-1 n = 11	4.87 ± 1.93 SD	48.98 ± 12.32 SD	52.58	5.01	0.0001	-0.74	-0.37	0.720	0.12
CB n = 12	4.53 ± 1.65 SD	32.99 ± 12.82 SD	34.65	2.94	0.015	-0.365	-0.15	0.885	0.04
Colchicine n = 9	6.85 ± 2.83 SD	35.25 ± 10.93 SD	52.66	6.50	0.0001	-2.541	-2.30	0.055	0.66

• Values shown for t_p and θ_{tp} are means ± standard deviations (SD).

CHAPTER 4

Force Equilibrium Analysis of an Adherent White Blood Cell in Shear Flow

Numerous analyses have been presented in the literature to model bond distribution within the contact zone between the leukocyte (WBC) and endothelial cell membrane during adhesion of these cells. Most of these models have been applied to a leukocyte rolling at a constant velocity. Dembo *et al.* (1988) applied a model of tape peeling, using the membrane equations of equilibrium and the bond kinetic equations for adhesion to determine both membrane shape and bond density distribution in the adherent region without hydrodynamic effect. Scott (1992) used a pure kinetic model of a rolling WBC, assuming a flat membrane shape in the adherent zone. He estimated a relationship between the bond density and cell rolling velocity. Tözeren and Ley (1992) used both bond kinetics, as well as, rolling kinematics for their analysis. They assumed the membrane shape to be spherical along the adherent surface for low blood velocities. No cell membrane equilibrium was involved in their analysis. The model presented here aims to predict the adhesive bond distribution which is required to maintain a WBC adherent to the endothelium based on the

mechanical equilibrium between hydrodynamic and adhesive forces. This model, however, does not include bond kinetics. The gap between WBC membrane and EC in the adhesion zone is assumed to be represented by an exponential decay from the point of maximum bond stretch at the peeling site to zero near the center of adhesion contact.

4.1 Analysis

The analysis presented here considers the equilibrium of hemodynamic shear forces versus bond adhesion forces that must be maintained in order for a WBC to remain adhered to the venular endothelium. The analysis yields the WBC bond density, bond normal stress, and membrane tension distribution for the bridged half of contact length that is in tension (Figure 4.1). It is assumed that the WBC is stationary ($V_{wbc} = 0$) and that there is no peeling velocity. This model is strictly a mechanical analysis and does not take into account the kinetics of bond formation. It was hypothesized that with appropriate assumptions for the shape of the WBC membrane in the zone of contact the results obtained through the mechanical analysis should be close to that obtained through kinetic analysis in earlier studies.

At equilibrium, there are two membrane regions; a free unbridged region, and a bridged region where the membranes are held together with receptor-ligand bonds. The bridged region or contact area is assumed to be

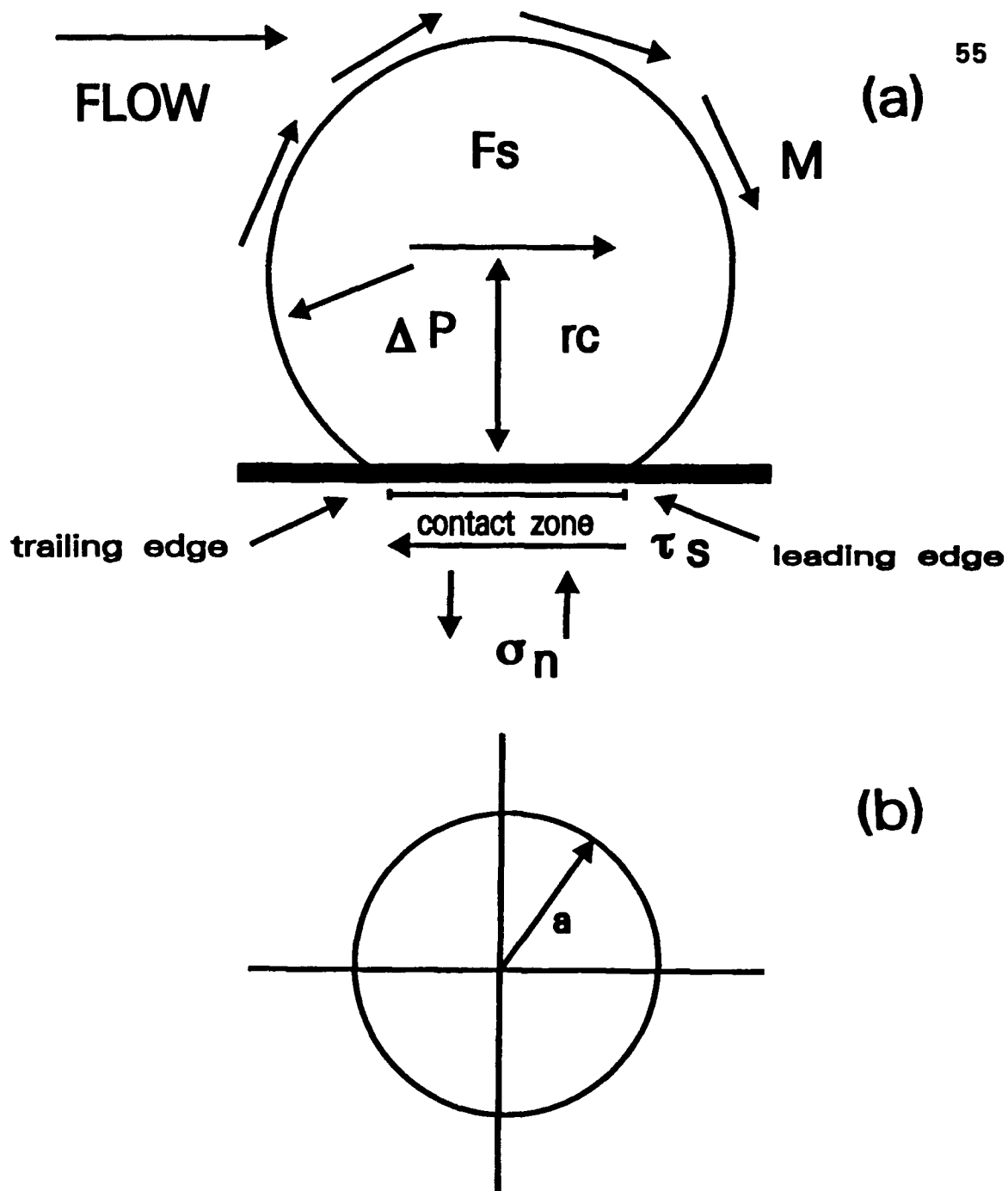


Figure 4.1 Schematic view of an adhering WBC. (a) Cross-sectional view of an adhering WBC. ΔP is the difference between the inside and outside of the cell. τ_s is the shear stress acting on the surface of the WBC, F_s is the resultant shear force, and M is the resultant torque. (b) The diagram shows the assumed contact area. (modified from Schmid-Schönbein, 1975)

circular with radius a . In order to counter the torque set up by the fluid which the bonds are assumed to be in tension, beginning with the trailing shear force acting on the cell, the normal stress due to the bonds in the adherent region must be non-uniform. Only the portion of the contact region in which the bonds are assumed to be in tension, beginning with the trailing edge of peeling zone, will be analyzed. The unbridged region and the leading edge of the contact zone which bonds are formed are not considered in this analysis except for requiring membrane tension continuity between the unbridged and bridged region.

Kinematics of the peeling process is considered in the lateral plane parallel to the direction of flow and the WBC membrane is considered as a two dimensional ring with the contact zone described by the coordinates (s, θ) where $s = 0$ at the leading edge of the peeling zone. In order to remain in equilibrium the hemodynamic and membrane (bond) stresses, as shown in Figure 4.2, must be balanced. The membrane tension, T_m , acts in the plane of the membrane. A transverse shear, Q_m , acting normal to the membrane, results from bending stresses in the membrane that are localized to the sharp bending adjacent to and within the adherent zone (Evans, 1985). The attractive normal stress, σ_n , arises from the forces acting on the receptor-ligand bonds in the bridged region is given as the product of force per bond (f) and bond density (Nb), i.e. $\sigma_n = f \cdot Nb$. The difference in pressure between the inside and outside of the cell, Δp , is assumed to be

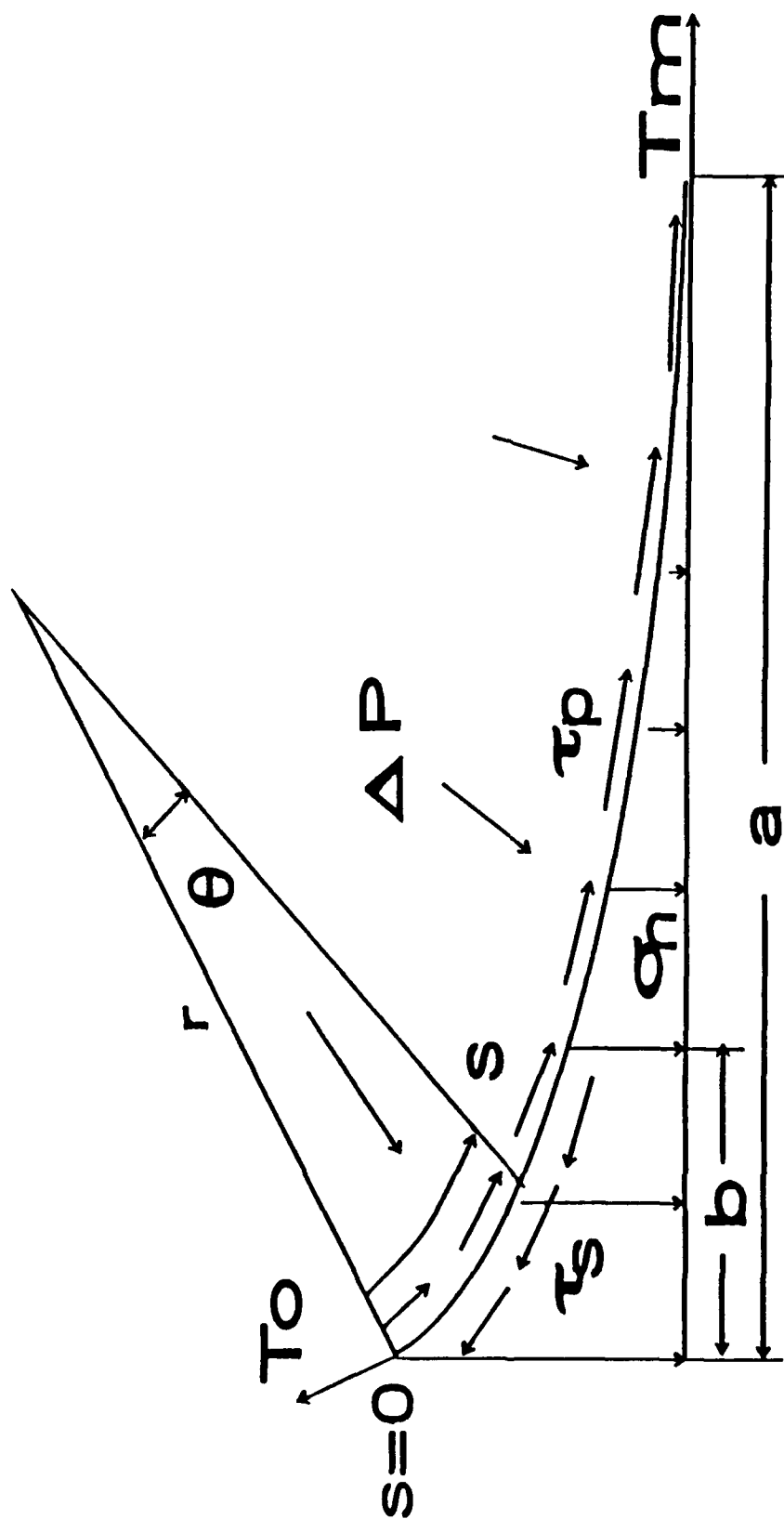


Figure 4.2 Schematic illustration of the stresses acting on the bridged region of the membrane. The intensive forces supported by the membrane include; the principle tension, T_m , that acts tangent to the plane of the membrane surface, the attractive stress, σ_n , which represents the adhesive bond stresses, the pressure difference, Δp , between the inside and outside of the cell, the resultant shear stress, τ_n , imparted by the adhesion to balance the fluid shear flow, and the internal shear stress, τ_p , due to cell deformation.

constant throughout. The resultant shear stress, τ_a , imparted to the WBC by the adhesion, balances the drag forces exerted by the blood flow. The internal cytoplasmic shear stress, τ_p , is due to cell deformation. Both τ_a and τ_p are assumed to be constant in the region they act.

The resultant shear stress in the model, τ_a , is assumed to be localized at the region of peeling of the bridged zone due to the fact that the dominant factor resisting the forward rolling motion of the cell occurs mostly at this peeling edge (Dembo *et al.*, 1988). Physically, the bonds at the peeling region will provide the greatest stress component in the tangential direction opposing the fluid shear. For this model, the bond stress is assumed to act normal to the endothelial surface; while, τ_a is a constant stress applied over a small peeling zone of the adherent region. To analyze the contributions of the peeling process to static equilibrium of the entire bridged zone, the zone of peeling is assumed to be localized over a distance, b . The ratio of the zone of peeling over the radius of contact (b/a) is denoted the non-dimensional parameter, δ , and is arbitrarily taken between 0.01 and 0.75.

4.1.1 Peeling Region

First, the peeling region of the bridged area will be considered¹. The local mechanical equilibrium of the membrane is given by the following equations (Evans and Skalak, 1980):

The balance of forces tangent to the surface is given by,

$$\frac{dT_m^{(1)}}{ds} - Q_m \cdot K_m + \sigma_n^{(1)} \cdot \theta = \tau_s - \tau_p \quad (4.1)$$

and the balance of forces normal to the surface is related to the membrane tension and bending modulus by:

$$T_m^{(1)} \cdot K_m + \frac{dQ_m}{ds} = -\sigma_n^{(1)} - \Delta p \quad (4.2)$$

where K_m is the local curvature of the meridional arc,

$$K_m = \frac{d\theta}{ds} \quad (4.3)$$

¹ Superscript 1 will be used to denote the peeling edge; superscript 2 will denote the remaining bridged region.

The local balance of moments for the membrane surface yields the relation that the transverse shear is equal to the gradient of the curvature multiplied by the bending modulus (Evans and Skalak, 1980).

$$Q_m = -B \cdot \frac{dK_m}{ds} \quad (4.4)$$

Since, it is a matter of debate whether or not the WBC membrane can offer a significant bending moment, zero bending modulus will be assumed.

Since, the curvature of the bridged zone is very small,

$$\sigma_n^{(1)} \cdot \theta \cong 0 \quad (4.5)$$

Therefore, equations (4.1) and (4.2) become, respectively,

$$\frac{dT_m^{(1)}}{ds} = T_s - T_p \quad (4.6)$$

and

$$T_m^{(1)} \cdot \frac{d\theta}{ds} = -\sigma_n^{(1)} - \Delta p \quad (4.7)$$

One method of solving the equations is to assume a membrane shape in the adherent region. Evans (1985) analyzed a similar problem without

shear flow and was able to solve for the membrane displacement from the equilibrium position with the approximation that membrane tension remained constant. A modified version of Evans' displacement will be assumed here;

$$\zeta = e^{-c\xi} \quad (4.8)$$

where

$$\zeta = \frac{r}{r_o} \quad (4.9)$$

and

$$\xi = \frac{s}{a} . \quad (4.10)$$

ζ denotes the non-dimensionalized membrane displacement from equilibrium or, equivalently, the non-dimensionalized bond stretch from zero, as shown in Figure 4.3. Bond stretch is denoted r ; the maximum bond stretch is r_o ; c is a non-dimensional parameter chosen to describe the exponential rate of decay of the membrane to equilibrium (equilibrium is assume to be a flat membrane in the same plane as the EC); and ξ is the spatial coordinate, s , in the meridional plane measured from the trailing edge normalized with respect to a , the radius of contact. Substituting the non-dimensionalized parameters into equations (4.6) and (4.7) yields:

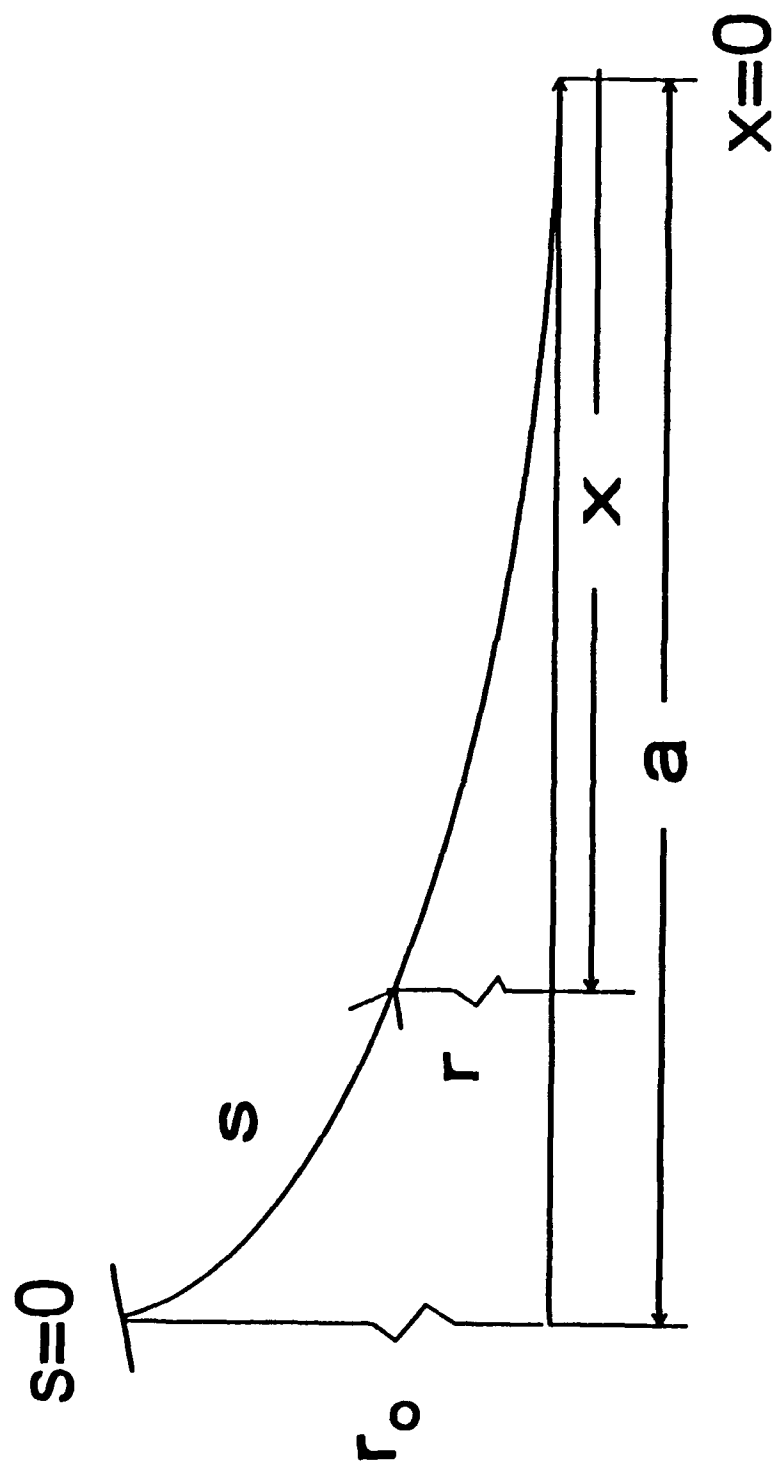


Figure 4.3 Membrane displacement from equilibrium.

$$\frac{dT_m^{(1)}}{a d\xi} = \tau_s - \tau_p \quad (4.11)$$

and

$$T_m^{(1)} \frac{d\theta}{a d\xi} = -\sigma_n^{(1)} - \Delta p \quad (4.12)$$

For membrane angles, measured relative to the equilibrium contact plane, that are $\leq 30^\circ$, the angle and curvature can be approximated by the first and second spatial derivative of the displacement (Evans, 1985).

$$K_m = \frac{d\theta}{ds} = -r_o \frac{d^2\zeta}{a^2 d\xi^2} \quad (4.13)$$

Therefore, equation (4.12) becomes;

$$T_m^{(1)} = \frac{a^2(\sigma_n^{(1)} + \Delta p)}{c^2 r_o e^{-c\xi}} \quad (4.14)$$

Equations (4.11) and (4.14) can be solved in terms of $T_m^{(1)}$, $\sigma_n^{(1)}$, τ_s , and τ_p by imposing the boundary conditions; $\xi = 0$, $T_m^{(1)} = T_o$ and $\sigma_n^{(1)} = \sigma_o$. Applying the boundary conditions to equation (4.14), yields an equation for Δp .

$$\Delta p = T_o \frac{c^2}{a^2} r_o - \sigma_o \quad (4.15)$$

Integrating equation (4.11), the balance of forces tangent to the membrane, yields:

$$T_m^{(1)} = (r_s - r_p) a \xi + T_o \quad (4.16)$$

Substituting for Δp , the balance of forces normal to the membrane becomes,

$$T_m^{(1)} = \frac{a^2(\sigma_n^{(1)} - \sigma_o)}{c^2 r_o e^{-cf}} + T_o e^{cf} \quad (4.17)$$

Setting equation (4.16) and (4.17) equal, the $\sigma_n^{(1)}$ distribution can be solved for the peeling region of the bridged zone.

$$\sigma_n^{(1)} = \frac{c^2}{a^2} r_o e^{-cf} [(r_s - r_p) a \xi + T_o (1 - e^{cf})] + \sigma_o \quad (4.18)$$

At this point, a linearized relation is introduced between the molecular adhesion force and membrane displacement. The relationship holds for the entire bonded region. Such that,

$$f = f_o \cdot \zeta \quad 0 < \zeta \leq 1 \quad (4.19)$$

and

$$f=0 \quad \zeta > 1 \quad (4.20)$$

where f is the force per bond, and f_o is the maximum force per bond.

Thus, the attractive bond stress, σ_n , is equal to the product of the force per bond and the bond density ($Nb(s)$).

$$\sigma_n = Nb(\xi) \cdot f = Nb(\xi) \cdot f_o \zeta = Nb(s) f_o e^{-\alpha f} \quad (4.21)$$

Now, $Nb(s)^{(1)}$ can be solved for the peeling region.

$$Nb(\xi)^{(1)} = \frac{c^2 r_o}{a^2 f_o} [(\tau_s - \tau_p) a \xi + T_o (1 - e^{-\alpha f})] + \frac{\sigma_o}{f_o e^{-\alpha f}} \quad (4.22) \quad \text{---}$$

4.1.2 Bonded Region - Outside of the Peeling Region

The assumptions made in the analysis of the peeling region concerning bending modulus and membrane curvature hold true for this region. Hence, the simplified equations of static equilibrium for this region are as follows:

First, the membrane equation in the tangential direction,

$$\frac{dT_m^{(2)}}{a d\xi} = -T_p \quad (4.23)$$

Next, the membrane equation in the normal direction,

$$T_m^{(2)} = \frac{a^2(\sigma_n^{(2)} + \Delta p)}{c^2 r_o e^{-c\xi}} \quad (4.24)$$

In order to ensure continuity between the peeling region and the rest of the bridged membrane, the boundary condition; at $\xi = b/a = \delta$, $T_m^{(2)}(\delta) = T_m^{(1)}(\delta)$, is imposed. Since Δp is assumed to be constant, it is the same in this region as in the peeling region. Therefore, substituting in for Δp and applying the boundary conditions, equations (4.23) and (4.24) become,

$$T_m^{(2)} = T_p a(\delta - \xi) + T_m^{(1)}(\delta) \quad (4.25)$$

and

$$T_m^{(2)} = \frac{\sigma_n^{(2)} + T_o \frac{c^2}{a^2} r_o - \sigma_o}{\frac{c^2}{a^2} r_o e^{-c\xi}} \quad (4.26)$$

Setting equations (4.25) and (4.26) equal, $\sigma_n^{(2)}$ and $Nb^{(2)}$ can be solved.

$$\sigma_n^{(2)} = \frac{c^2}{a^2} r_o e^{-c\xi} [\tau_p a(\delta - \xi) + T_m(\delta)] - T_o \frac{c^2 r_o}{a^2} + \sigma_o \quad (4.27)$$

$$Nb^{(2)} = \frac{c^2 r_o}{a^2 f_o} [\tau_p a(\delta - \xi) + T_m(\delta)] - \frac{(T_o \frac{c^2}{a^2} r_o - \sigma_o)}{f_o e^{-c\xi}} \quad (4.28)$$

σ_o is solved using the momentum balance between the hemodynamic forces and the sum of the forces due to the tensile and compressive bonds across the entire contact area. The stress distributions for the tensile and compressive bonds are assumed to be equal but opposite. The moment is taken about the center of the contact area so that the moment arms are equal. Therefore,

$$F_s \cdot r_c + M = 2 \int_A \sigma_n x \, dA \quad (4.29)$$

where F_s is the force exerted on the cell via the shear flow, r_c is the radius of the cell, and M is the resultant torque. The coordinate x is taken from the center of the contact area. In order to solve the momentum balance, F_s and

M are approximated by the following equations taken from work by Tözeren and Skalak;

$$F_s = C_1 6\pi\tau_w r_c^2 \quad (4.30)$$

and

$$M = C_2 4\pi\tau_w r_c^3 \quad (4.31)$$

where C_1 and C_2 are constants. To simplify the calculation of equation (4.29), the approximation $\xi \approx 1 - x/a$ can be made. By employing a trapezoidal numerical approximation, equation (4.29) is solved for $\xi = 0$ to 1 where $\sigma_n = \sigma_n^{(1)}$ for $0 \leq \xi \leq \delta$ and $\sigma_n = \sigma_n^{(2)}$ for $\delta \leq \xi \leq 1$, thereby, elucidating the value of σ_o .

4.2 Model Validation

The membrane tension, attractive normal stress, and bond density distribution are calculated with a Fortran program, DIST.EXE (Appendix C), using the parameters listed in Table 4.1. Nb_m , the maximum available bond density, is included in the model so that the bond density is capped within a physiologic range. If a greater bond density is required, the cell will no

Table 4.1
Parameter estimates

Parameter	Definition	Range	Reference
r_o	maximum bond interaction length	5.0×10^{-8} cm	Bell, 1978
f_o	maximum bond force	1.2×10^{-6} dyne/bond	Bell, 1978
r_c	WBC radius	$4.0 \mu\text{m}$	Schmid-Schönbein, 1975
T_o	membrane tension outside bridge region	0.031 - 0.035 dyne/cm	Dong, 1988 Evans, 1989
τ_w	wall shear stress	0.8 - 6.0 dyne/cm ²	current study
τ_p	shear stress due to cell deformation	0 - 3.0 dyne/cm ²	current study
a	radius of WBC-endothelium contact area	$2.0 - 6.0 \mu\text{m}$	current study
δ	peeling region (b/a)	0.01 - 0.75	current study
c	rate of decay of membrane shape	4 - 7	current study
C_1	constant that depends on the cell shape	1.7005	Tözeren, 1977
C_2	constant that depends of the cell shape	0.944	Tözeren, 1977
Nb_m	maximum available bond density	10^{10}	Dembo, 1988

longer be in equilibrium. If the bond density distribution does not change to accommodate the shortfall, the cell will be swept away by the shear flow.

Since the analysis contains two independent variables, δ and c , it is of interest to ascertain their effect on the model. The following set of parametric curves were run keeping all input parameters constant while varying only the independent parameter of interest. Figure 4.4 shows the membrane displacement from equilibrium for various values of parameter c . Physically, the parameter c will be dependent on both hemodynamic forces and cell deformability. The more deformable the cell the flatter the membrane will tend to be; the higher the value of c . As seen in Chapter 3, WBC deformability is influenced by shear stress, as well as, chemical treatment and degree of cell activation. However, the stronger the fluid shear force the more the WBC membrane will be peeled away from the EC and the lower the value of c . As shown by the figure, as c increases, the rate of exponential decay increases and the final displacement at $\xi = 1.0$ is closer to zero. Figure 4.5 is the bond density model sensitivity to the value of c . As c increases, the bond stretch associated with membrane displacement becomes less as ξ approaches 1. Since the force per bond has been linearized with the degree of stretch, the force per bond also decreases; therefore, the bond density increases with c to compensate. Figure 4.6 shows the sensitivity of σ_n to parameter c . As c increases, the value of σ_n increases, while the final value at $\xi = 1$ decreases. When c increases, the

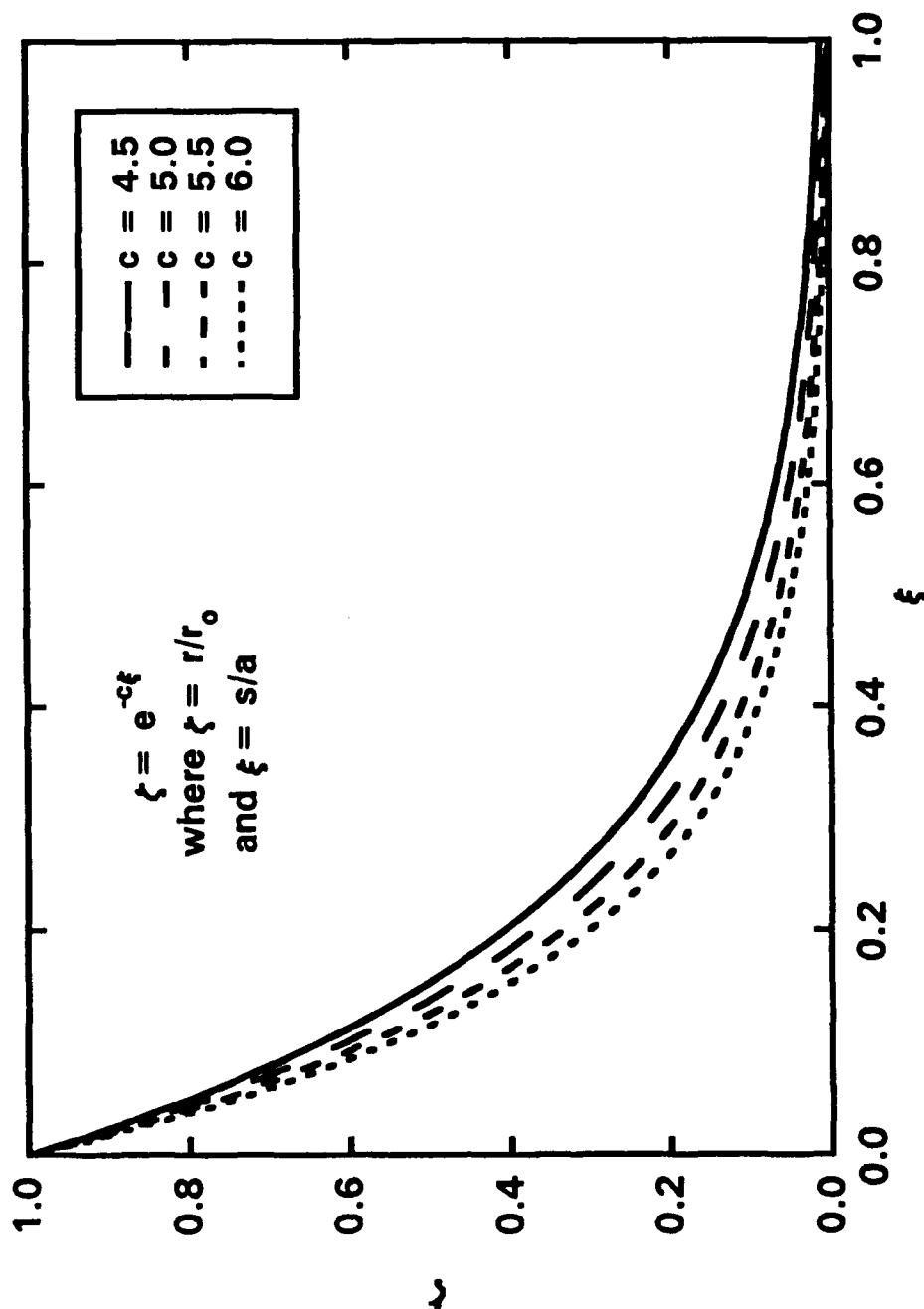


Figure 4.4 Assumed membrane displacements for various values of parameter c . Parameter c is a non-dimensional parameter describing the rate of exponential decay. The membrane displacement is equivalent to the bond stretch.

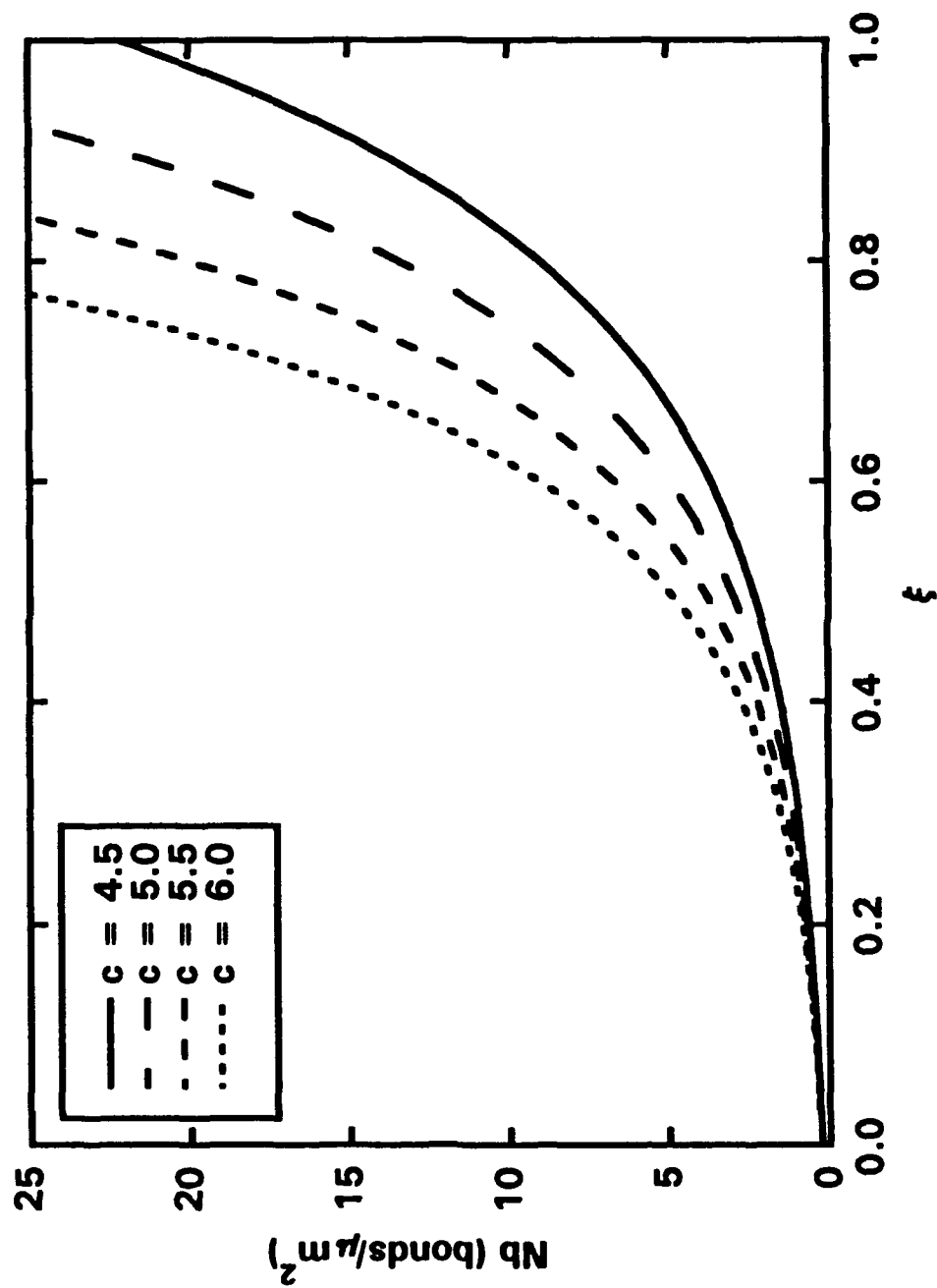


Figure 4.5 Bond density model sensitivity curves for independent parameter c . The following variables were used in the model calculations; $a = 3.5 \mu\text{m}$, $\delta = 0.10$, $\tau_w = 6.0 \text{ dyne/cm}^2$, $\tau_p = 0$, $f_o = 1.2 \times 10^{-5} \text{ dyne/bond}$ and $T_o = 0.035 \text{ dyne/cm}$.

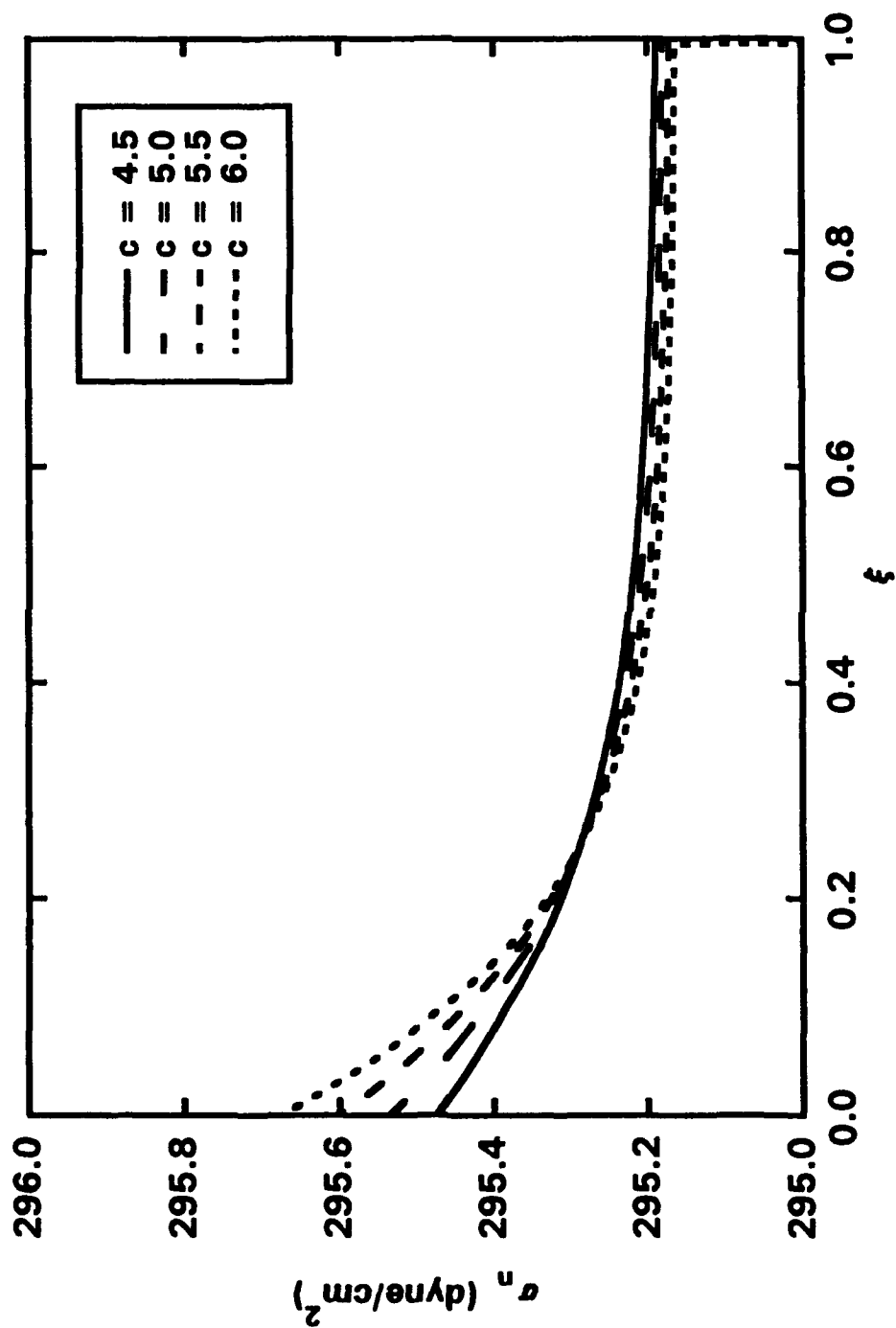


Figure 4.6 Bond normal stress versus non-dimensional distance from trailing edge for various gap thickness decay rates. The following variables were used in the model calculations; $a = 3.5 \mu\text{m}$, $\delta = 0.10$, $\tau_w = 6.0 \text{ dyne/cm}^2$, $\tau_p = 0$, $f_o = 1.2 \times 10^{-5} \text{ dyne/bond}$, and $T_o = 0.035 \text{ dyne/cm}$.

effective area in which the bonds providing the majority of the force required to counter the torque set up by the shear flow decreases. Since the required force is not changing, the initial stress increases. At $c = 6$, as shown in the figure, σ_n severely drops off just before $\xi = 1$; this is due to the physiologic bond density maximum being reached. The bond density at this point can not increase any further to compensate for the decreasing value of force per bond. The membrane tension is not effectively changed by the value of c since it is dependent only on r_a , r_p , and T_o .

Variation in the independent parameter δ does not effectively change the calculation of N_b (N_b decreases by 0.012% from analysis when $\delta = 0.01$ versus $\delta = 0.75$). The model of σ_n is also fairly insensitive to changes in δ since the bond normal stress is just the product of bond density and force per bond. Figure 4.7 shows the model membrane tension sensitivity to δ . The smaller the area that r_a acts, the quicker the membrane tension reaches its maximum value. The maximum value of membrane tension increases linearly as δ increases. This trend is the direct result of the membrane equation governing the membrane tension in the tangential direction.

Figure 4.8 through 4.11 show the membrane displacements, bond density, attractive normal stress, and tension distribution for a series of shear stresses (1, 2, 4, and 6 dyne/cm²) assuming the same membrane

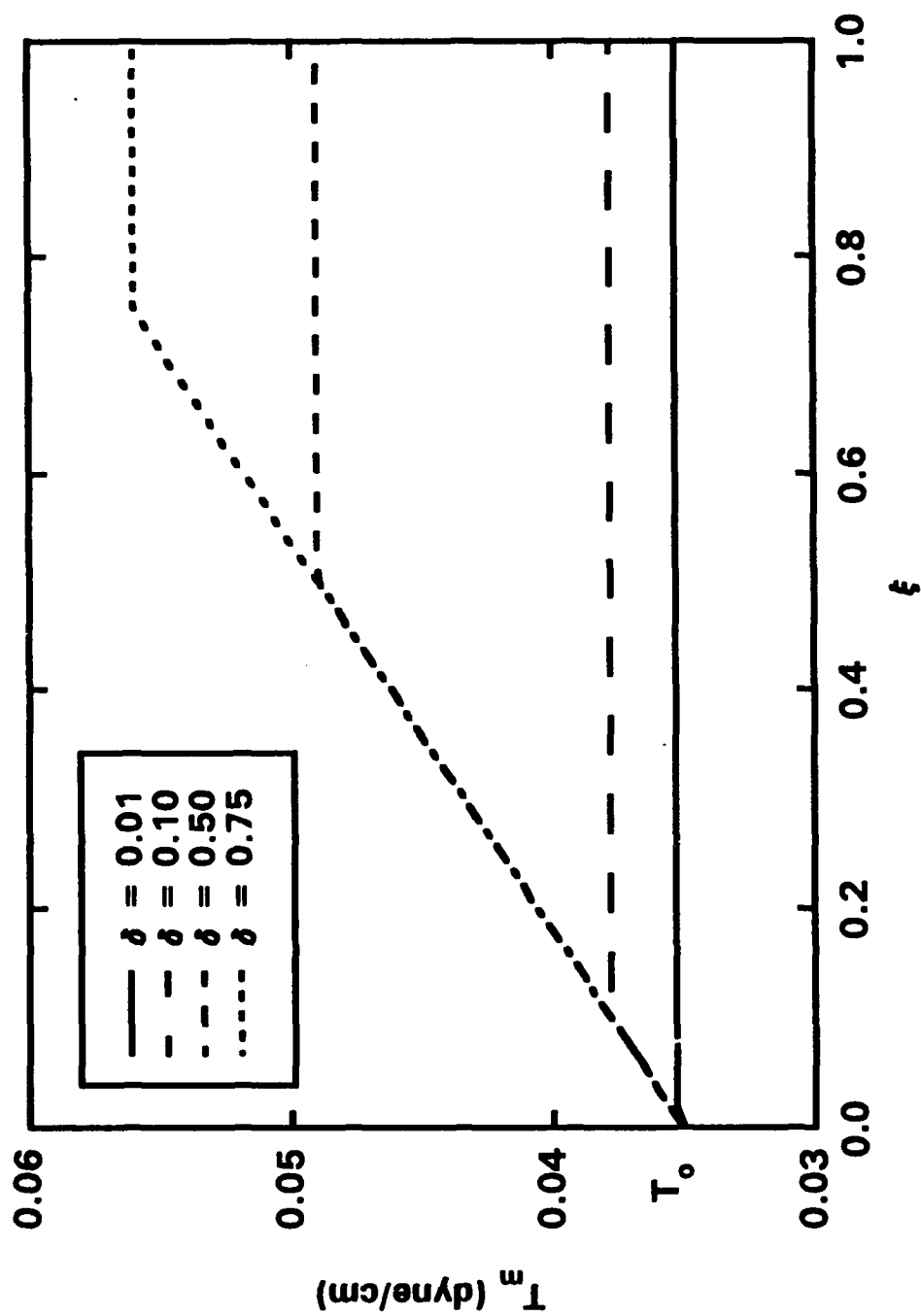


Figure 4.7 Membrane tension versus non-dimensional distance from trailing edge, where δ is the fraction of the contact zone with non-zero shear stresses (τ_s). Analysis was performed using the following parameters; $c = 5$, $a = 3.5 \mu\text{m}$, $\tau_w = 6.0 \text{ dyne/cm}^2$, $\tau_p = 0$, $f_o = 1.2 \times 10^{-5} \text{ dyne/bond}$, and $T_o = 0.035 \text{ dyne/cm}$.

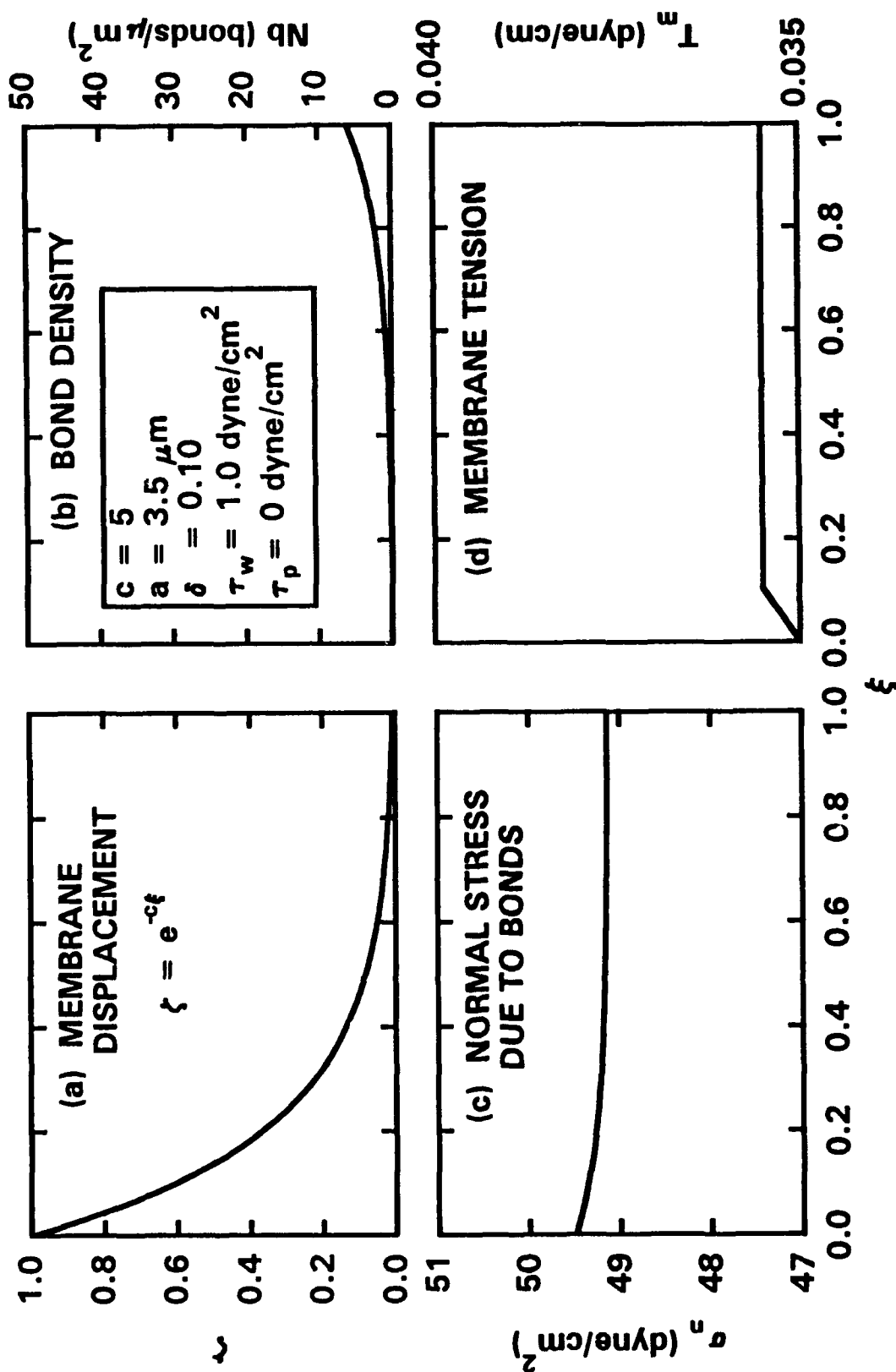


Figure 4.8 Membrane distributions for $\tau_w = 1.0 \text{ dyne/cm}^2$ and zero internal shear stress. Analysis was performed with $f_o = 1.2 \times 10^{-5} \text{ dyne/bond}$ and $T_o = 0.035 \text{ dyne/cm}$.

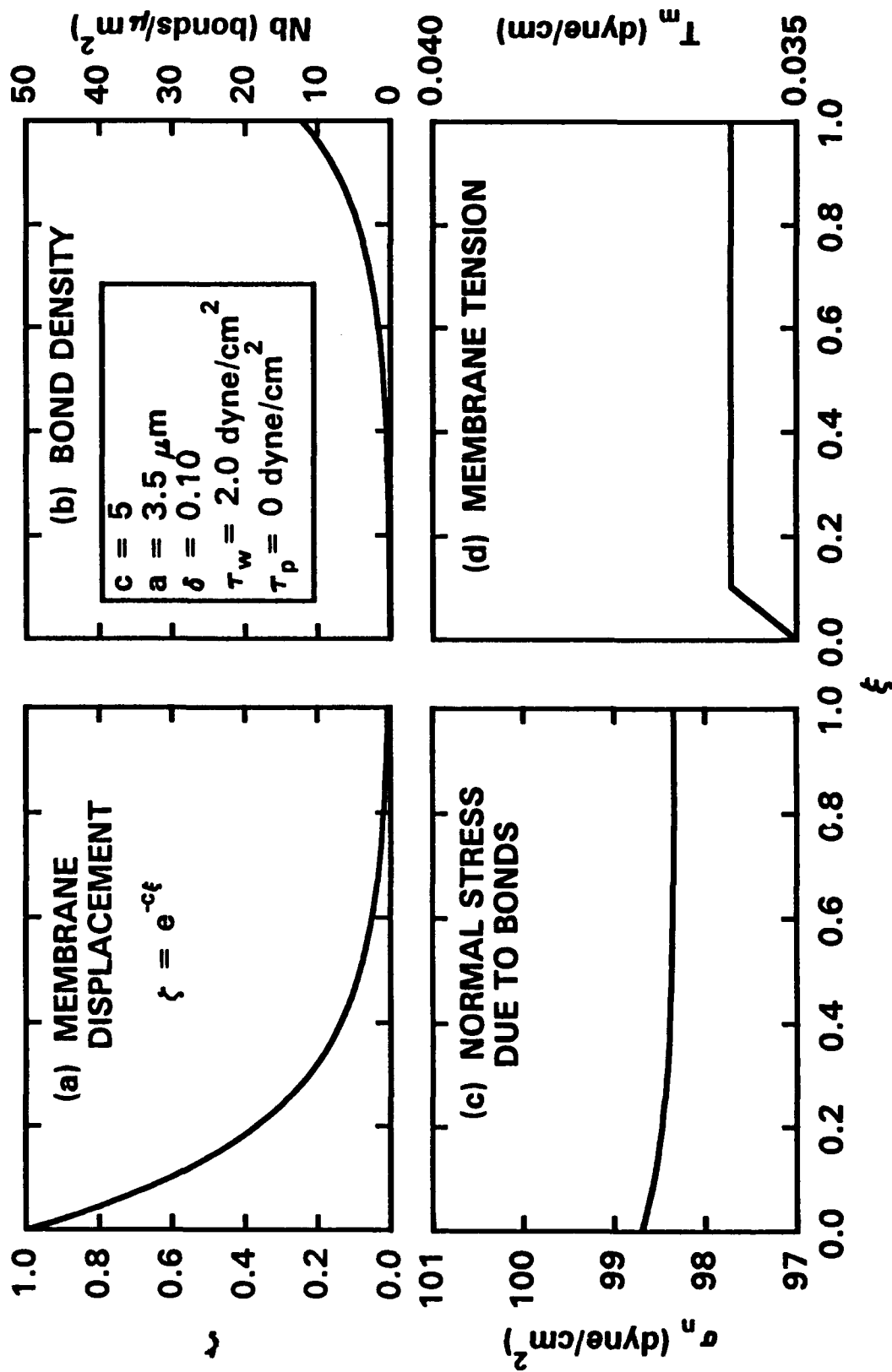


Figure 4.9 Membrane distributions for $\tau_w = 2.0 \text{ dyne/cm}^2$ and zero internal shear stress. Analysis was performed with $f_o = 1.2 \times 10^{-6} \text{ dyne/bond}$ and $T_o = 0.035 \text{ dyne/cm}$.

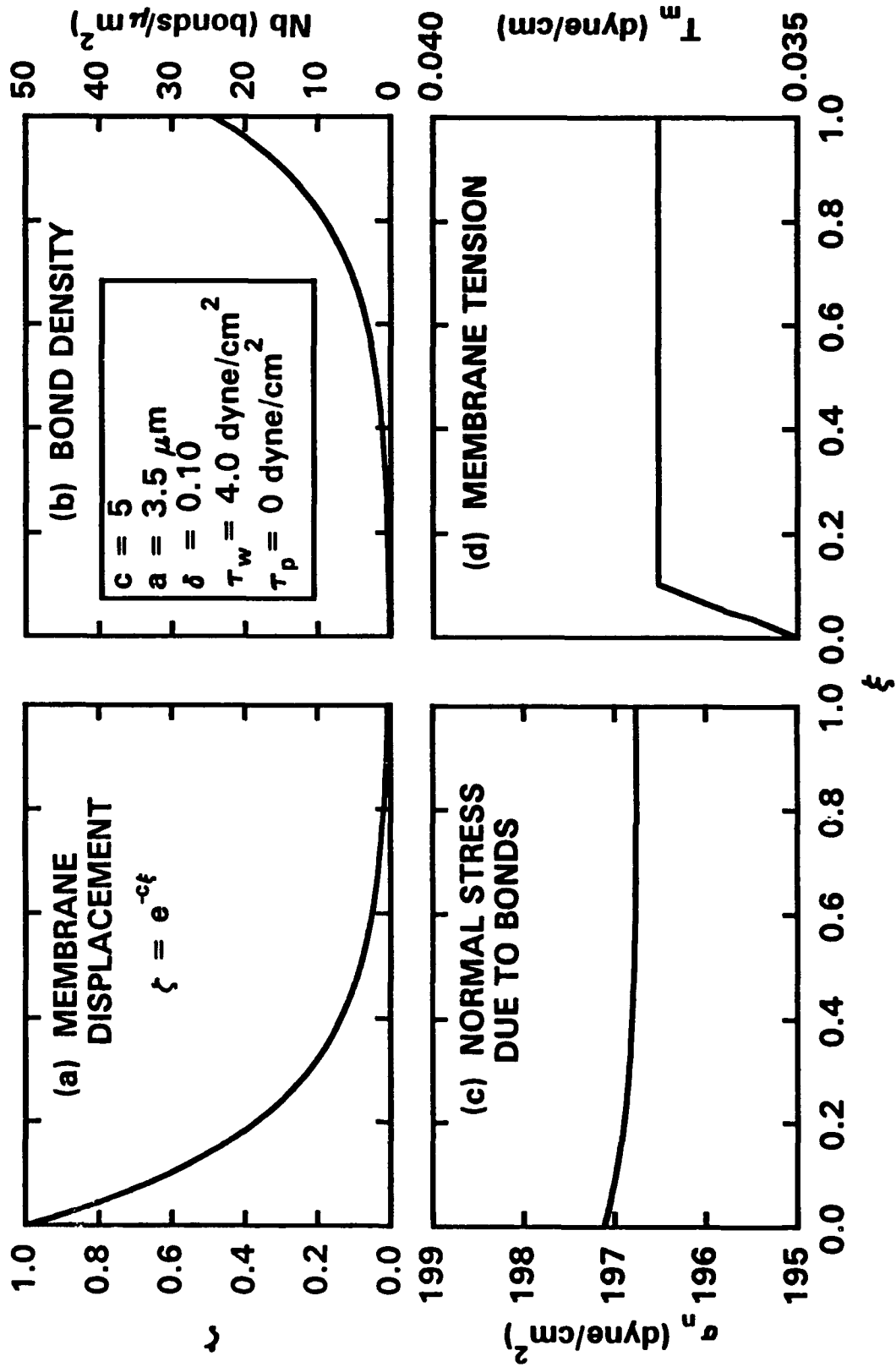


Figure 4.10 Membrane distributions for $\tau_w = 4.0 \text{ dyne/cm}^2$ and zero internal shear stress. Analysis was performed with $f_o = 1.2 \times 10^{-5} \text{ dyne/bond}$ and $T_o = 0.035 \text{ dyne/cm}$.

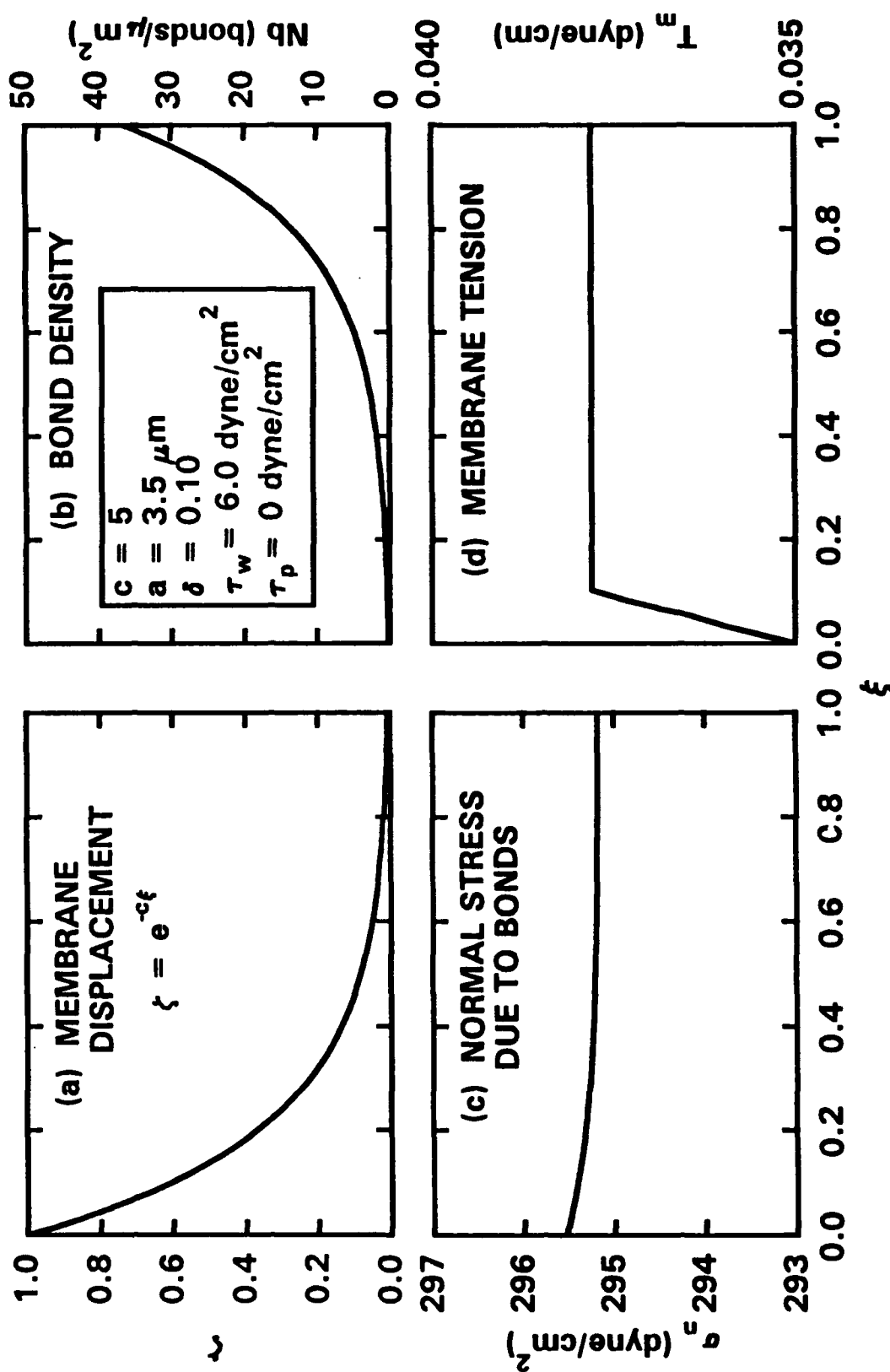


Figure 4.11 Membrane distributions for $\tau_w = 6.0 \text{ dyne/cm}^2$ and zero internal shear stress. Analysis was performed with $f_o = 1.2 \times 10^{-5} \text{ dyne/bond}$ and $T_o = 0.035 \text{ dyne/cm}$.

displacement function, contact radius, and peeling edge. τ_p is zero in all four cases. The membrane displacement was chosen so the bonds at the center of the cell contact area were virtually unstretched; therefore, providing very little force per bond. As discussed earlier, wall shear stress will influence the membrane displacement; however, for this comparison the value of c was kept constant for each trial.

As shear stress increases, so does the number of bonds required to maintain the cell in equilibrium. The bond distribution in each case rises exponentially from nearly zero at the peeling edge of the bridged membrane ($\xi = 0$) to a maximum at the center of the contact area. For all cases, the bond density at the center of the contact area is less than Nb_m ; hence, the estimates given by the analysis are within physiologic conditions. The normal stress distributions have the same profiles but different magnitudes for all shear stresses; σ_o , the stress at $\xi = 0$ increases proportionally with the level of wall shear stress. The normal stress distribution is similar to that predicted by Hammer and Lauffenburger (1989). Membrane tension increases slightly within the peeling zone and then remains constant for the remainder of the bridged region.

The conditions in Figure 4.11 were duplicated with the addition of a non-zero τ_p in the direction opposite of τ_o to take into account an internal cytoplasmic shear stress caused by cell deformation (Figure 4.12). The attractive stress distribution and bond density distributions do not change

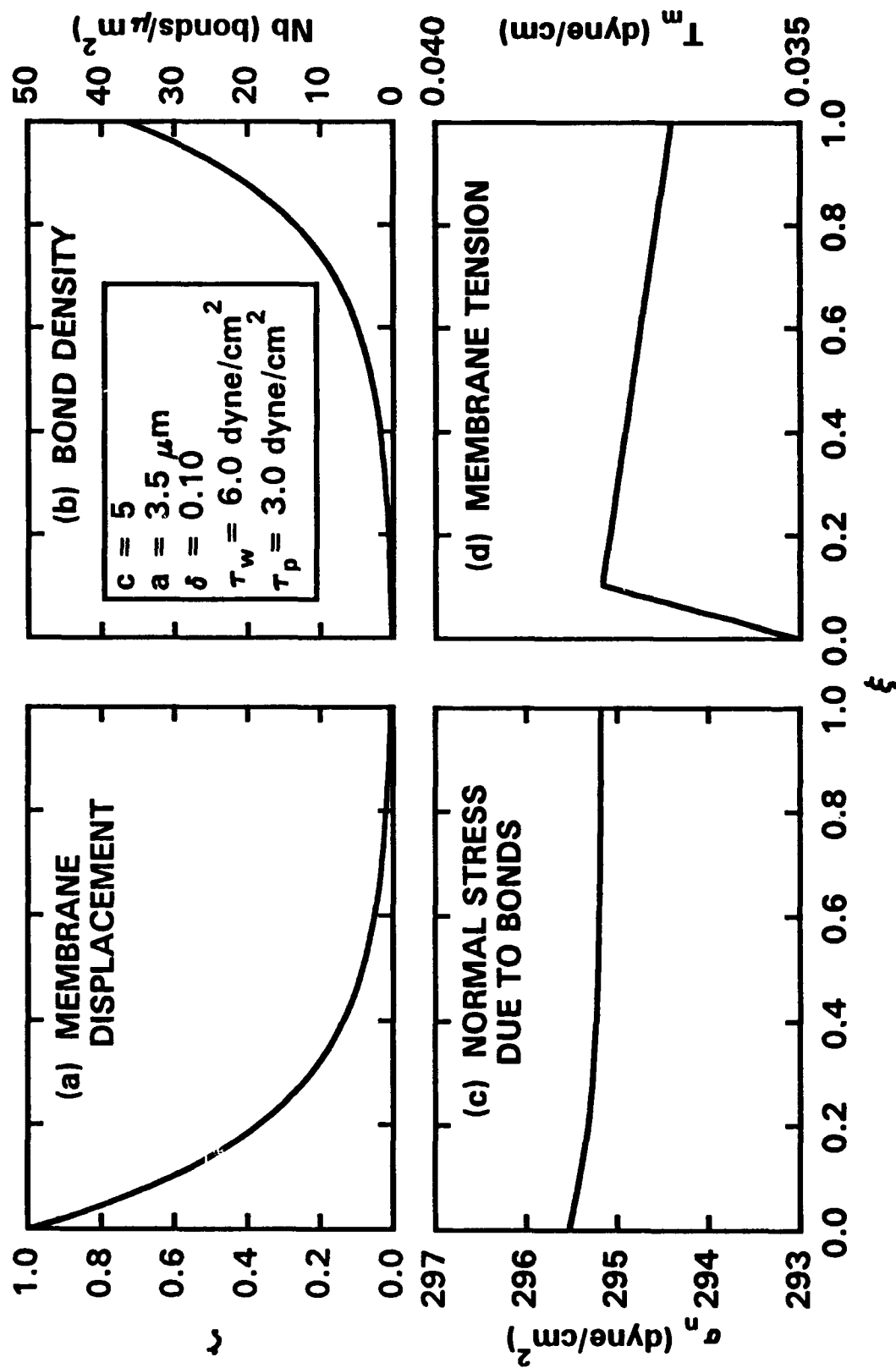


Figure 4.12 Membrane distributions for $\tau_w = 6.0 \text{ dyne/cm}^2$ and $\tau_p = 3.0 \text{ dyne/cm}^2$. Analysis was performed with $f_o = 1.2 \times 10^{-5} \text{ dyne/bond}$ and $T_o = 0.035 \text{ dyne/cm}$.

significantly; however, there is a steady decay in membrane tension as ξ approaches 1 outside the immediate peeling zone ($\delta \leq \xi \leq 1$). These results appear to indicate that as the cell deforms and an internal shear stress on the cell membrane within the contact region is produced in the same direction of the fluid flow, the membrane tension decreases from the maximum at the peeling edge to a minimum at the leading edge.

In order to assess the effect of deformation on the bond density distribution, the mechanical equilibrium equations were calculated over a range of contact lengths. Shear stress (τ_w) was held constant and the peeling region was equal to 10% of the contact radius for all cases. Once again, although deformation will influence the membrane displacement, the parameter c defining the rate of exponential decay for the membrane displacement was held constant. The results are shown in Figure 4.13(a), the bond density versus ξ and 4.13(b), a blow-up of (a) at the peeling region ($0 \leq \xi \leq \delta$). As the contact length increases, the bond density required to maintain the cell in equilibrium decreases at the center of the contact area, as does the bond density at the peeling edge. This result is consistent with the assumption that as contact area increases for the more deformable cells, the adherent WBC will be able to sustain higher shear forces. Thus, contact area is a chief determinant of adhesive force.

As seen in Chapter 3, the value of f_0 , the force per bond, can vary with chemical treatment. Therefore, it is of interest to examine the change

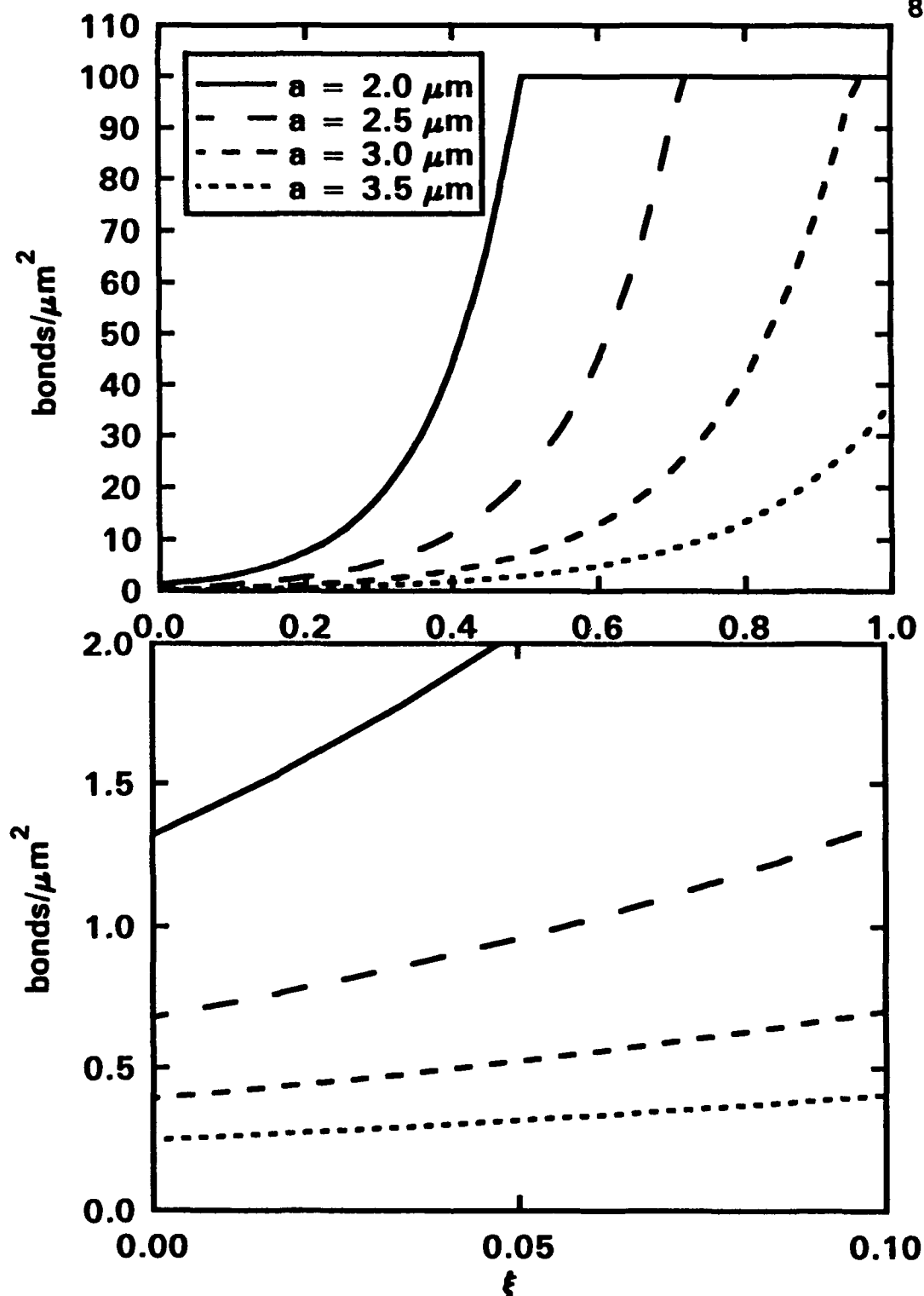


Figure 4.13 Effect of contact length on bond density distribution. (a) is full scale and (b) is a blow-up of the peeling edge. Analysis was performed using the following parameters; $c = 5$, $\delta = 0.10$, $t_w = 6.0 \text{ dyne/cm}^2$, $\tau_p = 0$, $f_o = 1.2 \times 10^5 \text{ dyne/bond}$, and $\tau_o = 0.035 \text{ dyne/cm}$.

in bond density distribution as a result of varying f_0 while keeping all other parameters constant (Figure 4.14). As expected, both the initial and final value of bond density decrease as the force per bond increases. However, within the small range of values ($1.5 \leq f_0 \leq 2.0 \times 10^{-5}$ dyne/bond) seen in Chapter 3 the variation in bond density is not great.

It is now of interest to compare the results obtained through this mechanical analysis to results obtained incorporating the kinetic behavior of the receptor-ligand bonds. As mentioned before, Tözeren and Ley (1992) analyzed the bond density distribution with a model taking into consideration bond kinetics and rolling kinematics. Figure 4.15 is a schematic of a rolling leukocyte used for their analysis. The model assumed the membrane shape to be a rigid cylinder and that the bonds had the mobility necessary for bond formation but no diffusivity. As the kinematics of rolling dictate, the adhesion bonds were first compressed than stretched during rolling. The compressed bonds were governed by both an attachment rate and detachment rate, while the stretched bonds were only governed by a detachment rate. Figure 4.16 shows the bond density distribution results Tözeren and Ley obtained. Implicit in their model was the assumption that the available leukocyte receptors interacted with their counter-receptors at any one instant. Therefore, the bond density reached the same maximum for both cases. The maximum bond density equaled the surface density of

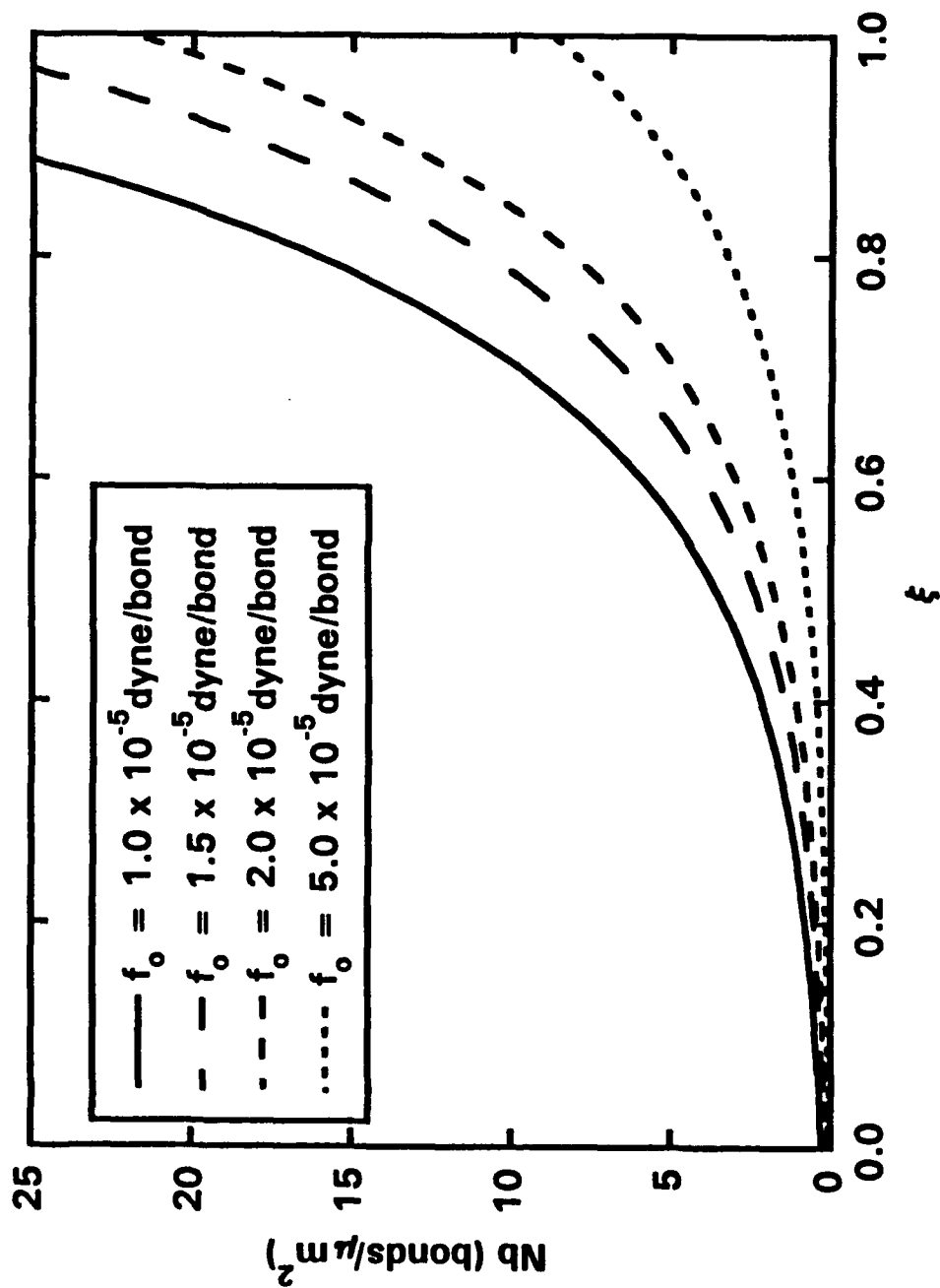


Figure 4.14 Bond density model sensitivity curves for f_o , the force per bond. The following variables were used in the model calculations; $c = 5$, $a = 3.5 \mu\text{m}$, $\delta = 0.10$, $\tau_w = 6.0 \text{ dyne}/\text{cm}^2$, $\tau_p = 0$, and $T_o = 0.035 \text{ dyne}/\text{cm}$.

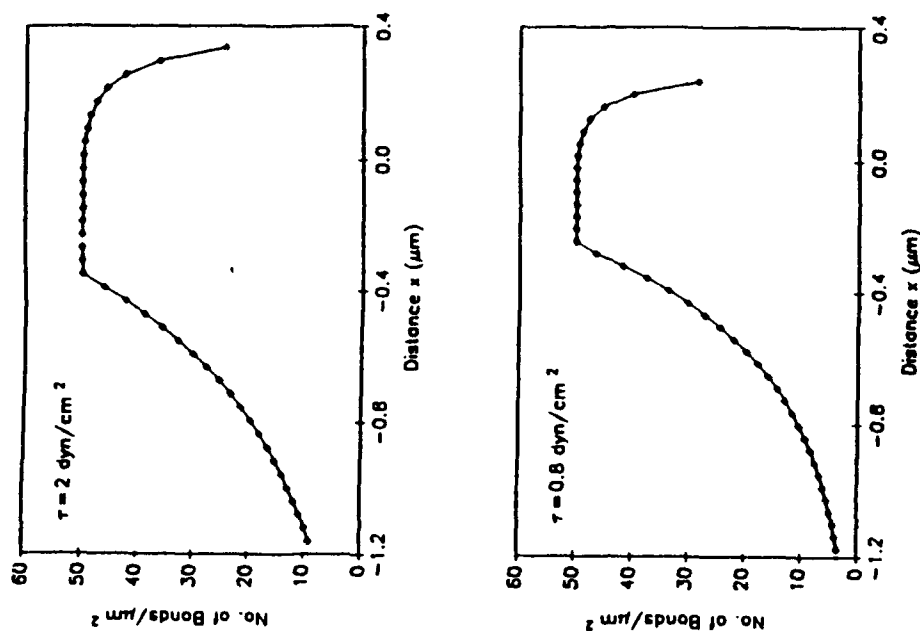


Figure 4.15 The schematic diagram of a leukocyte rolling on vascular endothelium. (Top) Geometric parameters used in the analysis are shown. (Bottom) Configuration of adhesion bonds in the contact area is shown schematically. (Reproduced from Tözzeren and Ley, 1992)

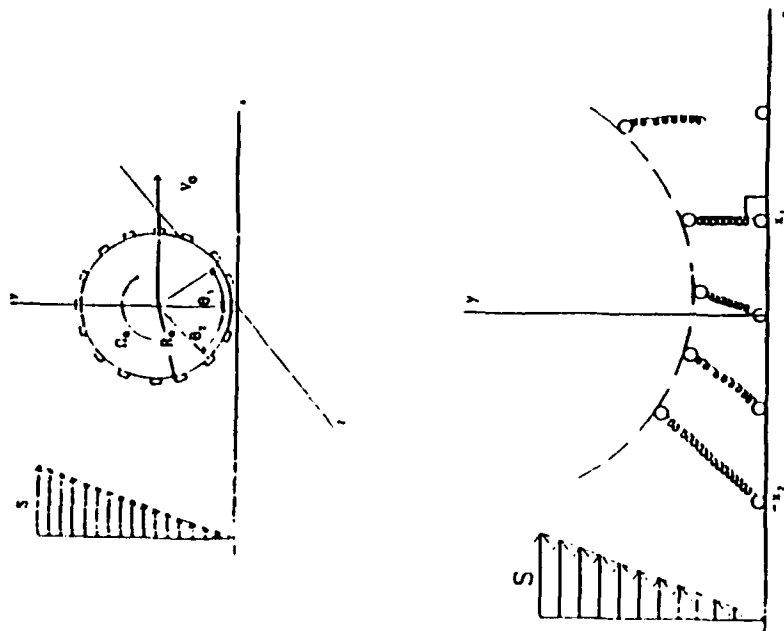


Figure 4.16 The surface density of adhesion bonds as a function of distance along the vascular endothelium (x). (Reproduced from Tözzeren and Ley, 1992)

endothelial receptors; the lower of the two receptor densities, leukocyte and endothelial. The number of stretched bonds in the detachment zone ($-1.2 \leq x \leq 0$) increased with increasing shear rate.

Figure 4.17 and 4.18 show the results obtained by the mechanical analysis presented here for similar conditions as used by Tözeren and Ley. The results obtained by Tözeren and Ley are also shown on the figure for comparison. The value of c used in Figure 4.17 is such that the bond length at the center of the contact area is very close to zero. Therefore, the bond density rose exponentially from a non-zero value at the peeling edge to the physiologic maximum, Nb_m , prior to the center of the contact area. In order to maintain the WBC adherent to the endothelium, one would expect that the bond distribution would shift to the left or the membrane shape would change to compensate for the bond density shortfall. Similar to the results obtained by Tözeren and Ley, the number of bonds within the contact region increases with shear stress. To keep the model results within physiologic range, the bonds at the center of the contact area were given a small initial amount of stretch by decreasing the parameter c . It is obvious from Figure 4.18 that the bond density required to keep the cell in equilibrium is drastically reduced when the bonds at the center can produce a greater force. Figure 4.18 also shows the same trends with shear stress as Figure 4.17. The mechanical model presented here correlates well with the kinetic and kinematic model introduced by Tözeren and Ley.

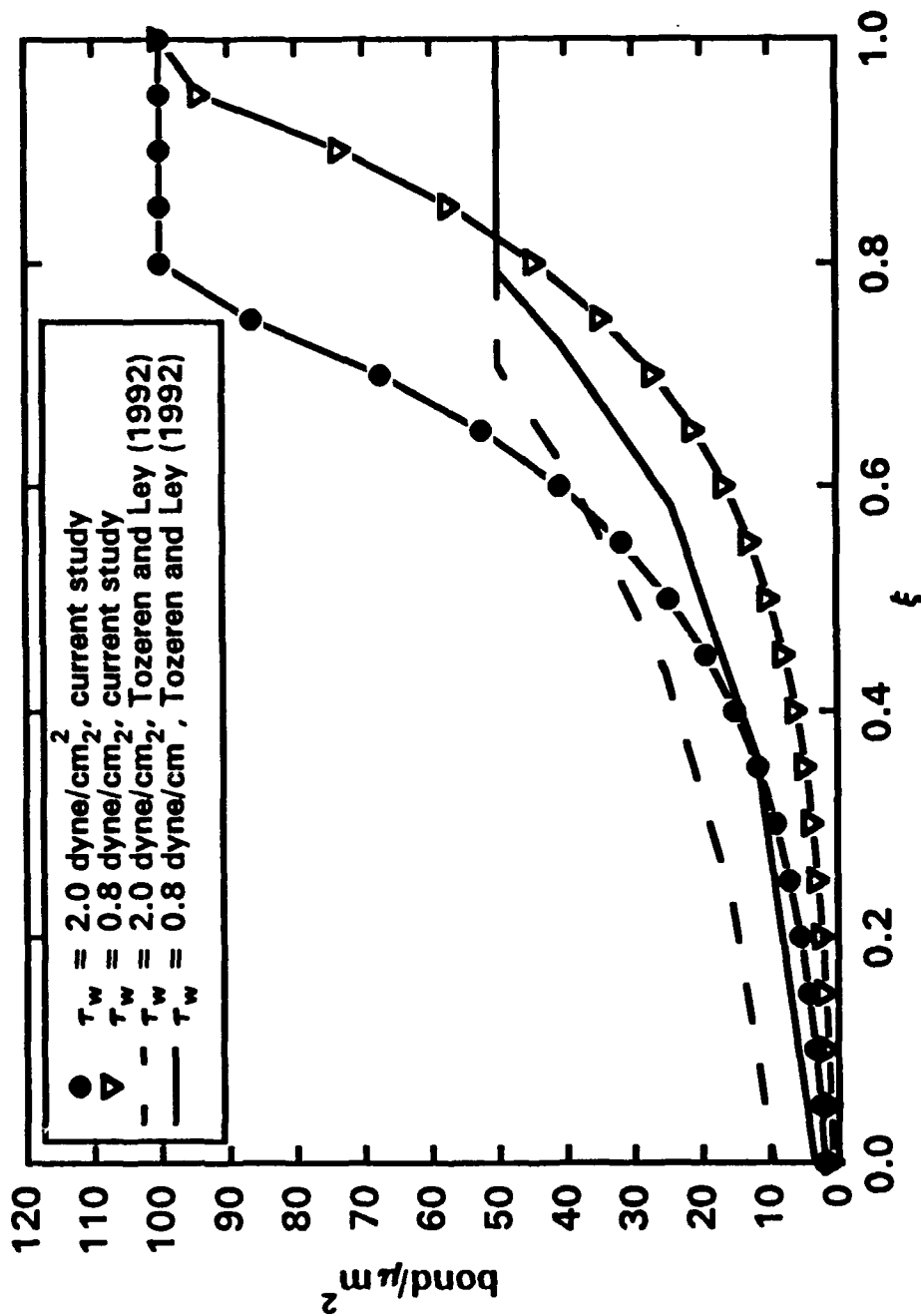


Figure 4.17 Bond density distribution for small membrane gap. Bond density distribution along the adherent membrane for the parameter values; $c = 5$, $a = 1.2 \mu\text{m}$, $\delta = 0.10$, $\tau_p = 0$, $f_0 = 1.2 \times 10^5$ dyne/bond, and $T_0 = 0.035$ dyne/cm. Wall shear stresses and contact area radius are the same as used by Tozeren and Ley (1992).

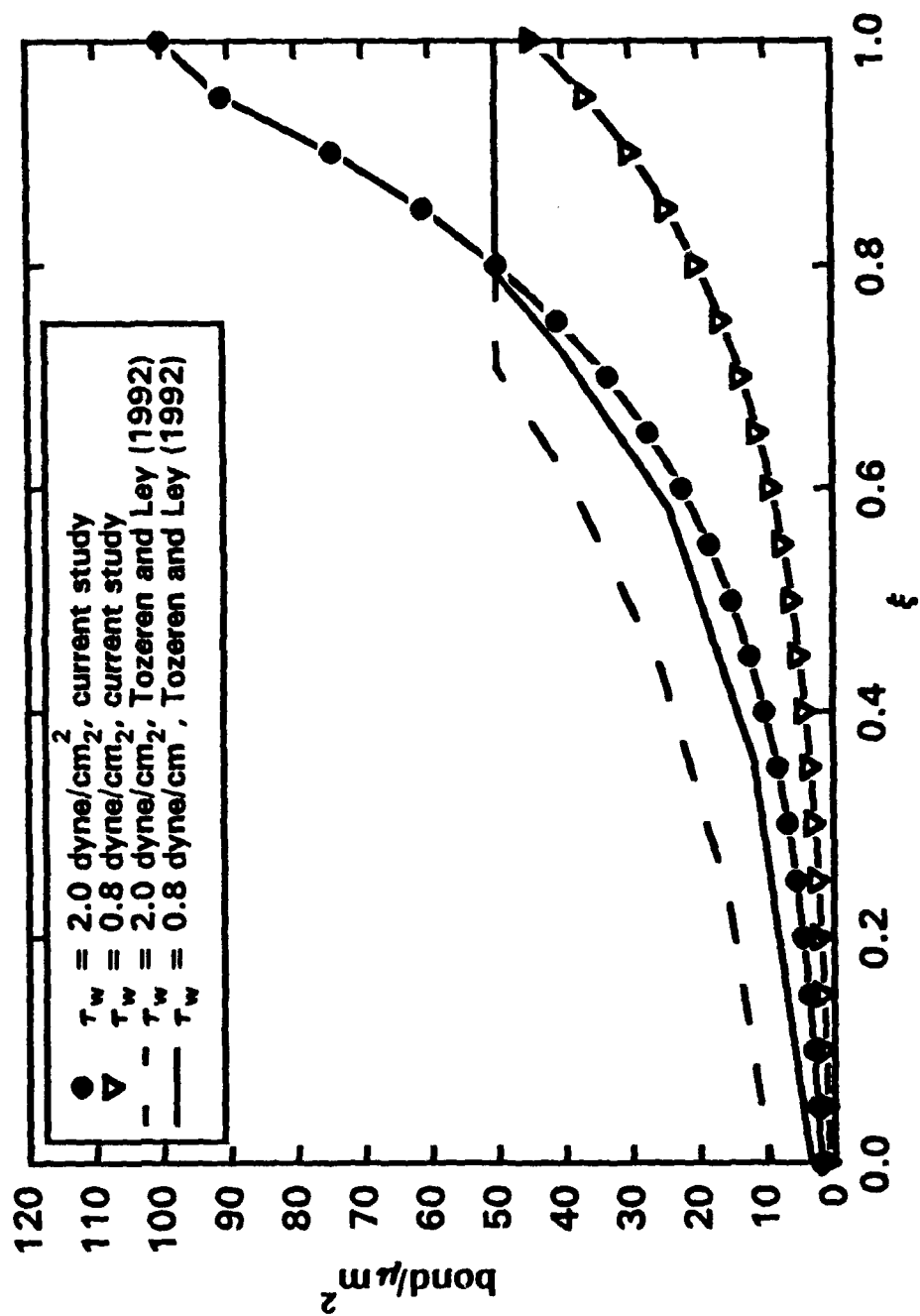


Figure 4.18 Bond density distribution for larger membrane gap. Bond density distribution along the adherent membrane for the parameter values; $c = 4$, $a = 1.2 \mu\text{m}$, $\delta = 0.10$, $\tau_p = 0$, $f_o = 1.2 \times 10^6$ dyne/bond, and $T_o = 0.035$ dyne/cm. Wall shear stresses and contact area radius are the same as used by Tozeren and Ley (1992).

Scott's pure kinetic model also produced a similar bond density curve as obtained here with the minimum bond concentration located at the peeling edge where $r = r_0$. The model assumed by Scott was of a flat linear membrane. The model in Scott's work produced a "fuller" curve where the exponential rise in bond density occurred prior to the half way point of the contact radius. As in both the mechanical model presented here and the model presented by Tözeren and Ley, the total number of bonds increased with shear rate.

Dembo *et al.*'s model incorporated both the peeling mechanics and bond kinetics. Their analysis also resulted in an exponential rise in bond density from the peeling edge reaching a constant value equal to the number of receptors available for bonding.

The mechanical analysis presented here provides remarkably similar results to that obtained by several different kinetic and kinematic models of bond density distribution. It has been shown the shape of the membrane in the adherent zone, the contact length, and the fluid shear stress all have a great effect on the number of bonds required within the adherent region to maintain the WBC in equilibrium. It is now of interest to incorporate the experimental results from Chapter 3 with the model presented here in order to analyze to the force equilibrium required to keep a WBC adherent to the EC under several conditions.

Chapter 5

Discussion of Bond Density Distributions for Control Conditions and FMLP and IL-1 Stimulated Adhesion

The *in vivo* measurements of transients in contact zone length yielded the force per bond (f_o) for control, FMLP, and IL-1 stimulated adhesion. These parameters, as listed in Table 5.1, were incorporated into the mechanical peeling analysis so that membrane bond density could be calculated for control conditions and stimulated adhesion. With the addition of f_o , a kinetic parameter was included in the model that was directly related to the life time of the bonds. The internal shear stress, τ_p , was assumed to be zero for all analysis.

Figures 5.1 through 5.3 depict the membrane distributions for displacement, bond density, normal stress, and membrane tension for control, FMLP, and IL-1, respectively. The membrane distributions are over the half of the contact area that is in tension normalized by the length of the contact radius.

The bond density was greatest for FMLP stimulated adhesion and least for IL-1 stimulated adhesion. Since the mean wall shear stress was greatest for FMLP, the bond density required to maintain the WBC in force equilibrium

Table 5.1

Model parameters and average bond density for control, FMLP, and IL-1 conditions.

Treatment	Radius of contact (μm)	Peeling region (δ)	c	τ_w (dyne/cm ²)	f_o (dyne/bond)	Average Nb (bonds/ μm^2)
Control n = 18	4.2	0.10	5	7.13	$1.638 \times 10^{-5} \pm 0.012 \times 10^{-5}$ SD	3.65 ± 0.02 SD
FMLP n = 13	4.4	0.10	5	11.65	$1.683 \times 10^{-5} \pm 0.007 \times 10^{-5}$ SD	5.05 ± 0.02 SD
IL-1 n = 12	5.1	0.10	5	7.43	$1.646 \times 10^{-5} \pm 0.009 \times 10^{-5}$ SD	2.12 ± 0.02 SD

* Values given for f_o and average Nb are means and standard deviations (SD). Standard deviations for average Nb are due to f_o SD.

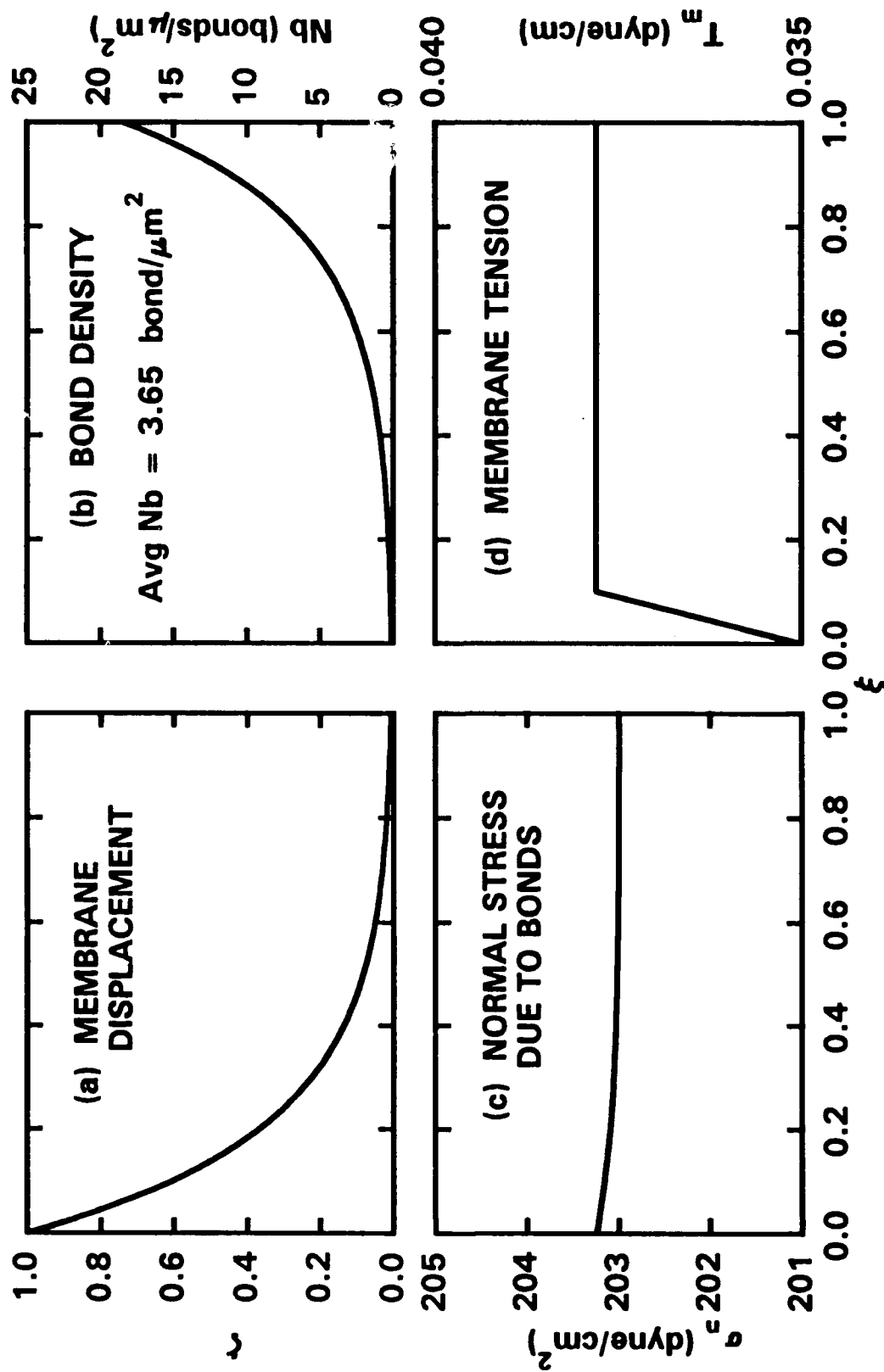


Figure 5.1 Membrane distributions for WBC adhesion under control conditions. Analysis was performed with $\tau_w = 7.13 \text{ dyne/cm}^2$, $a = 4.2 \mu\text{m}$, $\delta = 0.10$, $c = 5$, $f_o = 1.64 \times 10^{-5} \text{ dyne/bond}^2$ and $T_o = 0.035 \text{ dyne/cm}$. Average bond density for control conditions was $3.65 \text{ bonds}/\mu\text{m}^2$.

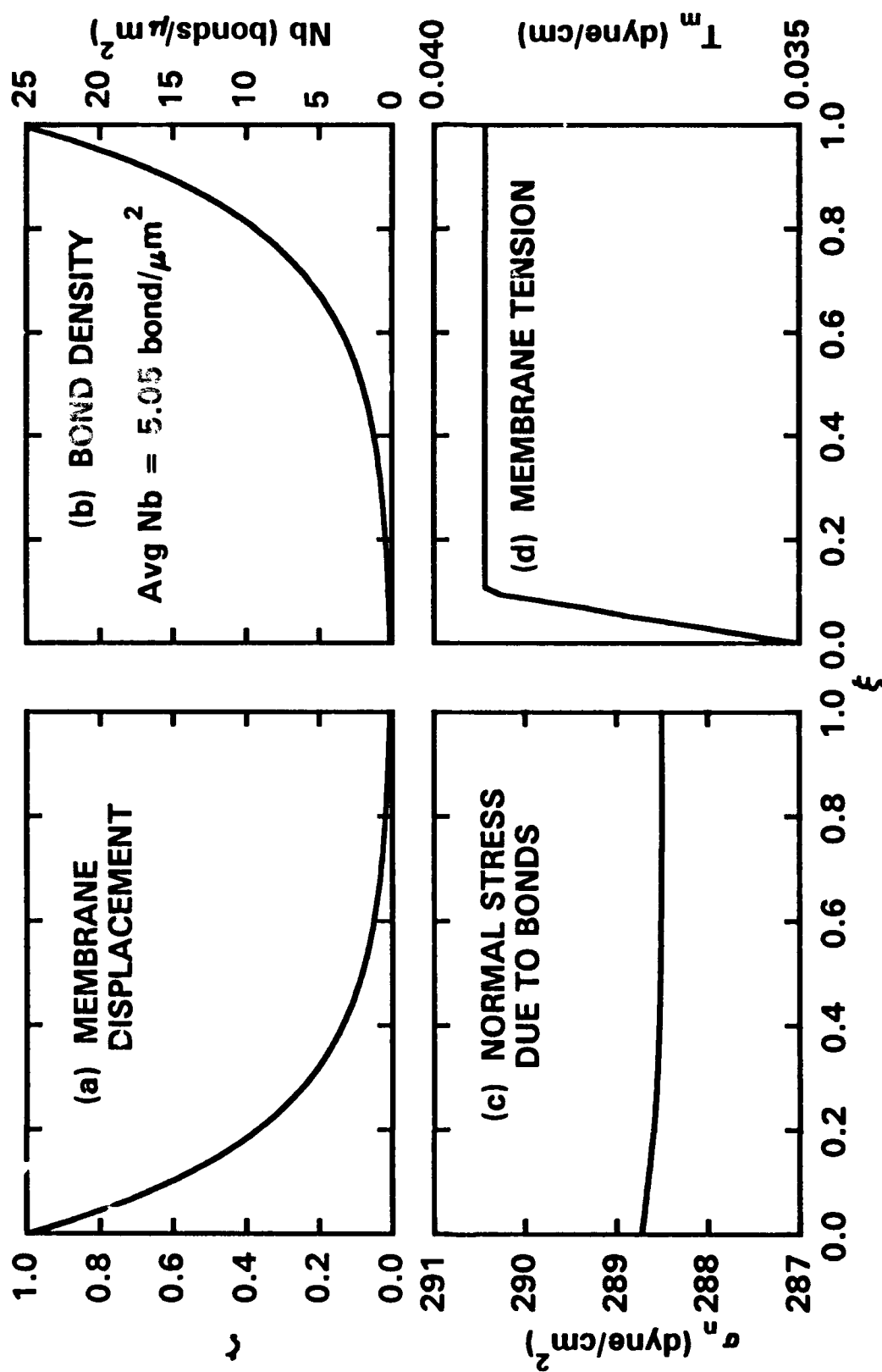


Figure 5.2 Membrane distributions for WBC FMLP stimulated adhesion. Analysis was performed with $\tau_w = 11.65$ dyne/cm², $a = 4.4$ μm , $\delta = 0.10$, $c = 5$, $f_o = 1.68 \times 10^{-5}$ dynes/bond and $T_o = 0.035$ dyne/cm. Average bond density for FMLP stimulated adhesion was 5.05 bonds/ μm^2 .

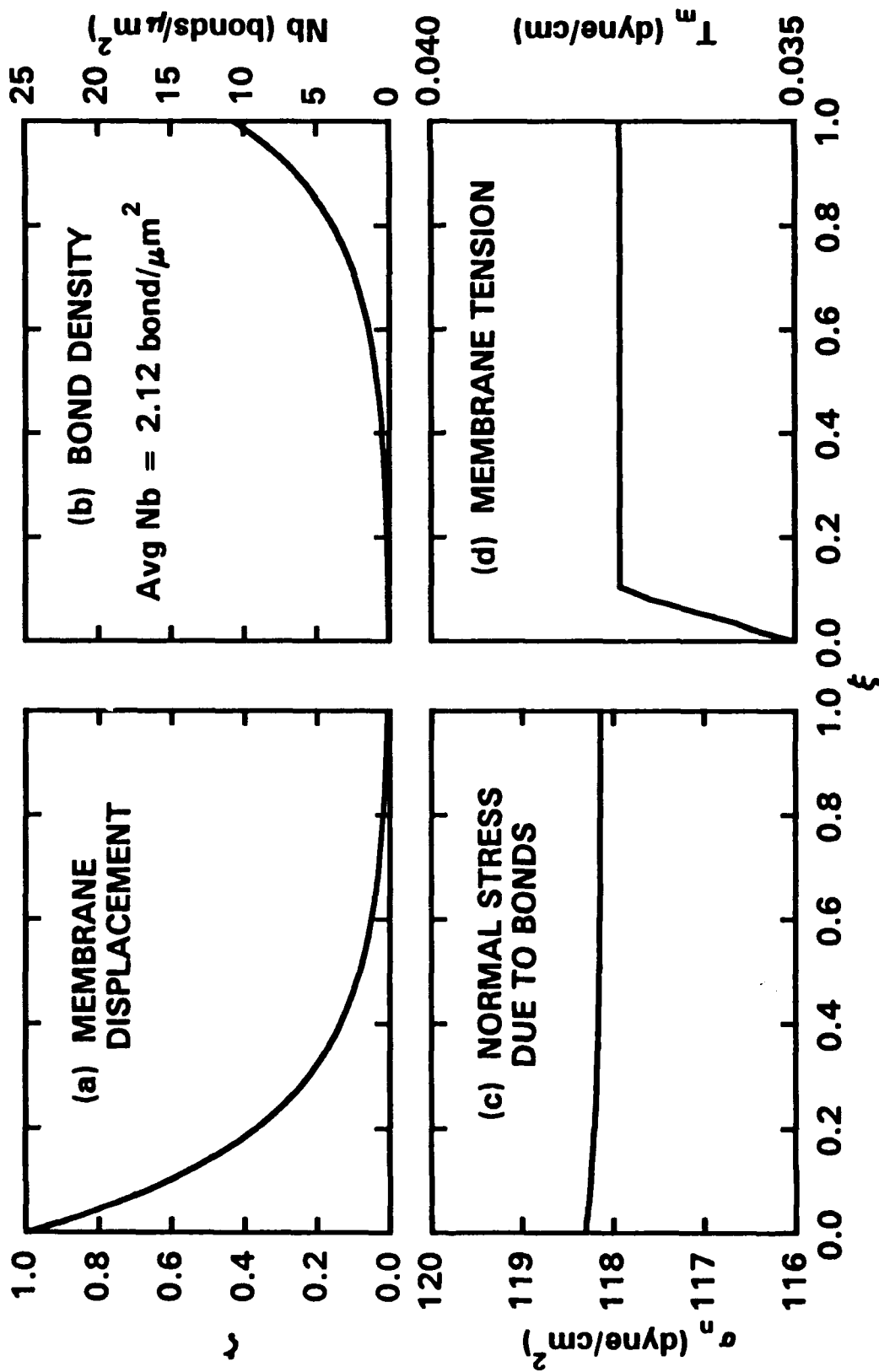


Figure 5.3 Membrane distributions for WBC IL-1 stimulated adhesion. Analysis was performed with $\tau_w = 7.43$ dyne/cm², $a = 5.1$ μm , $\delta = 0.10$, $c = 5$, $f_o = 1.65 \times 10^{-5}$ dynes/bond and $T_o = 0.035$ dyne/cm. Average bond density for IL-1 stimulated adhesion was 2.12 bonds/ μm^2 .

was greatest even though the force per bond was also the largest for FMLP. In order to accurately assess the contribution that the increased value of f_o played in determining the average bond density for FMLP stimulated adhesion, Figure 5.4 depicts the average bond density versus the force per bond, f_o , holding all other parameters constant. It is clear from this figure that for $f_o \leq 2.5 \times 10^{-5}$ dyne/bond small changes in bond force will have a large effect on the average bond density required to maintain the WBC in force equilibrium. However, for the very small variations in f_o determined for the three conditions from the peeling measurements, there will be a minimal effect on the potential number of adhesion bonds. IL-1 stimulated adhesion and adhesion under control conditions occurred at similar hemodynamic forces and yielded nearly identical values of force per bond. Yet, the required bond density was less for IL-1 stimulated adhesion. The reason for the difference is due to the increased mean contact length seen with IL-1. Figure 5.5 is a composite of the bond density distributions for all three conditions. The average bond densities calculated for each condition for a unit depth are shown in Figure 5.6. The average bond density for FMLP was $5.05 \text{ bonds}/\mu\text{m}^2$ versus $3.65 \text{ bonds}/\mu\text{m}^2$ for control and $2.12 \text{ bonds}/\mu\text{m}^2$ for IL-1 stimulated adhesion. The standard deviations for the average bond densities in Table 5.1 and Figure 5.6 were derived from the standard deviations in f_o .

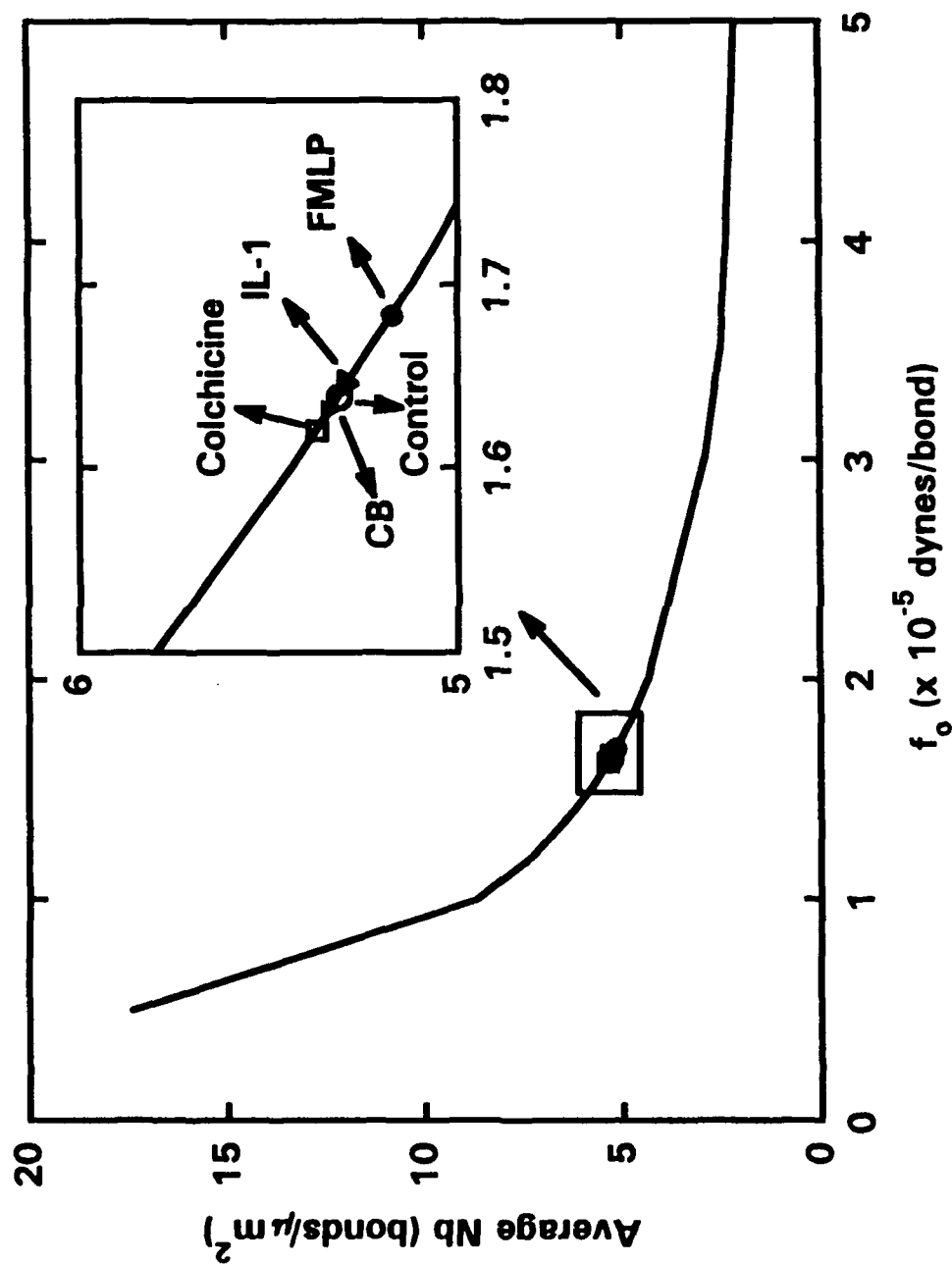
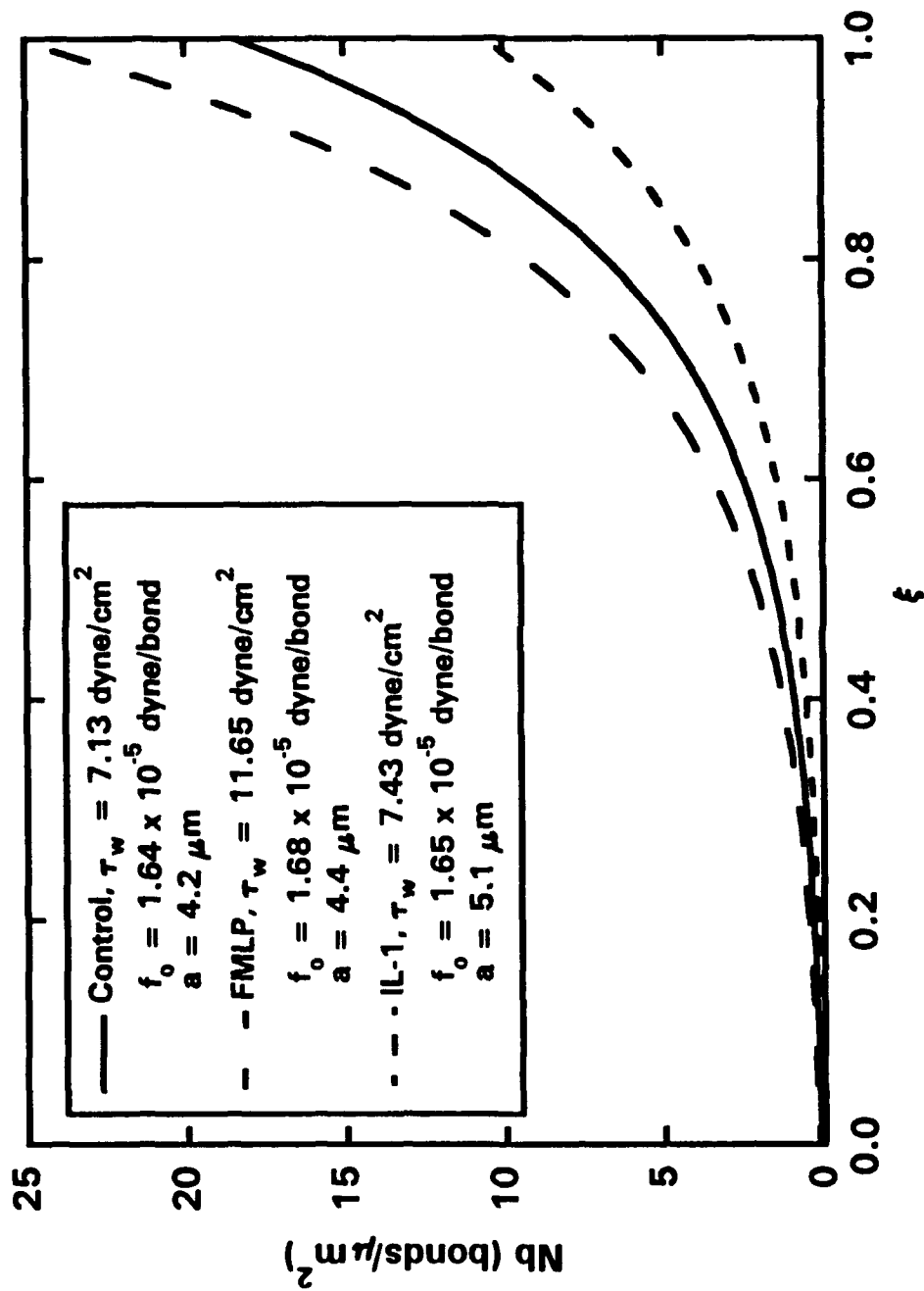
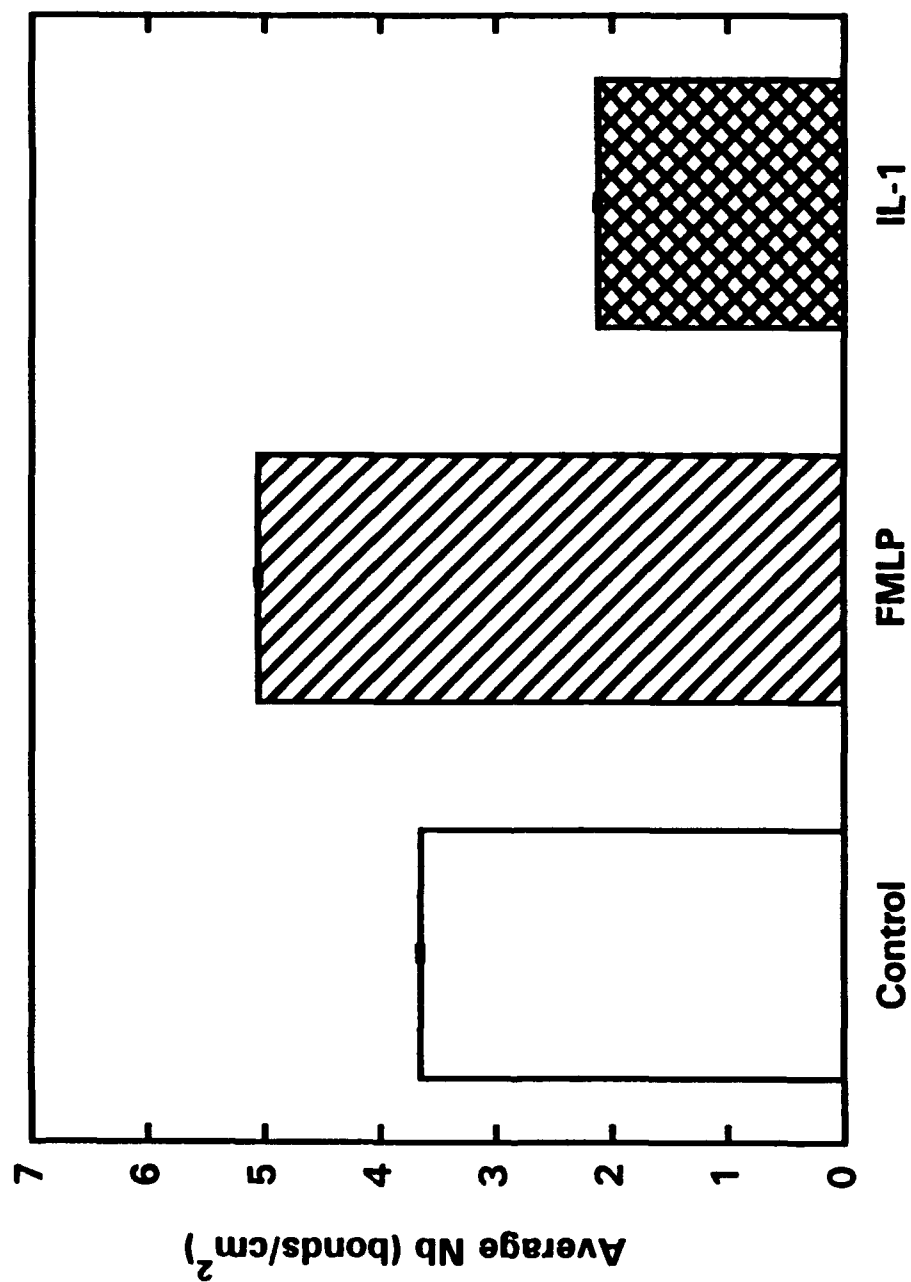


Figure 5.4 Average bond density versus force per bond. Analysis was performed with $a = 3.5 \mu\text{m}$, $\delta = 0.10$, $c = 5$, $\tau_w = 6 \text{ dyne/cm}^2$, $\tau_p = 0$, and $T_o = 0.035 \text{ dyne/cm}$. The inset graph is a blow-up of the boxed region depicting the average bond density for each of the experimental conditions for f_o determined through the peeling process.



5.5 Bond density comparison for control conditions and FMLP and IL-1 stimulated adhesion. Analysis was performed for the parameter listed above and $c = 5$, $\delta = 0.10$, and $T_o = 0.035$ dyne/cm.



5.6 Average bond density for control conditions and FMLP and IL-1 stimulated adhesion. The error bars represent the variance in Nb due to the standard deviation for f_0 .

Since $\sigma_n = f \cdot Nb$, it is not surprising to see that bond normal stress followed the same trends as bond density being greatest for FMLP and least for IL-1. The order of magnitude of normal stress was within the same range as cited by Schmid-Schönbein and others (1975) for the normal stress of interaction between the WBC and endothelium. The total force can be calculated for each condition by integrating the stress distribution over the area. Since the stress distribution was nearly constant, an approximation of total force was made by multiplying the initial stress, σ_o , by the contact area (πa^2) taken at t_p . This yielded the total force for each condition required to maintain the WBC in static equilibrium with the EC as follows; for control conditions - 1.13×10^{-4} dynes, for FMLP - 1.76×10^{-4} dynes and for IL-1 stimulated adhesion - 1.539×10^{-4} dynes. The order of magnitude obtained for force were consistent with in vitro experimental data obtained by Tözeren *et al.* (1989) for cell to cell adhesion of a cytotoxic T-cell and a target cell separated using micromanipulation techniques.

While the normal stress was almost twice as great for control versus IL-1, the membrane tension distributions were comparable. In the present analysis, the membrane tension was dictated solely by the hemodynamic stress, T_o , and the distance along the peeling edge, δ . Therefore, bond density and normal stress distribution did not appreciably affect T_m . Since the wall shear stress for control and IL-1 stimulated adhesion was virtually the same, so were the T_m distributions.

A number of inferences can be made from the discussion above. First, the increased strength of adhesion seen with FMLP does not appear to be due to the avidity of the bond but rather the increased bond density. Secondly, deformability plays a significant role in decreasing the required bond density by increasing the contact area between the WBC and EC as clearly shown in the comparison between the control condition and IL-1 stimulated adhesion.

Chapter 6

Summary and Conclusion

Both WBC-EC contact angle and contact length versus wall shear stress gave a relatively good measure of cell deformability that was consistent with previously reported data. Contact length increased while adhesive bonds were being formed and decreased when the rate of bonds breaking exceeded the rate of bond formation. This transition time was identified as the time to peeling coincident with the maximum contact length. The disruption of WBC-EC bonds as indicated by the time to peeling appeared to be consistent with the kinetic theory of fracture. Using the kinetic theory of fracture, the bond adhesion energy and bond force under control conditions, FMLP and IL-1 stimulated adhesion, and CB and colchicine treatment were elucidated. The bond adhesion energy and bond force were significantly greater for FMLP as compared to control and IL-1; however, not by a great enough magnitude to conclude whether a different type of bond or bonding mechanism was involved. Since the bond adhesion energy was statistically the same for both control and IL-1 activated adhesion, it was concluded that both conditions induced WBC sticking through similar mechanisms.

A theoretical analysis was presented in which the bond density, normal stress, and membrane tension distributions were elucidated for an adherent WBC in shear flow. The WBC membrane was considered as a cortical shell with an assumed shape. In order to maintain the cell in static equilibrium, the adhesive forces due to the bonds keeping the WBC stuck to the EC were required to equal the hemodynamic forces tending to peel the WBC off the EC. It was seen that both shear stress magnitude and deformability, as indicated by contact length, were important parameters in determining the bond density distribution. The model provided an estimate of bond density, normal stress, and membrane tension that was consistent with other kinetic based analysis.

The values of f_0 determined experimentally for control, FMLP, and IL-1 were incorporated into the model along with the mean hemodynamic parameters for each of these conditions. The inclusion of f_0 into the mechanical model incorporated a kinetic parameter that was directly related to the bond life time. The average bond density varied for control versus IL-1 even though the hemodynamic force and bond force were nearly identical. The average bond density was lower for IL-1 due to the increased contact area. Finally, since the avidity of the receptor-ligand bonds for integrin (FMLP) versus selectin (IL-1) adhesion was similar in magnitude, the FMLP adhesion appeared to be much stronger due to the increase in average bond density as calculated using the theoretical model rather than the bond force.

One may speculate as to the plausible physiologic consequence of this conclusion. Selectin mediated adhesion, as demonstrated with IL-1 treatment, occurs in response to low levels of antigens and primes the system for a greater immune response through integrin mediated WBC adhesion. This pre-activation includes the influx of WBCs into the area of inflammation and increased WCB rolling along the post-capillary venular endothelium. This is in accord with the lower levels of adhesive force seen in the present study for IL-1. Integrin mediated adhesion, as demonstrated with FMLP, is the primary cellular immune response resulting in not only increased WBC adhesion but greater cell motility; therefore, precipitating the emigration of WBCs through the microvessel walls. In this light, the results obtained for FMLP stimulated adhesion are consistent with the critical role integrin mediated adhesion plays in the body's response to acute infection.

The present study logically leads to ideas for future research. It would be advantageous for both the study of the peeling process and WBC deformability to control the wall shear stress using a technique, such as, micro-occlusion. The use of monoclonal antibodies to block one or more of the receptors on the WBC or EC could lead to a more precise interpretation of the role of the individual adhesion molecules. Finally, the theoretical analysis could be improved so that the membrane shape could be determined analytically and cell deformability included.

References

- ADAMSON, A. W. (1976). "Physical Chemistry of Surfaces" 340-341. John Wiley & Sons, Inc. New York.
- ASAKO H., KUBES, P., BAETHGE, B. A., WOLF, R. E., AND GRANGER D. N. (1992). Colchicine and methotrexate reduce leukocyte adherence and emigration in rat mesenteric venules. *Inflammation* 16, 45-56.
- ATHERTON, A. AND BORN, G. V. R. (1973) Relationship between the velocity of rolling granulocytes and that of the blood flow in venules. *J. Physiol.* 233, 157-165.
- BAGGE, U. (1984). Leukocytes and capillary perfusion in shock. *In* "White Cell Mechanics: Basic Science and Clinical Aspects" (H. J. Meiselman, M. A. Lichtman, and P. L. LaCelle, Eds.), 16, 285-294. Alan R. Liss, Inc., New York.
- BARROSO-ARNANDA, J., SCHÖNBEIN-SCHMID, G. W., ZWEIFACH, B. W., AND ENGLER, R. L. (1988). Granulocytes and no-reflow phenomenon in irreversible hemorrhagic shock. *Circ. Res.* 63, 437-447.
- BELL, G. I. (1978). Models for the Specific Adhesion of Cells to Cells. *Science* 200, 618-627.
- BELL, G. I., DEMBO, M., AND BONGRAND, P. (1984). Cell adhesion - competition between nonspecific repulsion and specific bonding. *Biophys. J.* 45, 1051-1064.
- COOPER, J. A. (1987). Effects of cytochalasin and phalloidin on actin. *J. Cell Biol.* 105, 1473-1478.
- DAHLGREN, M. D., PETERSON, M. A., ENGLER, R. L., AND SCHONBEIN-SCHMID, G. W. (1984). Leukocyte rheology in cardiac ischemia. *In* "White Cell Mechanics: Basic Science and Clinical Aspects" (H. J. Meiselman, M. A. Lichtman, and P. L. LaCelle, Eds.), Vol. 16, pp. 271-283. Alan R. Liss, Inc., New York.

- DEMBO, M., TORNEY, D. C., SAXMAN, K., AND HAMMER, D. (1988). The reaction-limited kinetics of membrane-to-surface adhesion and detachment. *Proc. R. Soc. Lond.* **234**, 55-83.
- DONG, C., SKALAK, R., SUNG, K. P., SCHMID-SCHÖNBEIN, G. W., AND CHIEN, S. (1988). Passive deformation analysis of human leukocytes. *J. Biomech. Eng.* **110**, 27-36.
- ENGLER, R. L., SCHMID-SCHÖNBEIN, G. W., AND PAVELEC, R. S. (1983). Leukocyte capillary plugging in myocardial ischemia and reperfusion in the dog. *Am. J. Pathol.* **111**, 98-111.
- ENGLER, R. L., DAHLGREN, M. D., MORRIS, D. D., PERTERSON, M. A., AND SCHÖNBEIN-SCHMID, G. W. (1986). Role of leukocytes in response to acute myocardial ischemia and reflow in dogs. *Am. J. Physiol.* **251**, H314-H322.
- ENGLER, R. L. (1989). Free radical and granulocyte-mediated injury during myocardial ischemia and reperfusion. *Am. J. Cardiol.* **63**, 19E-23E.
- EVANS, E. A. (1985). Detailed mechanics of membrane-membrane adhesion and separation. *Biophys. J.* **48**, 175-183.
- EVANS, E. A. AND YEUNG, A. (1989). Apparent viscosity and cortical tension of blood granulocytes determined by micropipet aspiration. *Biophys. J.* **56**, 151-160.
- FIGDOR, C. G. AND VAN KOOYK (1992). Regulation of Cell Adhesion. In "Adhesion - Its Role in Inflammatory Disease" (J. M. Harlan and D. Y. Liu, Eds.), 117-150. W. H. Freeman and Company, New York.
- FIRRELL, J. C. AND LIPOWSKY, H. L. (1989). Leukocyte margination and deformation in mesenteric venules of rat. *Am. J. Physiol.* **256**, H1667-H1674.
- FLUGGE, W. (1962). "Stresses in Shells" 18-21. Springer-Verlag, Berlin.
- GRANGER, D. N., BENOIT, J. N., SUZUKI, M., AND GRISHAM, M. B. (1989). Leukocyte adherence to venular endothelium during ischemia-reperfusion. *Am. J. Physiol.* **257**, G683-G688.

- GRANT, L. (1973). The sticking and emigration of white blood cells in inflammation. *In* "The Inflammatory Process - II" (B. W. Zweifach, L. Grant, and R. T. McCluskey, Eds.), 205-244. Academic Press, New York.
- HAMMER, D. A. AND LAUFFENBURGER D. A. (1989). A dynamical model for receptor-mediated cell adhesion to surfaces in viscous shear flow. *Cell Biophys.* 14, 139-173.
- HARLAN, J. M., WINN, R. K., VEDDER, N. B., DOERSCHUK, C. M., AND RICE, C. L. (1992). *In vivo* models of leukocyte adherence to endothelium. *In* "Adhesion - Its Role in Inflammatory Disease" (J. M. Harlan and D. Y. Liu, Eds.), 117-150. W. H. Freeman and Company, New York.
- HOUSE S. D. AND LIPOWSKY H. L. (1987). Leukocyte-endothelium adhesion: microhemodynamics in mesentery of the cat. *Microvas. Res.* 34, 363-379.
- HOUSE S. D. AND LIPOWSKY H. L. (1988). *In vivo* determination of the force of leukocyte-endothelium adhesion in the mesenteric microvasculature of the cat. *Circ. Res.* 63, 658-668.
- HOUSE S. D. AND LIPOWSKY H. L. (1991). Dynamics of leukocyte-endothelium interactions in the splanchnic microcirculation. *Microvas. Res.* 42, 288-304.
- KAWAOKA, E. J., MILLER, M. E., AND CHEUNG, A. T. (1981). Chemotactic factor-induced effects upon deformability of human polymorphonuclear leukocytes. *J. Clin. Immunol.* 1, 41-44.
- LASKY, L. A. (1992). The homing receptor (LECAM 1/L selectin): a carbohydrate-binding mediator of adhesion in the immune system. *In* "Adhesion - Its Role in Inflammatory Disease" (J. M. Harlan and D. Y. Liu, Eds.), 117-150. W. H. Freeman and Company, New York.
- LAWRENCE, M. B. AND SPRINGER, T. A. (1991). Leukocytes roll on a selectin at physiologic flow rates: distinction from and prerequisite for adhesion through integrins. *Cell* 65, 859-873.
- LEY, K., GAEHTGENS, P., AND SPANEL-BOROWSKI, K. (1992). Differential adhesion of granulocytes to five distinct phenotypes of cultured microvascular endothelial cells. *Microvas. Res.* 43, 119-133.

- LIPOWSKY, H. H. AND ZWEIFACH, B. W. (1978). Application of the "two-slit" photometric technique to the measurement of microvascular volumetric flow rates. *Microvas. Res.* **15**, 93-101.
- LIPOWSKY, H. H., RIEDEL, D., AND SHI, G. S. (1991). *In vivo* mechanical properties of leukocytes during adhesion to venular endothelium. *Biorheology* **28**, 53-64.
- MAYROVITZ, H. N. AND WIEDEMAN, M. P. (1976). Leukocyte adhesiveness as influenced by blood velocity. In "Microcirculation" (J. Grayson and G. Zingg, Eds.), 128-129. Plenum Press, New York.
- MAYROVITZ, H. N., WIEDEMAN, M. P., AND TUMA, R. F. (1977). Factors influencing leukocyte adherence in microvessels. *Thromb. Haemostasis* **38**, 823-830.
- MAYROVITZ, H. N., KANG, S. J., HERSCOVICI, B., AND SAMPSELL, R. N. (1987). Leukocyte adherence initiation in skeletal muscle capillaries and venules. *Microvas. Res.* **33**, 22-34.
- SCHMID-SCHÖNBEIN, G. W., FUNG, Y. C., AND ZWEIFACH, B. W. (1975). Vascular endothelium-leukocyte interaction, sticking shear force in venules. *Circ. Res.* **36**, 173-184.
- SCHMID-SCHÖNBEIN, G. W., USAMI, S., SKALAK, R., AND CHIEN, S. (1980). The interaction of leukocytes and erythrocytes in capillary and postcapillary vessels. *Microvas. Res.* **19**, 45-70.
- SCHMID-SCHÖNBEIN, G. W., SKALAK, R., SIMON, S. I., AND ENGLER, R. L. (1987). The interaction between leukocytes and endothelium *in vivo*. In "Blood in Contact with Natural and Artificial Surfaces" (E. F. Leonare, V. Turito, and L. Vroman, Eds.), 348-361. NY Acad. Sci., New York.
- SCHMID-SCHÖNBEIN, G. W. AND ENGLER, R. L. (1990). Perspectives of leukocyte activation in the microcirculation. *Biorheology* **27**, 859-869.
- SCOTT, D. A. (1992). "In Vivo Mechanics of Leukocyte Rolling on Venular Endothelium: The Role of Deformability and Adhesion", M.S. Thesis, Bioengineering Program, The Pennsylvania State University, University Park, PA.

- SUZUKI, M., ASAKO, H., KUBES, P., JENNINGS, S., GRISHAM, M. B., AND GRANGER, D. N. (1991). Neutrophil-derived oxidants promote leukocyte adherence in postcapillary venules. *Microvas. Res.* **42**, 125-138.
- TÖZEREN, A. AND SKALAK, R. (1977). Stress in a suspension near rigid boundaries. *J. Fluid Mech.* **82**, 289-307.
- TÖZEREN, A., SUNG, K. L. P., AND CHIEN, S. (1989). Cross-bridge migration during cell disaggregation. *Biophys. J.* **55**, 479-487.
- TÖZEREN, A. AND LEY K. (1992). How do selectins mediate leukocyte rolling in venules. *Biophys. J.* **63**, 700-709.
- VADAS, M. A., GAMBLE, J. R., AND SMITH, W. B. (1992). Regulation of myeloid blood cell-endothelial interaction by cytokines. *In* "Adhesion - Its Role in Inflammatory Disease" (J. M. Harlan and D. Y. Liu, Eds.), 65-81. W. H. Freeman and Company, New York.
- ZHURKOV, S. N. (1965). Kinetic concept of the strength of solids. *Int. J. Fract. Mech.* **1**, 311-323.

Appendix A
Hemodynamic Data

A.1 Hemodynamic Data - Control

CELL ID	DATE	TIME	V _{rec} (mm/sec)	DIAM (μ m)	SHEAR RATE (s ⁻¹)	τ_w (dyne/cm ²)
CONT1	8/2/88	15:21:19:26	3.00	43.3	346.44	8.661
CONT2	8/2/88	15:22:57:32	3.00	43.3	346.44	8.661
CONT3	8/4/88	00:54:11:26	1.40	33.0	212.12	5.303
CONT4	8/11/88	12:51:29:52	1.40	16.20	432.08	10.802
CONT5	8/11/88	13:00:09:49	1.40	20.00	323.00	8.075
CONT6	8/2/88	15:20:51:16	3.00	43.30	346.44	8.661
CONT7	10/28/88	10:55:11:16	1.05	40.00	131.00	3.275
CONT8	8/3/92	13:00:38:65	2.00	25.90	386.10	9.653
CONT9	8/13/92	12:37:21:84	1.40	22.70	308.37	7.709
CONT10	8/13/92	12:37:49:81	1.50	20.00	375.00	9.375
CONT11	8/13/92	12:50:20:32	0.90	20.30	221.68	5.542
CONT12	8/13/92	12:56:27:33	0.75	20.20	185.64	4.641
CONT13	8/19/92	11:51:42:29	1.20	23.60	254.00	6.350
CONT14	8/13/92	12:30:16:03	1.00	19.60	271.52	6.788
CONT15	8/13/92	12:32:01:13	1.00	19.40	257.72	6.443
CONT16	8/13/92	12:34:19:92	1.00	19.40	257.72	6.443

CELL ID	DATE	TIME	V_{rec} (mm/sec)	DIAM (μ m)	SHEAR RATE (s^{-1})	τ_w (dyne/cm ²)
CONT17	8/13/92	12:37:07:19	1.40	20.00	350.00	8.750
CONT18	7/30/92	12:43:56:39	0.60	25.00	120.00	3.000
MEAN	--	--	1.50	26.40	285.35	7.12
\pm S.D.	--	--	0.76	9.57	88.67	2.22

A.2 Hemodynamic Data - FMLP

CELL ID	DATE	TIME	V _{rec} (mm/sec)	DIAM (μ m)	SHEAR RATE (s ⁻¹)	τ_w (dyne/cm ²)
FMLP1	8/5/88	00:42:23:45	2.00	26.0	384.20	9.605
FMLP2	9/1/88	12:48:10:10	2.30	32.0	395.40	9.885
FMLP3	12/5/88	00:47:29:70	2.50	26.3	475.32	11.883
FMLP4	8/5/88	00:44:39:05	2.30	28.0	410.72	10.268
FMLP5	12/5/88	00:44:06:32	2.20	27.6	398.60	9.965
FMLP6	8/11/88	13:46:23:84	2.60	28.0	464.28	11.607
FMLP7	8/19/88	14:38:42:56	1.60	39.0	205.12	5.128
FMLP8	9/1/88	11:53:12:42	3.00	22.0	681.80	17.045
FMLP9	9/1/88	11:53:51:36	3.00	22.0	681.80	17.045
FMLP10	9/1/88	11:54:43:92	3.00	22.0	681.80	17.045
FMLP11	9/1/88	12:19:38:56	3.00	22.0	681.80	17.045
FMLP12	9/1/88	12:24:21:66	1.80	33.0	272.72	6.818
FMLP13	9/1/88	12:48:14:90	2.30	32.0	375.40	9.385
MEAN	--	--	2.43	27.69	465.95	11.65
\pm S.D.	--	--	0.48	5.23	165.52	4.14

A.3 Hemodynamic Data - IL-1

CELL ID	DATE	TIME	V _{asc} (mm/sec)	DIAM (μ m)	SHEAR RATE (s ⁻¹)	τ_w (dyne/cm ²)
IL1	11/1/88	04:26:49:29	1.60	23.0	347.80	8.695
IL2	11/1/88	03:34:14:25	2.30	31.8	170.20	4.255
IL3	11/1/88	04:44:27:26	1.60	23.0	347.80	8.695
IL4	11/1/88	04:45:03:70	1.60	23.0	347.80	8.695
IL5	11/1/88	05:04:35:97	1.60	23.0	347.80	8.695
IL6	11/1/88	05:04:53:02	1.60	23.3	347.80	8.695
IL7	11/11/88	15:20:59:89	0.70	18.0	194.40	4.860
IL8	11/11/88	13:24:31:33	1.10	27.5	200.00	5.000
IL9	11/16/88	15:33:50:66	2.50	31.6	395.60	9.890
IL10	11/16/88	15:41:41:09	2.50	31.0	403.20	10.080
IL11	11/1/88	03:44:52:71	1.00	30.6	163.40	4.085
IL12	11/1/88	03:39:26:13	0.70	31.9	109.72	2.743
MEAN	--	--	1.57	26.45	297.26	7.43
\pm S.D.	--	--	0.63	4.81	100.43	2.51

A.4 Hemodynamic Data - CB

CELL ID	DATE	TIME	V _{asc} (mm/sec)	DIAM (μ m)	SHEAR RATE (s ⁻¹)	τ_w (dyne/cm ²)
CB1	11/29/88	05:08:20:10	1.50	22.7	330.40	8.260
CB2	11/29/99	05:11:32:69	1.30	25.5	254.92	6.373
CB3	11/29/88	05:12:25:19	1.30	25.5	254.92	6.373
CB4	11/29/88	05:48:43:66	1.20	23.3	257.52	6.438
CB5	11/28/88	13:01:06:43	1.20	22.8	263.16	6.579
CB6	11/28/88	13:12:49:12	1.80	25.2	357.16	8.929
CB7	11/28/88	13:13:12:65	2.00	25.2	396.84	9.921
CB8	11/28/88	13:13:40:02	2.00	24.1	414.92	10.373
CB9	11/28/88	13:42:54:37	1.50	21.5	348.84	8.721
CB10	11/28/88	13:55:42:12	1.70	20.6	412.64	10.316
CB11	11/28/88	13:15:42:65	2.30	25.5	451.00	11.275
CB12	11/28/88	13:16:49:06	1.90	26.0	365.44	9.136
CB13	11/28/88	13:17:02:39	1.90	23.20	409.48	10.237
MEAN	--	--	1.66	23.93	347.47	8.69
± S.D.	--	--	0.36	1.72	70.02	1.75

A.5 Hemodynamic Data - Colchicine

CELL ID	DATE	TIME	V _{rec} (mm/sec)	DIAM (μ m)	SHEAR RATE (s ⁻¹)	τ_w (dyne/cm ²)
COLC1	12/21/88	14:55:00:95	1.30	25.20	257.92	6.448
COLC2	12/21/88	13:04:47:59	1.30	37.90	171.52	4.288
COLC3	12/21/88	13:17:51:27	1.20	25.70	233.52	5.838
COLC4	12/21/88	14:54:32:25	1.30	25.20	257.92	6.448
COLC5	12/21/88	13:05:32:99	1.30	37.90	171.52	4.288
COLC6	12/21/88	13:04:47:46	1.30	37.50	173.32	4.333
COLC7	12/21/88	13:08:24:23	1.30	41.20	157.80	3.945
COLC8	12/21/88	13:10:52:29	0.80	41.20	97.12	2.428
COLC9	12/21/88	13:11:44:52	0.80	38.80	103.12	2.578
COLC10	12/21/88	13:17:47:20	1.30	38.80	167.52	4.188
COLC11	12/21/88	13:41:27:02	1.00	27.90	179.32	4.483
MEAN	--	--	1.17	34.30	179.12	4.48
\pm S.D.	--	--	0.21	6.73	53.50	1.34

Appendix B
Experimental Analysis

B.1 Experimental Analysis - Control

CELL ID	τ_w (dyne/cm ²)	t_p (sec)	L_c at t_p (μ m)	total time adhered (s)	θ at t_p (degrees)	% of total θ by t_p
CONT1	8.661	2.760	10.210	2.76	31.5	100
CONT2	8.661	3.675	10.136	4.77	43.02	96.62
CONT3	5.303	4.665	10.689	7.40	41.47	99.59
CONT4	10.802	1.729	8.885	3.18	27.44	92.57
CONT5	8.075	1.814	10.531	3.00	42.80	99.53
CONT6	8.661	2.011	8.808	2.62	46.09	99.49
CONT7	3.275	4.246	8.025	5.36	48.35	90.98
CONT8	9.653	2.156	8.383	3.54	52.20	96.94
CONT9	7.709	4.722	8.654	7.24	46.31	85.59
CONT10	9.375	4.162	9.000	9.29	43.56	99.81
CONT11	5.542	6.162	7.102	7.64	60.33	99.97
CONT12	4.641	4.343	7.288	8.68	66.57	98.84
CONT13	6.350	2.974	9.700	5.00	52.59	82.47
CONT14	6.788	2.502	7.023	5.30	46.20	99.83
CONT15	6.443	1.655	7.987	2.42	•	•
CONT16	6.443	4.940	4.330	4.94	46.65	100

CELL ID	τ_w (dyne/cm ²)	t_p (sec)	L_c at t_p (μ m)	total time (sec)	θ at t_p (degrees)	% of total θ by t_p
CONT17	8.750	1.535	7.577	2.57	•	•
CONT18	3.000	5.86	7.080	5.86	53.40	100
MEAN	7.118	3.439	8.412	5.09	46.78	96.39
\pm S.D.	2.22	1.502	1.585	2.21	9.53	5.57

• Values could not be determined due to image quality.

B.2 Experimental Analysis - FMLP

CELL ID	r_w (dyne/cm ²)	t_p (sec)	L_c at t_p (μ m)	total time adhered (s)	θ_p at t_p (degrees)	θ_p at total time
FMLP1	9.605	9.566	11.048	31.71	33.55	61.02
FMLP2	9.885	10.700	11.151	20.12	75.64	87.70
FMLP3	11.883	9.883	10.143	31.72	60.18	82.77
FMLP4	10.268	14.130	10.650	45.24	30.82	83.99
FMLP5	9.965	21.270	9.3291	34.45	49.70	54.11
FMLP6	11.607	5.621	9.926	23.10	58.22	67.83
FMLP7	5.128	17.255	5.917	31.82	52.43	57.57
FMLP8	17.045	3.704	6.738	30.94	84.59	89.92
FMLP9	17.045	3.680	6.270	15.73	70.56	63.35
FMLP10	17.045	5.349	5.673	16.60	92.89	59.58
FMLP11	17.045	6.820	8.003	14.80	*	*
FMLP12	6.818	9.655	7.463	23.60	72.23	68.14
FMLP13	9.385	8.290	12.355	19.07	44.88	84.25
MEAN	11.65	9.445	8.820	26.069	60.47	71.69
\pm S.D.	4.14	5.453	2.257	9.042	19.39	13.10

* Values could not be determined due to image quality.

B.3 Experimental Analysis - IL-1

CELL ID	τ_w (dyne/cm ²)	t_p (sec)	L_c at t_p (μ m)	total time adhered (s)	θ_p at t_p (degrees)	% of total θ_p by t_p
IL1	8.695	5.125	10.740	6.43	*	*
IL2	9.040	4.255	9.468	5.54	56.09	93.96
IL3	8.695	4.512	11.018	4.70	40.36	99.95
IL4	8.695	4.150	13.438	4.50	71.51	94.83
IL5	8.695	5.324	7.931	6.55	46.73	86.84
IL6	8.695	3.378	7.561	4.03	55.05	97.15
IL7	4.860	5.120	9.233	5.74	56.96	96.10
IL8	5.000	4.120	9.900	4.12	62.59	100.00
IL9	9.890	2.554	13.056	4.70	35.64	100.00
IL10	10.080	3.316	11.579	4.00	33.71	98.07
IL11	4.085	9.983	9.398	10.70	43.54	88.78
IL12	2.743	3.605	9.351	7.50	36.59	99.10
MEAN	7.43	4.872	10.223	5.7099	48.98	95.89
± S.D.	2.51	1.933	1.822	1.934	12.32	4.52

* Values could not be determined due to image quality.

B.4 Experimental Analysis - CB

CELL ID	τ_w (dynes/cm ²)	t_p (sec)	L_c at t_p (μ m)	total time adhered (s)	θ at t_p (degrees)	% of total θ by t_p
CB1	8.260	6.331	11.67	6.96	20.33	95.38
CB2	6.373	5.458	10.44	10.00	12.27	99.49
CB3	6.373	3.093	11.42	5.54	26.73	96.43
CB4	6.438	8.495	8.64	11.79	52.56	77.70
CB5	6.579	4.575	12.07	8.06	28.50	85.69
CB6	8.929	2.896	9.05	8.04	44.42	91.33
CB7	9.921	4.128	14.82	5.34	47.02	85.16
CB8	10.373	5.139	12.39	7.07	21.80	99.13
CB9	8.721	3.272	9.09	16.16	35.00	97.88
CB10	10.316	7.128	13.84	8.95	*	*
CB11	11.275	2.964	9.00	4.84	49.80	65.18
CB12	9.136	3.728	15.28	5.10	28.30	79.02
CB13	10.237	4.275	10.40	6.63	29.19	96.24
MEAN	8.687	4.729	11.393	8.037	32.99	89.05
\pm S.D.	1.751	1.734	2.435	3.178	12.82	10.73

* Values could not be determined due to image quality.

B.5 Experimental Analysis - Colchicine

CELL ID	τ_w (dyne/cm ²)	t_p (sec)	L_c at t_p (μ m)	total time adhered (s)	θ at t_p (degrees)	% of total θ by t_p
COLC1	6.448	6.905	13.09	9.10	22.36	99.25
COLC2	4.288	10.906	11.36	11.93	27.42	97.08
COLC3	5.838	5.690	11.00	5.69	36.05	100.00
COLC4	6.448	4.068	14.66	4.30	34.42	99.88
COLC5	4.288	7.440	9.40	7.44	39.60	100.00
COLC6	4.333	11.393	10.46	12.46	26.46	97.75
COLC7	3.945	11.700	9.12	11.70	*	*
COLC8	2.428	4.560	12.50	4.56	*	*
COLC9	2.578	2.922	8.61	30.85	53.91	41.36
COLC10	4.188	5.463	10.25	5.60	49.96	99.87
COLC11	4.480	6.873	9.88	12.25	27.08	95.59
MEAN	4.478	7.084	10.939	10.54	35.25	92.31
\pm S.D.	1.337	3.034	1.845	7.46	10.93	19.17

* Values could not be determined due to image quality.

Appendix C
Bond Distribution Program

Bond Distribution Program

```

PROGRAM DIST
C  PROGRAM SOLVES NB, STRESS, AND TENSION DISTRIBUTION FOR
C  WBC-EC ADHESION.

C  WRITTEN BY ERIKA J. STRUBLE, 29 JANUARY 1993
C  MODIFIED 15 FEBRUARY 1993 TO INCLUDE TWO REGIONS
C  .....

REAL C,A,TW,TP,RO,FO,C1,C2,RC,PI,FS,M,TS,TO,DLTAX,X,DLTAP,F1JX,
* F1JXX,F1JXN,IF1,F2JX,F2JXX,F2JXN,IF2,SIG0,S,NB,SIGN,TM,S1,b,
* F1XB,F2XB,F3JX,F3JXX,F3JXN,IF3,TMb,SS,NBMAX,NB1b,NB10,NB2A,
* NB2b,NNB,CN,BN,ZETA,ZETAN,AU

INTEGER N,J,Z,I

CHARACTER*20 FLNAM

DATA IOUT /21/

C  FORMAT STATEMENTS

7 FORMAT(' ',F4.2,' ',F20.4,' ',F9.4,' ',F9.4,' ',F9.4,' ',F9.4,' '
*      ,F9.4)

C  PROGRAM ASKS FOR THE FOLLOWING INFORMATION:

C  FLNAM = FILE TO CONTAIN NB, SIGMA, AND TENSION DISTRIBUTION
C  CN = NON-DIMENSIONAL PARAMETER DESCRIBING EXPONENTIAL DECAY
C  A = RADIUS OF CONTACT AREA (CM)
C  AU RADIUS OF CONTACT AREA (uM)
C  TW = WALL SHEAR STRESS (DYNE/CM2)
C  TP = INTERIOR SHEAR STRESS (DYNE/CM2)
C  bN = NON-DIMENSIONALIZED REGION OF PEELING

WRITE(*,*)'INPUT VALUE OF CN:'
READ(*,*)CN
WRITE(*,*)'INPUT RADIUS OF CONTACT AREA (um):'
READ(*,*)AU
WRITE(*,*)'INPUT VALUE OF bN:'
READ(*,*)bN
WRITE(*,*)'INPUT VALUE OF TW:'
READ(*,*)TW
WRITE(*,*)'INPUT VALUE OF TP:'
READ(*,*)TP
WRITE(*,*)'INPUT VALUE OF FO (DYNE/BOND):'
READ(*,*)FO

```

C DIMENSIONALIZE CN AND bN

$A = AU \cdot 1E-4$
 $C = CN/A$
 $b = bN \cdot A$

C DEFINE CONSTANTS

$FLNAM = 'A:DIST.OUT'$
 $RO = 0.5E-7$
 $C1 = 1.7005$
 $C2 = 0.944$
 $RC = 4.0E-4$
 $PI = 3.1415927$
 $TO = 0.035$
 $NBMAX = 100$

C CALCULATE FS, M, TS

$FS = C1 \cdot 6 \cdot PI \cdot TW \cdot RC^{**2}$
 $M = C2 \cdot 4 \cdot PI \cdot TW \cdot RC^{**3}$
 $TS = FS / (PI \cdot A^{**2})$

$WRITE(*,*)FS = ',FS$
 $WRITE(*,*)M = ',M$
 $WRITE(*,*)TS = ',TS$
 $WRITE(*,*)TO = ',TO$
 $WRITE(*,*)'CALCULATING SIG0, NB, SIGN, AND TM DISTRIBUTION'$
 $WRITE(*,*)'WRITING TO FILE A:DIST.OUT'$

C CALCULATE SIGMA 0 USING TRAPAZOIDAL NUMERICAL APPROXIMATION

$N = 100$
 $DLTAX = A/100$

C F1(X) = 0

$F1XB = ((TS-TP) \cdot (A-b) + TO-TO \cdot EXP(C \cdot (A-b))) \cdot EXP(-C \cdot (A-b)) \cdot b \cdot$
 $\cdot SQRT(A^{**2}-b^{**2})$

C SUMMATION OF F1(J*DELTAX)

$F1JX = 0$
 $F1JXX = 0$

DO 10 J = 1, N-1, 1

C INITIALIZE F1JXN

F1JXN=0
X=J*DLTAX

IF (X .LE. b) THEN

• F1JXN=((TS-TP)*(A-X) + TO-TO*EXP(C*(A-X)))*EXP(-C*(A-X))*X*
SQRT(A**2-X**2)

F1JXX=F1JX + F1JXN
F1JX=F1JXX

ENDIF

10 CONTINUE

C NUMERICAL SOLUTION FOR INTEGRAL F1(X)

IF1=(DLTAX/2)*(F1XB + 2*F1JX)

C F2(X)

F2XB=(TS*b-TP*(A-b) + TO-TO*EXP(C*(A-b)))*EXP(-C*(A-b))*b*
SQRT(A**2-b**2)

C F2X0=0

C SUMMATION OF F2(J*DLTAX)

F2JX=0
F2JXX=0

DO 20 J=1,N-1,1

C INITIALIZE F2JXN

F2JXN=0
X=J*DLTAX

IF (X .GT. b) THEN

• F2JXN=(TS*b-TP*(A-X) + TO-TO*EXP(C*(A-X)))*EXP(-C*(A-X))*X*
SQRT(A**2-X**2)

F2JXX=F2JX + F2JXN
F2JX=F2JXX

ENDIF

20 CONTINUE

C NUMERICAL SOLUTION FOR INTEGRAL F2(X)

IF2 = (DLTAX/2)*(F2XB + 2*F2JX)

C F3(X)

C F3(0) = 0

C F3(A) = 0

C SUMMATION OF F3(J*DLTAX)

F3JX = 0

F3JXX = 0

DO 30 J = 1, N-1, 1

C INITIALIZE F3JXN

F3JXN = 0

X = J*DLTAX

F3JXN = X*SQRT(A**2 - X**2)

F3JXX = F3JX + F3JXN

F3JX = F3JXX

30 CONTINUE

C NUMERICAL SOLUTION FOR INTEGRAL F3(X)

IF3 = DLTAX*F3JX

C SOLVE FOR SIGMA 0 AND DELTA P

SIG0 = (((FS*RC + M)/4) - C**2*RO*(IF1 + IF2))/(IF3)

WRITE(*,*)'SIGMA 0 = ', SIG0

DLTAP = TO*C**2*RO - SIG0

WRITE(*,*)'DELTA P = ', DLTAP

C CALCULATE NB, SIGN, TM, NORMALIZED ZETA AND WRITE TO FILE

TMb = (TS-TP)*b + TO

OPEN(UNIT = IOOUT, FILE = FLNAM)

C WRITE(IOOUT, 6)

Z = 100

S = 0

```
WRITE(*,*)Z
DO 40 I=0,Z,1
```

```
IF (S .LE. b) THEN
```

```
C NB IS CALCULATED FOR BONDS/UM2
```

```
• NB = ((C**2*RO/FO)*((TS-TP)*S + TO-TO*EXP(C*S)) + SIGO/(FO*EXP
  (-C*S))) * 1E-8
```

```
IF (NB .GE. NBMAX) THEN
```

```
NB = NBMAX
```

```
ENDIF
```

```
SIGN = (NB*1E8)*FO*EXP(-C*S)
```

```
TM = (TS-TP)*S + TO
```

```
ZETA = RO*EXP(-C*S)
```

```
ZETAN = ZETA/RO
```

```
ELSE
```

```
• NB = ((C**2*RO/FO)*(TP*(b-S) + TMb) - (TO*C**2*RO-SIGO)/
  (FO*EXP(-C*S))) * 1E-8
```

```
IF (NB .GE. NBMAX) THEN
```

```
NB = NBMAX
```

```
ENDIF
```

```
SIGN = (NB*1E8)*FO*EXP(-C*S)
```

```
TM = TP*(b-S) + TMb
```

```
ZETA = RO*EXP(-C*S)
```

```
ZETAN = ZETA/RO
```

```
ENDIF
```

```
SS = S*1E4
```

```
WRITE(IOUT,7)SS,NB,SIGN,TM,DLTAP,SIGO,ZETAN
```

```
S1 = S + 6E-6
```

```
S = S1
```

40 CONTINUE

 CLOSE(UNIT=IOUT)

 STOP
 END